Studies on Properties of Peripherally Modified Antiaromatic Norcorroles

YOSHIDA Takuya

Studies on Properties of Peripherally Modified Antiaromatic Norcorroles

周辺修飾された反芳香族ノルコロールの物性に関する研究

YOSHIDA Takuya

吉田　拓矢

Department of Applied Chemistry, Graduate School of Engineering,

Nagoya University

名古屋大学大学院工学研究科

化学・生物工学専攻　応用化学分野

2018

Preface

The studies in this thesis were carried out under the guidance of Prof. Dr. Hiroshi Shinokubo at Graduate School of Engineering, Nagoya University during the period from April 2015 to February 2018.

These studies mainly focus on the synthesis and properties of peripherally modified antiaromatic norcorroles. In the field of organic chemistry, antiaromatic compounds have attracted much attention due to their distinctly different properties from those of conventional aromatic compounds. However, comprehensive studies on antiaromatic compounds have been hampered by their synthetic difficulties and unstable nature. The main aim of the research in this thesis is a creation of novel antiaromatic compounds with unique properties thorough the peripheral modification of norcorrole, which is an exceptionally stable antiaromatic porphyrinoid.

Table of Contents

List of Abbreviations

Å	ångström unit
Ac	acetyl
ACID	anisotropy of the induced current density
aq	aqueous solution
Ar	aryl
B3	Becke's three-parameter hybrid exchange functional
BCOD	bicyclo[2,2,2]octadiene
BLA	bond length alternation
BS	symmetry-broken
Bu	n-butyl
calcd	calculated
cod	1,5-cyclooctadiene
CT	charge transfer
CuTc	copper(I) 2-thiophenecarboxylate
δ	chemical shift
DDQ	2,3-dichloro-5,6-dicyano-1,4-benzoquinone
DFT	density functional theory
DMF	N,N-dimethylformamide
ε	absorption coefficient
ESI-MS	electrospray ionization mass spectrometry
ESR	electron spin resonance
Eq.	equation
equiv	equivalent(s)
Et	ethyl
f	oscillator strength
Fc	ferrocene
FP-TRMC	flash-photolysis time-resolved microwave conductivity
h	hour(s)
HOMA	harmonic oscillator model of aromaticity
HOMO	highest occupied molecular orbital
HR-MS	high resolution mass spectrometry infrared
J	coupling constant (NMR)
J_{S-T}	intramolecular magnetic coupling constant
λ	wavelength
LC	long-range correction
LUMO	lowest occupied molecular orbital

List of Abbreviations

LYP	Lee–Yang–Parr correlation functional
M	metal or molar
Me	methyl
Mes	mesityl
*m*CPBA	*m*-chloroperoxybenzoic acid
min	minute(s)
MO	molecular orbital
NBS	*N*-bromosuccinimide
NICS	nucleus-independent chemical shift
NIR	near infrared
NIS	*N*-iodosuccinimide
NMP	*N*-methylpyrrolidone
NMR	nuclear magnetic resonance
Ph	phenyl
OEFT	organic field-effect transistor
ppm	parts per million
R	an organic group or restricted
RT	room temperature
SOMO	singly occupied molecular orbital
SQUID	superconducting quantum interference device
TBAPF$_6$	tetrabutylammonium hexafluorophosphate
TD	time-dependent
TEA	triethylamine
TFA	trifluoro aceticacid
THF	tetrahydrofuran
TMS	tetramethylsilane
TPP	tetraphenylporphyrin
U	unrestricted
UV	ultraviolet
vis	visible
VT	variable temperature
y	diradical character
$\chi_p T$	temperature-dependent magnetic susceptibility

Chapter 1

General Introduction

Contents

1-1. Antiaromatic compounds and antiaromaticity

According to the Hückel's rule, planar cyclic molecules which have (4n+2) π-electrons in their conjugation systems show aromaticity, as represented by aromatic benzene. On the other hand, planar cyclic molecules which have 4n π-electrons in their conjugation systems are called antiaromatic compounds (Figure 1-1). Although antiaromatic compounds are generally unstable unlike aromatic compounds, they exhibit distinct and intriguing physical properties. One of the commonly known features of antiaromatic compounds is their paratropic ring current, of which direction is opposite to the diatropic ring current associated with aromaticity.[1] Electrochemical properties of antiaromatic compounds are also notable. Basically, antiaromatic compounds are easily oxidized and reduced, and their oxidation and reduction processes often show good reversibility. Antiaromatic compounds are potential candidates for semiconductor materials because of such redox properties. The difference between aromatic and antiaromatic compounds is also found in their optical properties. Antiaromatic compounds does not have any emission, and their absorption in the low-energy region (red to near-IR region) are fairly weak, due to the forbidden nature of the lowest excited state. Importantly, all of physical properties listed above are eventually attributed in the small HOMO–LUMO energy gap and electronic configuration of antiaromatic compounds.   While an aromatic annulene has enlarged HOMO–LUMO energy gap compared with the corresponding (4n+2) π-electron polyene, an antiaromatic annulene have small HOMO–LUMO energy gap compared with the 4n π-electron polyene (Figure 1-2). The smaller gap of the antiaromatic annulene can be accounted for by phase interactions through cyclization of polyenes, in which the HOMO level is destabilized and the LUMO level is stabilized by opposite phase interaction and same phase interaction, respectively.[2] In theory, an antiaromatic compound with an ideal symmetric structure should have degenerated two SOMOs to become an open-shell triplet diradical, because these orbitals have same numbers of nodes (Figure 1-3a).[3] However, such electronic configuration is so unstable that antiaromatic compounds choose distorted structure through Jahn-Teller effect to split degenerated orbitals into HOMO and LUMO (Figure 1-3b). 4n π-Electron molecules which experimentally exhibited triplet ground states with degenerated SOMOs have been limited to cyclopentadienyl cations (Figure1-4).[4,5] Consequently, antiaromatic compounds generally have the closed-shell singlet ground state with small HOMO–LUMO gaps.
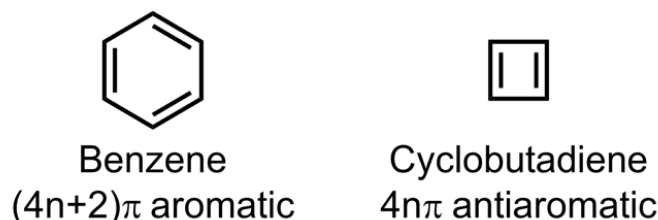

Figure 1-1. Benzene and cyclobutadiene as representatives of aromatic and antiaromatic compounds, respectively.
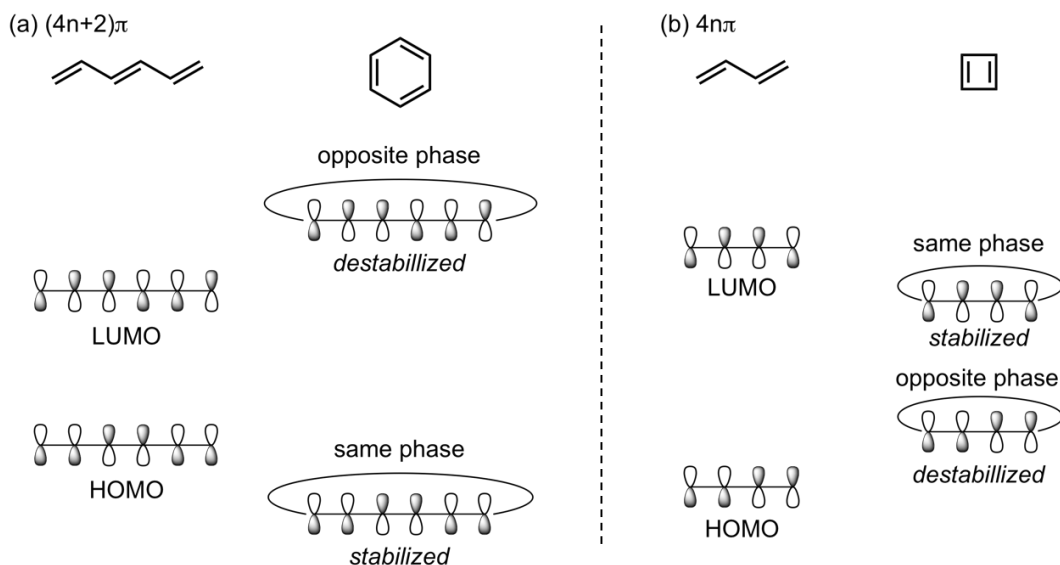
Figure 1-2. Change in energy levels of HOMO and LUMO through cyclization of polyenes to form (a) $(4n+2)$ π-electron and (b) $4n$ π-electron systems, described by using benzene and cyclobutadiene, respectively. The figure describes an enlarged energy gap of an aromatic compound and a reduced energy gap of an antiaromatic compound.
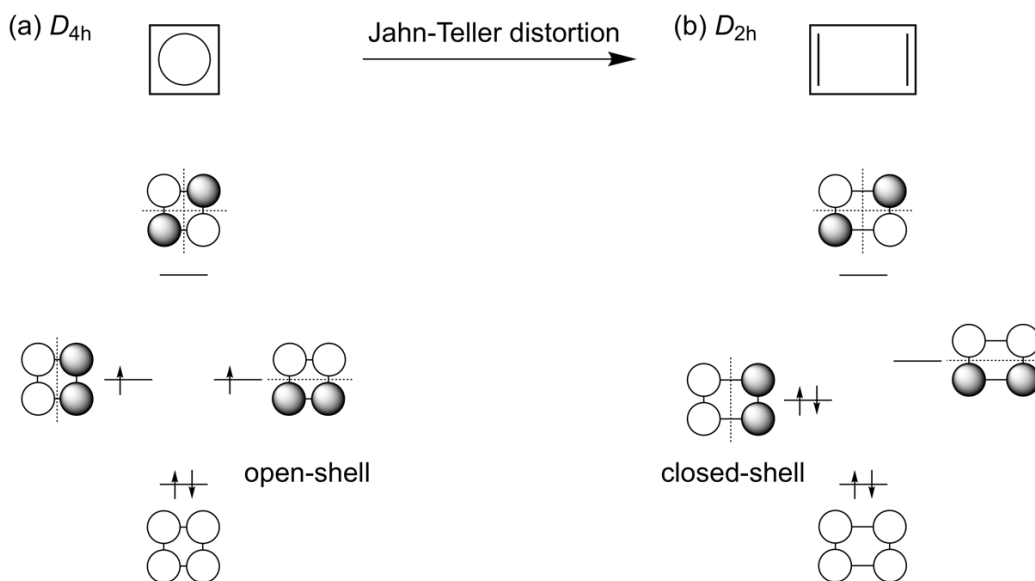

Figure 1-3. Electronic configurations of (a) D_{4h} and (b) D_{2h} cyclobutadienes. Dashed lines represent nodes of π-orbitals. Degenerated orbitals (SOMOs) of D_{4h} cyclobutadiene are split into HOMO and LUMO of D_{2h} cyclobutadiene by Jahn-Teller distortion.
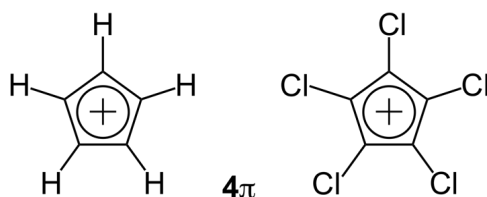

Figure 1-4. 4π cyclopentadienyl cations which have triplet ground states.[4,5]

There are several criteria for antiaromaticity.[1] The chemical shifts in the ^{1}H NMR spectrum of a particular π-system are an experimentally observable criterion to evaluate antiaromaticity. (Figure 1-5). Antiaromatic compounds exhibit the anticlockwise paratropic ring current under an external magnetic field. Due to a magnetic field induced by the paratropic ring current, an inner hydrogen atom of a conjugation system undergoes downfield shift, whereas an outer hydrogen atom undergoes upfield shift. These changes in chemical shifts are completely opposite to the cases of aromatic compounds, which have clockwise diatropic ring current under an external magnetic field. Consequently, ^{1}H NMR spectroscopy is the effective method to distinguish aromatic and antiaromatic compounds.
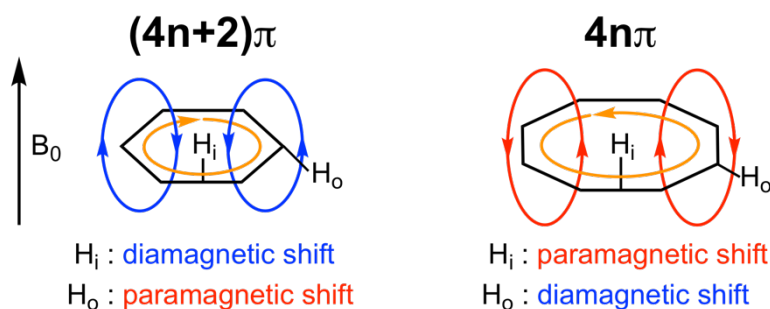

Figure 1-5. Diatropic ring current of an aromatic compound (left) and paratropic ring current of ring current of an antiaromatic compound (right). H_i: inner hydrogen atom, H_o: outer hydrogen atom, B_0: external magnetic field.
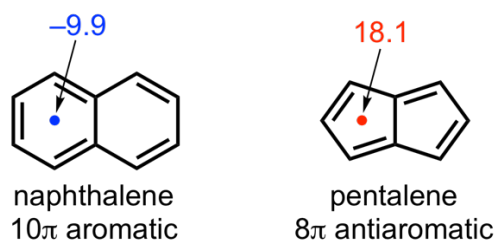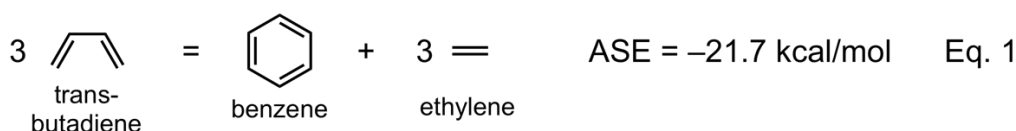

Figure 1-6. NICS values of naphthalene and pentalene.[6]

The effects of ring currents are also evaluated by computational methods. Nuclear independent chemical shift (NICS)[6,7] is an absolute chemical shift at a virtual nucleus, which can be calculated using standard quantum chemical programs. For instance, the internal NICS value of 10π naphthalene is calculated to be negative and 8π pentalene to be positive, because of the effects of diatropic and paratropic ring currents, respectively (Figure 1-6). NICS is particularly useful for molecules which have no internal proton. Recent developments of computational studies have also enabled direct visualization of ring currents of (anti)aromatic compounds. The anisotropy of the induced current density (ACID) program[8] is representative of such methods, and commonly employed to recognize the direction and strength of ring currents.

Bond length alternation (BLA) of a conjugation system is also sometimes used to evaluate antiaromaticity. Since a 4n π-electron system is inherently unfavorable conjugation, antiaromatic compounds generally show large BLA to decrease the symmetry of molecules (Figure 1-3). An extent of BLA is usually quantified by the harmonic oscillator model of aromaticity (HOMA)[9] value, which is close to 1 in an ideally delocalized aromatic molecule. Antiaromatic compounds normally show smaller HOMA values due to the larger BLA than those of

aromatic compounds. However, a 4n π-electron molecule with a very small HOMA value results in destruction of the conjugation system. Such molecule eventually loses its antiaromaticity and is classified as a nonaromatic compound. Thus, a small HOMA value can suggest the existence of antiaromaticity, but is not criterion for antiaromaticity.

Aromatic stabilization energy (ASE) is the energetic criterion for aromaticity, and is calculated based on difference in energy between annulenes and corresponding olefins/polyenes.[1] Eq. 1 in Scheme 1-1 shows that aromaticity of benzene stabilizes the energy of the right-hand side relative to the left-hand side by 21.7 kcal/mol. Conversely, the energy of the right-hand side relative to the left-hand side is destabilized by 36.7 kcal/mol in Eq. 2, due to antiaromaticity of cyclobutadiene. The value of destabilization by antiaromaticity is called antiaromatic destabilization energy (ADE). Delocalization energy per electron (DEPE), Dewar's resonance energy (DRE), and Hess-Schaad resonance energy (HSRE), etc. are employed as criteria of (anti)aromaticity besides ASE and ADE.

$$3 \quad \text{trans-butadiene} \quad = \quad \text{benzene} \quad + \quad 3 \quad \text{ethylene} \qquad \text{ASE} = -21.7 \text{ kcal/mol} \qquad \text{Eq. 1}$$

$$2 \quad \text{cyclobutene} \quad - \quad \text{cyclobutane} \quad = \quad \text{cyclobutadiene} \qquad \text{ADE} = 36.7 \text{ kcal/mol} \qquad \text{Eq. 2}$$

Scheme 1-1. Aromatic stabilization energy (ASE) of benzene (Eq. 1) and aromatic destabilization energy (ADE) of cyclobutadiene (Eq. 2).[1]

The small HOMO–LUMO gaps of antiaromatic compounds provide possibility of application in several fields. Several antiaromatic compounds have been developed as semiconductor materials by taking advantage of their easily oxidized and reduced nature.[10-14] Nuckolls and Haley *et al.* reported that diarylated indenofluorene behaved as an ambipolar semiconductor in an organic field-effect transistor (OFET).[11] Nishinaga and Kunugi *et al.* also synthesized fused cyclooctatetraene (COT) with planar structure, which showed ambipolar character in an OFET device (Figure 1-7).[12] These researches successfully utilize high HOMO and low LUMO of antiaromatic compounds for creating conductive materials.

The other applicative feature of antiaromatic compounds is their high reactivity,[15-17] which is also induced by small HOMO–LUMO gap. Piers *et al.* achieved metal-free activation of molecular dihydrogen (H$_2$) by antiaromatic pentaarylborrole (Figure 1-8a).[18,19] The driving force of the activation is disruption of antiaromaticity of 4π borrole as well as highly Lewis acidic boron center, and pentaarylborrole is converted to nonaromatic boracyclopentene after the addition of dihydrogen. Silylated 1,4-dihydropyrazine reported by Kaim exhibits exceptionally low ionization potential stemmed from its 8π antiaromaticity and electron rich N-heterocyclic system.[20] This highly electron-rich 1,4-dihydropyrazine reagent can serve as a strong reductant to generate low valent metal species (Figure 1-8b).[21,22]
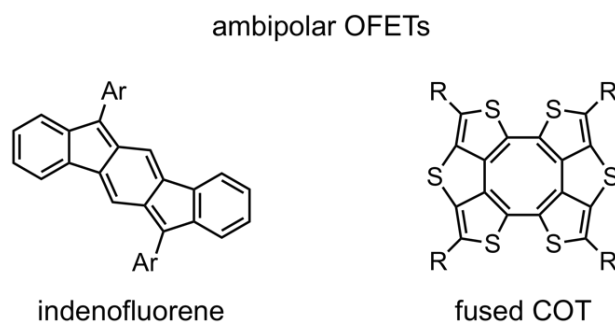
ambipolar OFETs

indenofluorene   fused COT

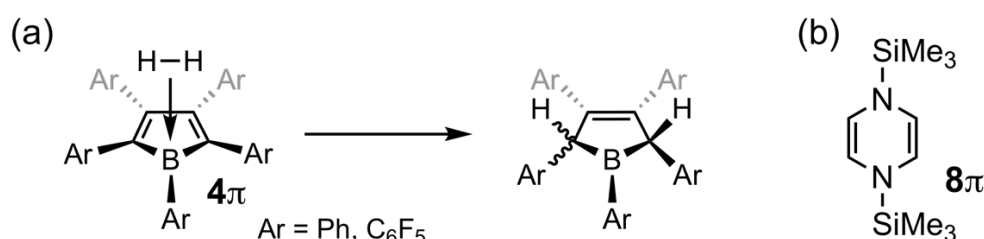**Figure 1-7.** Antiaromatic compounds which function as ambipolar OFETs.[11,12]


Figure 1-8. Examples of highly reactive antiaromatic compounds. (a) Activation of dihydrogen by pentaarylborrole[18,19] and (b) silylated 1,4-dihydropyrazine[20-22] as a strong reducing agent.

Recently, exited state (anti)aromaticity (so called Baird's rule) also has been received much attentions.[23-25] The main claim of Baird's rule is that ground state Hückel aromaticity and antiaromaticity are inverted in exited states. The concept of Baird's rule is partly related to the exited state intramolecular proton transfer (ESIPT). Introducing the concept of the exited state (anti)aromaticity would help designing of novel functional π-molecules.

In spite of these achievements, further development in antiaromatic compounds has been still hampered by their synthetic difficulties and unstable nature. The chemistry of antiaromatic compounds lags far behind the chemistry of aromatic compounds, in which a variety of functional molecules have been produced to date. Easily accessible and stable antiaromatic compound has been highly desired toward further development of the field.

1-2. Antiaromatic porphyrinoids

While porphyrins are normally known as aromatic compounds with 18π electron systems, a number of antiaromatic porphyrinoids have been synthesized and reported.[26-29] Since multiple conjugation pathways can be adopted in the structure of porphyrin, simple two-electron oxidation or reduction of aromatic porphyrins sometimes afford the corresponding antiaromatic systems (Scheme 1-2). Relatively large cyclic π systems of porphyrins and local aromaticity of pyrrole rings are also advantages to stabilize and isolate such oxidized or reduced forms of antiaromatic porphyrins.
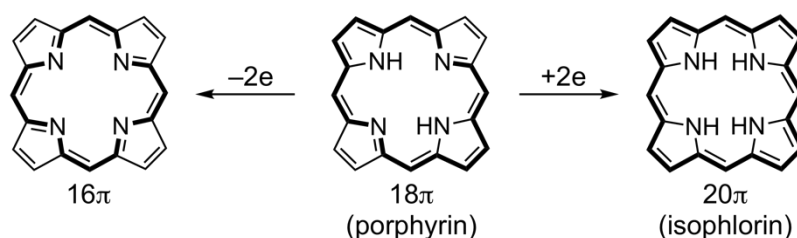
Scheme 1-2. The regular 18π aromatic porphyrin and 16π/20π porphyrins.

Series of 16π porphyrins have been comprehensively investigated by Yamamoto *et al.*[30-32] Since some of them readily lost antiaromaticity by structural deformation, 16π porphyrins showing antiaromaticity were isolated as rigid zinc complexes without sterically demanding substituents (Figure 1-9). Vaid *et al.* also reported 16π antiaromatic porphyrin as a lithium complex.[33] 20π porphyrin is generally known as an unstable isophlorin containing four NH groups in the core cavity. Although pristine isophlorin should be weakly antiaromatic or nonaromatic owing to its distorted structure induced by repulsion among central hydrogen atoms, Vaid *et al.* and Brothers *et al.* have synthesized and isolated 20π isophlorin derivatives displaying distinct antiaromaticity (Figure 1-10a). Such isophlorins contain silicon atom,[34] dibroron group,[35] and C=C group[36] in their cavities instead of four hydrogen atoms to suppress the distortion of structures. Another strategy to design antiaromatic isophlorin is replacement of pyrrole rings with other heterocycles. Anand *et al.* successfully synthesized tetraoxaisophlorin and dioxadithiaporphyrin, which adopt planar structure to show 20π antiaromatic character (Figure 1-10b).[37] In addition, Matano *et al.*[38] and Shinokubo *et al.*[39] independently reported synthesis of 20π diazaporphyrins, whose conjugation systems are different from those of isophlorins (Figure 1-10c).
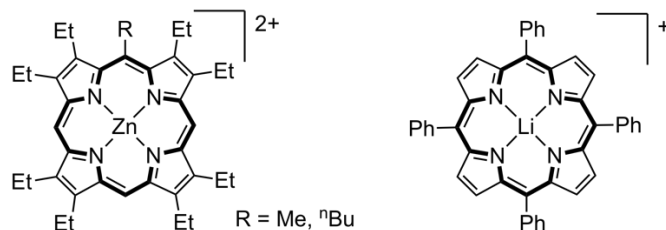

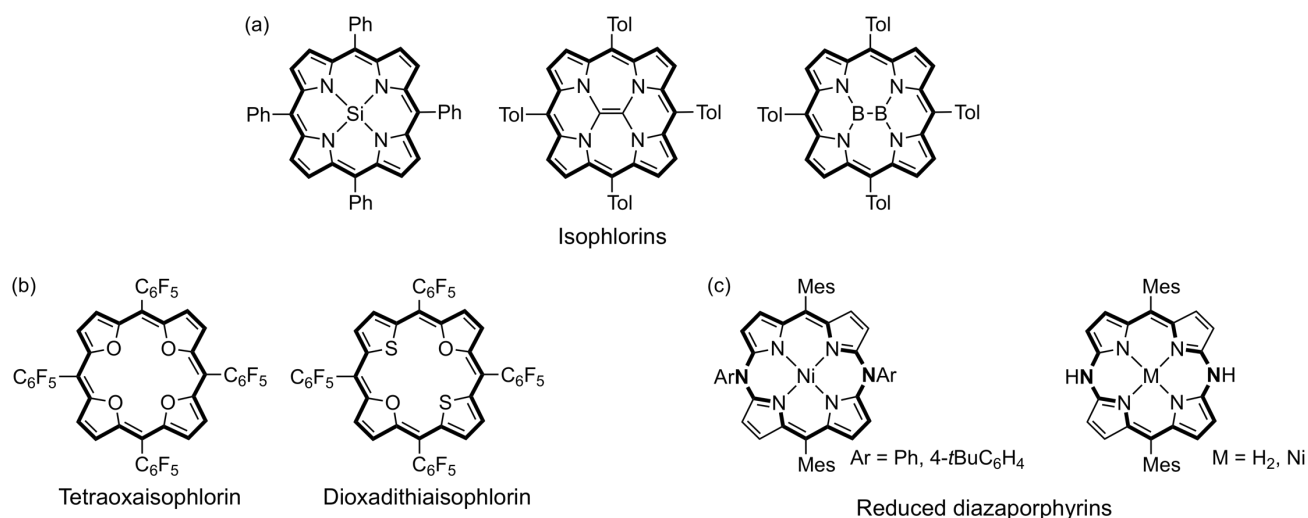**Figure 1-9.** Examples of 16π antiaromatic porphyrins.[31,33]

Figure 1-10. Examples of 20π antiaromatic porphyrins.[34-39]

Expanded porphyrins have been also extensively investigated in the chemistry of porphyrinoids, some of which display antiaromatic character. Osuka *et al.* have reported a series of hexaphyrins,[27,40] that is constructed of six pyrrole rings with six bridged *meso*-carbons. The large π system of hexaphyrins enables formation of multiple electronic states through oxidation or reduction. For instance, reduction of 26π aromatic hexaphyrin Au[III] complexes easily produce the corresponding stable 28π antiaromatic hexapyrins (Scheme 1-3).[41] The switchable aromaticity and antiaromaticity of hexaphyrin allowed to study difference in physical properties between aromatic and antiaromatic systems in a systematic fashion. Kobayashi *et al.* fully analyzed UV-vis-NIR absorption bands of both of aromatic and antiaromatic hexaphyrins by DFT calculations and magnetic circular dichroism (MCD) spectroscopy.[42] Kim *et al.* experimentally elucidated the lifetime of exited states of aromatic and antiaromatic vinylene-bridged hexaphyrins by transient absorption spectroscopy, and provided the important insight about energy relaxation dynamics of antiaromatic systems.[43] As well as these examples, researches on expanded porphyrins have contributed the development of notable antiaromaticity, such as Möbius antiaromaticity,[44,45] Baird's antiaromaticity with spectroscopic evidence,[46] and antiaromaticity over large conjugation systems.[47,48]
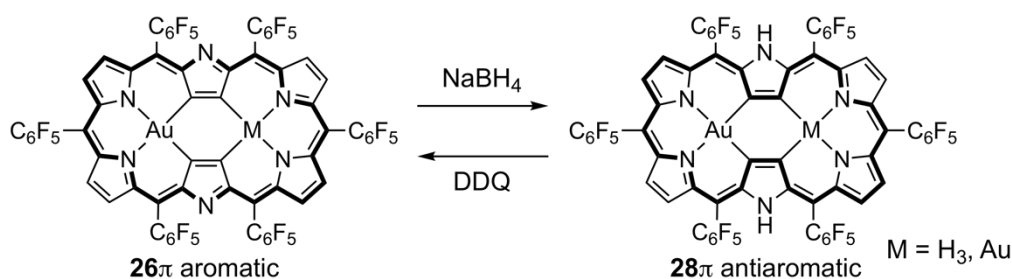
Scheme 1-3. Switchable aromaticity/antiaromaticity of hexaphyrin Au[III] complexes.[41,42]

As a variety of antiaromatic porphyrinoids have been prepared, porphyrinoids can be attractive macrocycles to construct novel antiaromatic compounds. However, most of the researches of antiaromatic porphyrinoids focus on their synthesis and properties, and further modification and application of antiaromatic porphyrinoids are still a challenging issue.

1-3. Norcorroles

Norcorrole is a ring-contracted porphyrin with a 16 π-electron system, whose structure lacks two-*meso* carbon atoms from a regular porphyrin (Figure 1-11). Norcorrole was firstly reported by Bröring *et al.* as an unstable Fe[III] complex, which is rapidly converted into a nonaromatic dimerized product to break antiaromaticity of norcorrole (Scheme 1-4).[49] The Fe[III] norcorrole was observed only by ^{1}H NMR and mass spectrometry and was not isolable due to the quick dimerization.
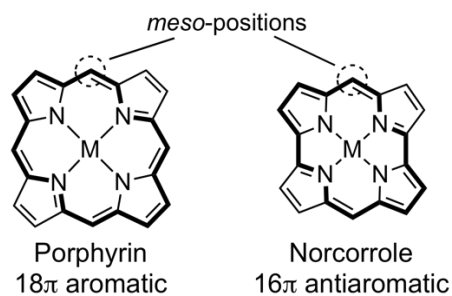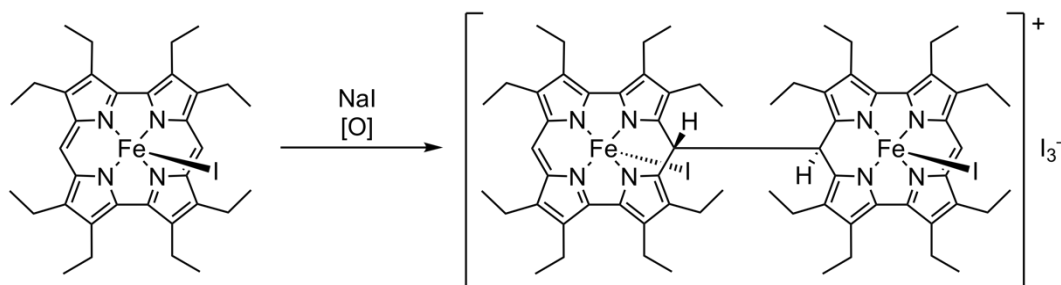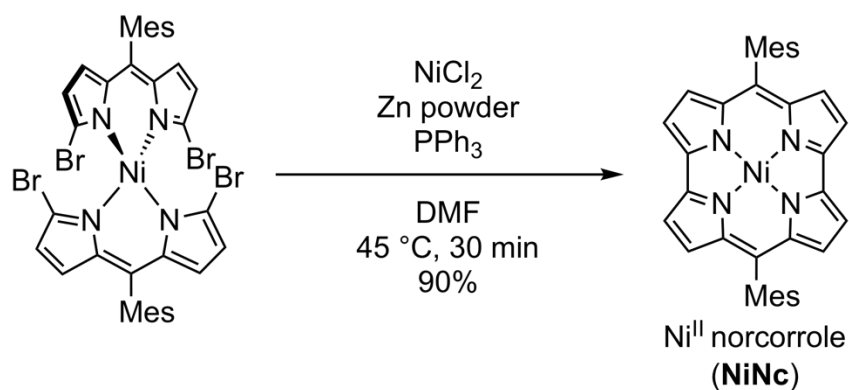
**Figure 1-11.** Structures of porphyrin and norcorrole.

Scheme 1-4. Fe[III] norcorrole and its dimerization.[49]

Scheme 1-5. Synthesis of Ni[II] norcorrole (**NiNc**).[50]

After several years of Bröring's report, Shinokubo *et al.* successfully prepared a norcorrole Ni[II] complex substituted with dimesityl groups in high yield by intramolecular coupling reaction of a bisdipyrrin Ni[II] complex (Scheme 1-5).[50] Surprisingly, this Ni[II] norcorrole **NiNc** was obtained as an air- and moisture-stable product and could be isolated by ordinary silica gel column chromatography. For the synthesis and stabilization of **NiNc**, the central Ni[II] and mesityl groups at *meso*-positions play crucial roles. Ni[II] in the precursor complex is necessary as a template atom to construct the norcorrole macrocycle upon the reductive coupling reaction. The small ionic radius of Ni[II] is also an important factor for the macrocyclization and fixing the structure of norcorrole, because the central cavity of norcorrole is fairly small due to the ring-contracted structure. In fact, coupling reaction with the precursor containing larger Pd[II] ion in the center leaded to intermolecular coupling to produce a ring-expanded Pd[II] octaphyrin instead of Pd[II] norcorrole (Scheme 1-6).[51] Peripheral dimesityl groups of **NiNc** kinetically stabilize the molecule by steric protection of *meso*-positions, which were not protected in the case of previous Fe[III] norcorrole. Since the dimerization of Fe[III] norcorrole occurred through the bond formation

11

between *meso*-positions, introducing bulky substituent to *meso*-positions of norcorrole should be effective strategy to enhance its stability. The distinct antiaromaticity of **NiNc** based on the 16 π-electron system was confirmed by ^{1}H NMR analysis, in which protons on pyrrole rings appeared at δ = 1.57 and 1.47 ppm in the upfield region. The large NICS value (+39.4 ppm) inside the macrocycle and small HOMO–LUMO gap (1.5 eV) of **NiNc** estimated by DFT calculations also supported its antiaromaticity. X-ray structural analysis elucidated a highly planar core structure of **NiNc** (Figure 1-12), which would sustain the antiaromatic nature.
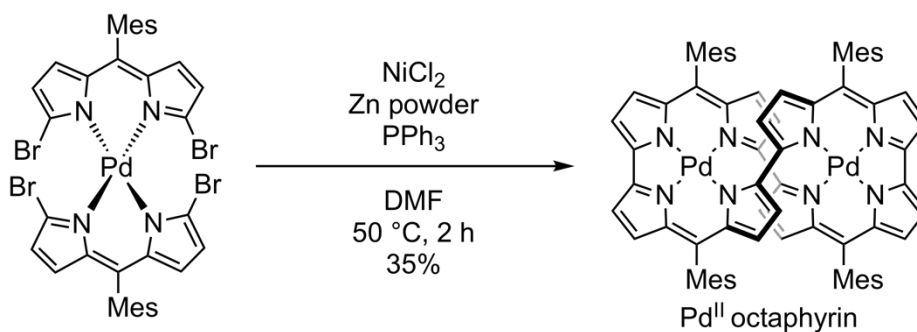
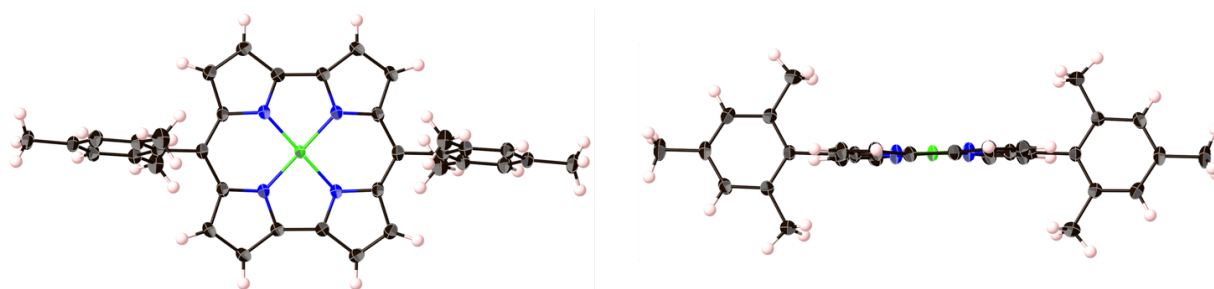**Scheme 1-6.** Synthesis of Pd[II] octaphyrin.[51]

Figure 1-12. Crystal structure of **NiNc**.[50]

The small HOMO–LUMO gap of **NiNc** was also confirmed by using cyclic voltammetry, and **NiNc** displayed perfectly reversible two oxidation waves and two reduction waves. The stability for redox processes is accounted for by aromatic nature of two-electron oxidized 14π species and two-electron reduced 18π species (Figure 1-13). The remarkable redox properties were applicable to a rechargeable organic battery, whose electrodes are composed of **NiNc**.[52] This is the first report applying antiaromatic porphyrinoids to practical material science, to the best of the author's knowledge.
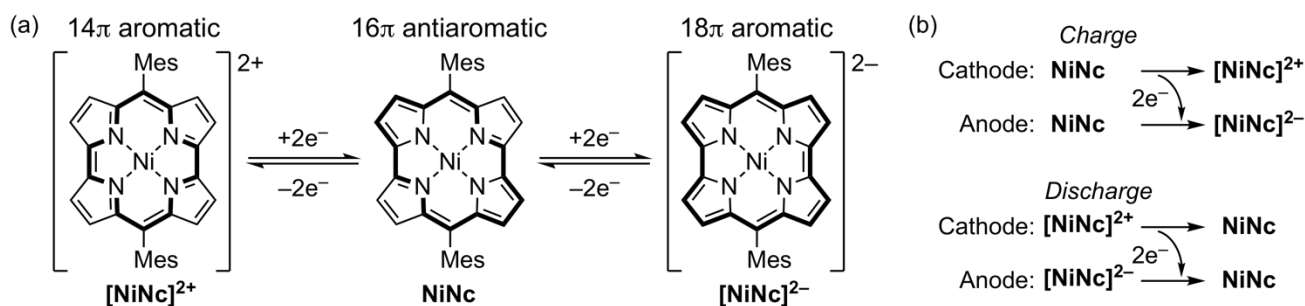

Figure 1-13. (a) Two-electron oxidation and reduction of **NiNc** and (b) outline of the norcorrole battery.[52]

With this easily accessible and stable antiaromatic compound in hand, reactivity and functionalization of norcorroles have been explored. **NiNc** dissolved in DMF is gradually oxidized by O_2 at high temperature to produce 18π aromatic 10-oxacorrole, in which an oxygen atom is inserted between pyrrole α-carbons of **NiNc** (Scheme 1-7).[50] Oxidation of **NiNc** with *m*CPBA also afforded the 10-oxacorrole at low temperature. The reaction of **NiNc** with a silylene resulted in insertion of silicon atoms in a different manner from the oxygen-insertion (Scheme 1-8).[53] The pyrrole ring of **NiNc** was opened by treatment with 1.0 equivalent of silylene to afford a silylated product containing a six-membered ring in a quantitative yield. Interestingly, the product exhibited intense near-IR absorption bands because of considerable change in the π-conjugation system. Furthermore, the addition of an excess amount of the silylene to **NiNc** resulted in formation of a muti-silylated compound. The intriguing reactivity of **NiNc** is induced by the antiaromatic character, because a regular aromatic porphyrin never underwent any reaction with the silylene reagent.
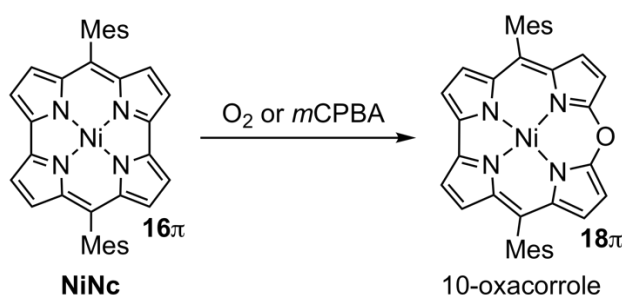
Scheme 1-7. Oxidation reaction of **NiNc**.[50]
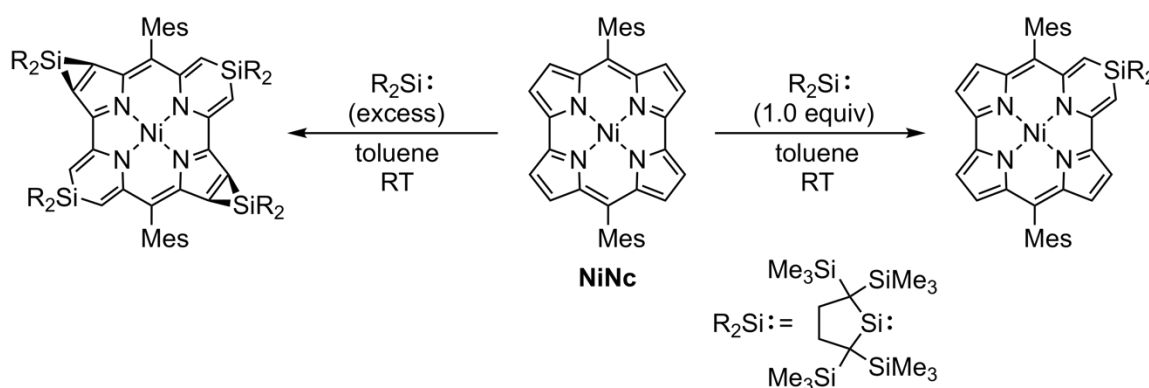
Scheme 1-8. Silylation reactions of **NiNc**.[53]

Two types of hydrogenation of **NiNc** have been reported. The firstly reported reduction is hydrogenation with Raney Ni, which produced hexahydronorcorrole with nonaromatic character (Scheme 1-9a).[54] On the other hand, *p*-tosylhydrazide with Zn powder was employed for reduction of **NiNc** in the second report, in which weakly antiaromatic chlorin- and bacteriochlorin-like norcorroles were obtained as resultant products (Scheme 1-9b).[55]
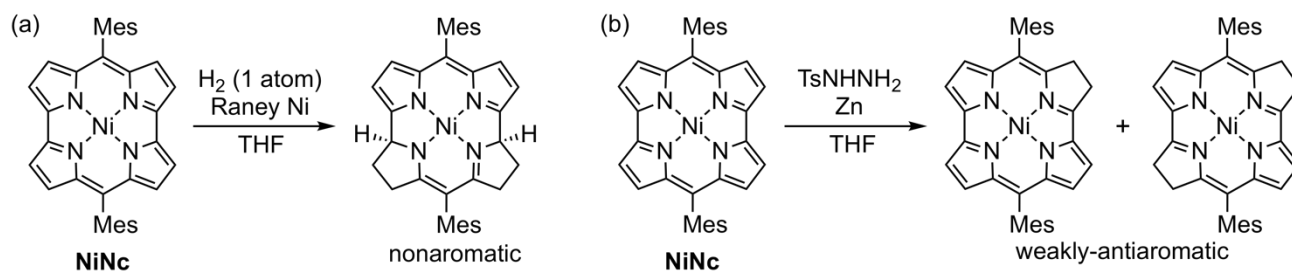
Scheme 1-9. Hydrogenation of norcorrole by (a) H$_2$ with Raney Ni[54] and (b) *p*-tosylhydrazide with Zn.[55]

Nucleophilic and electrophilic substation reactions are applicable to **NiNc**, owing to its low LUMO level and high HOMO level resulted from the antiaromaticity. The pyrrole β-positions of **NiNc** were regioselectively substituted via reactions with nucleophiles such as cyanide, alkoxide, and thiolate (Scheme 1-10).[56] The introduced functional groups affected optical and electrochemical properties of norcorrole. Tetrathiolated norcorrole exhibited further decreased HOMO–LUMO gap in particular. The reaction of **NiNc** with electrophilic nitrite provided regioselectively nitrated norcorroles (Scheme 1-11).[57] The nitration enabled observation of reduced species of norcorroles which were stabilized by electron-withdrawing nitro groups. Electrophilic bromination of **NiNc** with *N*-bromosuccinimide (NBS) and the following migration reaction afforded two regioisomeric brominated norcorroles (Scheme 1-12).[58] These brominated products could be scaffolds for regioselective functionalization of norcorroles by cross-coupling reactions.
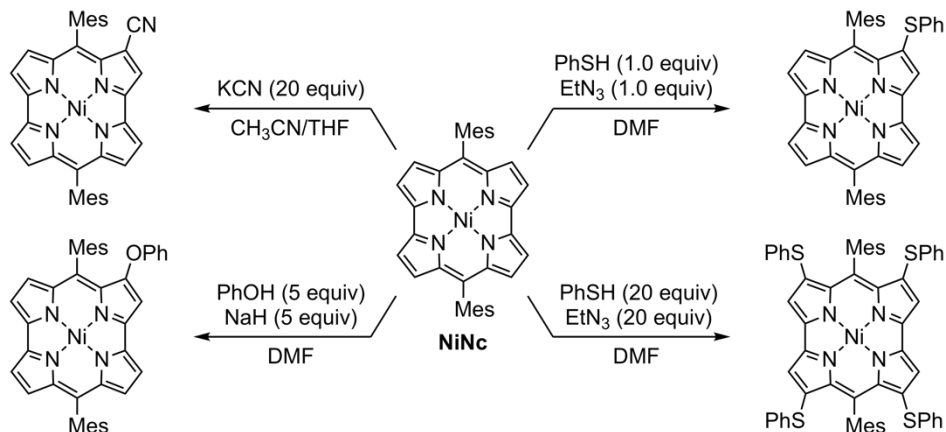
**Scheme 1-10.** Nucleophilic cyanation, alkoxylation, and thiolation reactions of **NiNc**.[56]
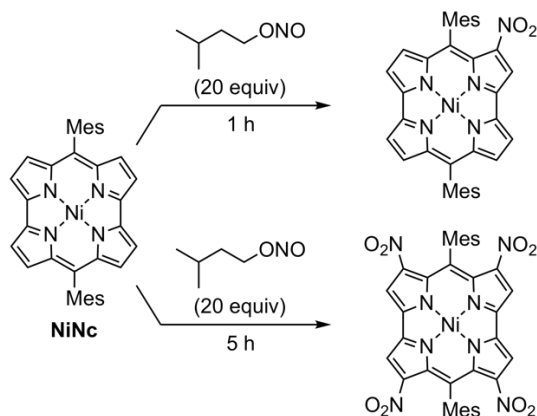
**Scheme 1-11.** Electrophilic nitration reaction of **NiNc**.[57]
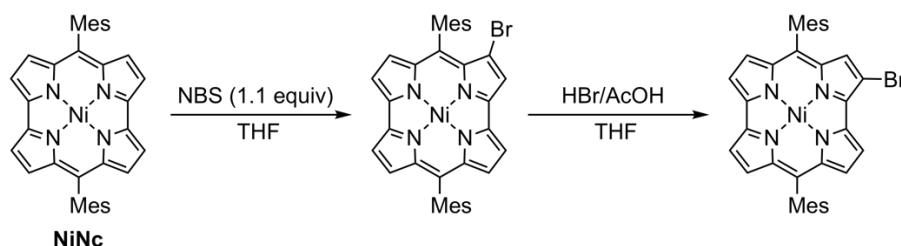
Scheme 1-12. Electrophilic bromination and the following migration reactions of **NiNc**.[58]

The development of such functionalization of norcorrole is not only useful for tuning its properties, but also for the creation of a novel antiaromatic compound. Shinokubo *et al.* employed the nucleophilic thiolation reaction to synthesize a tethered norcorrole dimer, which adopts π-stacked conformation both in crystal and in solution (Scheme 1-13).[59] Thorough analyses of the stacked norcorrole dimer experimentally revealed emergence of three-dimensional aromaticity in π-stacked antiaromatic compounds, that had been theoretically predicted but never been demonstrated by an actual molecule.[60,61]
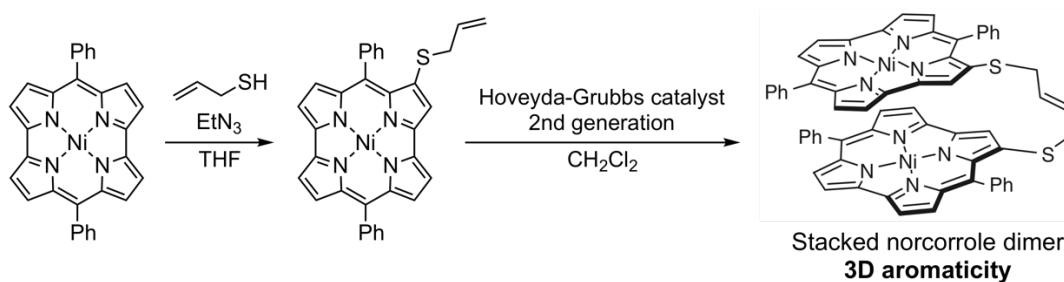
Scheme 1-13. Synthesis of stacked norcorrole dimer showing 3D aromaticity.[59]

Changing the central metal is an interesting topic in the chemistry of porphyrinoids. Although all norcorroles had been isolated as Ni^{II} complexes, recently a free-base norcorrole was successfully prepared via synthesis and demetallation reaction of Cu^{II} norcorrole (Scheme 1-14).[62] Pd^{II} insertion reaction to the free-base norcorrole afforded Pd^{II} complex, which showed a bowl-shaped structure because of the large ionic radius of Pd^{II} (Figure 1-14). Pd^{II} norcorrole maintained distinct antiaromaticity despite its distorted structure, and thus this molecule can be classified as a bowl-shaped antiaromatic compound. Furthermore, bowl-to-bowl inversion of Pd^{II} norcorrole was observed by analyses of variable temperature ^1H NMR spectra. The energy for bowl-to-bowl inversion (9.2 kcal/mol) was experimentally determined.
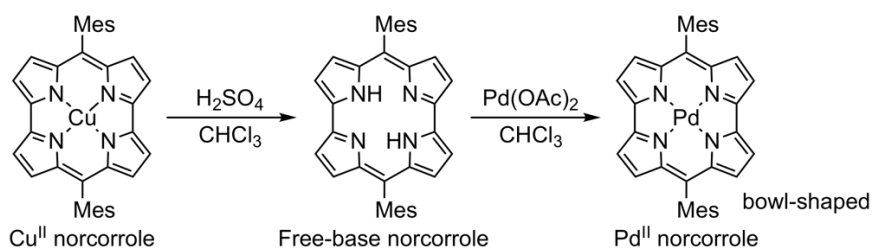
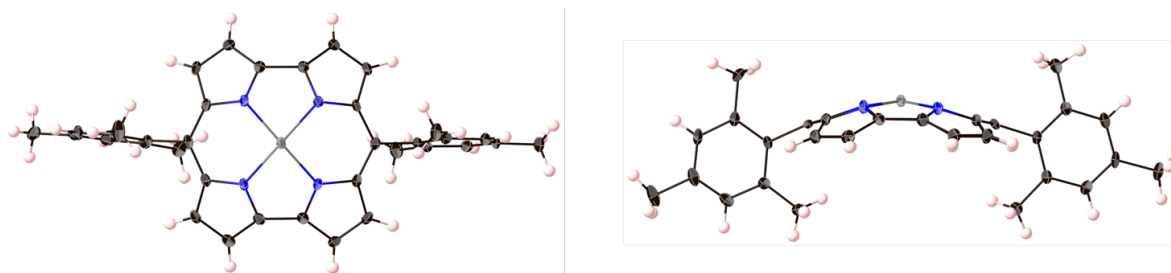**Scheme 1-14.** Synthesis of free-base norcorrole and the following Pd^{II} insertion reaction.[62]

Figure 1-14. Crystal structure of Pd^{II} norcorrole.[62]

As overviewed in this section, the exceptional stability and easy preparation of norcorrole have enabled to explore the practical use, reactivity, and novel properties of antiaromatic compounds. Such comprehensive researches have been impossible in the cases of other antiaromatic hydrocarbons, heterocycles, and porphyrinoids, because of difficulties in synthesis and isolation. Consequently, norcorrole can be considered as a promising motif to develop the chemistry of antiaromatic compounds.

1-4. Overview of this thesis

This thesis describes the synthesis of peripherally modified norcorroles and systematic studies on changes in their physical properties. The author expected that modification of norcorrole would uncover novel chemistry of antiaromatic compounds. In Chapter 2, substituent effects at *meso*-position of norcorrole are presented. Dissymmetrical substitution allowed designing stable *meso*-modified norcorroles, which showed fairly different optical properties form those of the regular norcorrole. Since these norcorroles took various packing structures depending on the *meso*-substituents, their carrier conductivity were evaluated. In Chapter 3, a facile amination reaction of norcorrole and the effect of introduced amino groups are discussed. The amination proceeded with perfect regioselectivity, which was accounted for by molecular orbitals. The resultant aminonorcorroles exhibited highly electron-rich nature. In Chapter 4 and Chapter 5, synthesis and properties of norcorroles fused by aromatic benzene rings (benzonorcorroles) are presented. Benzonorcorroles exhibited unexpectedly strong antiaromaticity by the effect of peripheral benzene rings and their diradical character were also disclosed. The narrow HOMO–LUMO gaps of benzonorcorroles induced the enhanced aromaticity and the open-shell character.
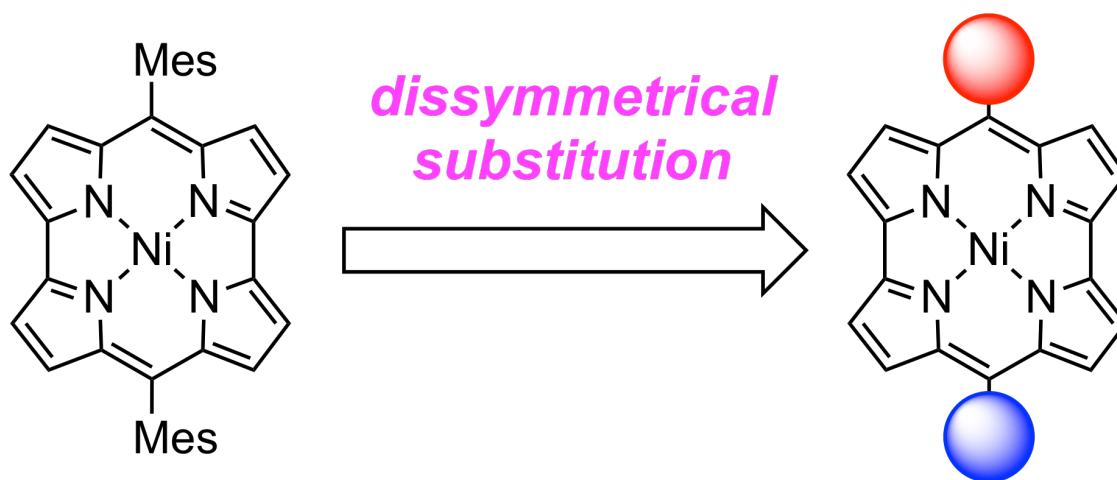
1-5. References

1. P. v. R. Schleyer, H. Jiao, *Pure & Appl. Chem.* **1996**, *68*, 209.

2. T. Kubo, in *CSJ Current Review, Vol. 12* (Ed. The Chemical Society of Japan), Kagaku-Dojin Publishing Company, INC, **2013**, pp. 12-19.

3. U. Höweler, J. W. Downing, J. Fleischhauer, J. Michl, *J. Chem. Soc., Perkin Trans. 2*, **1998**, 1101.

4. R. Breslow, H. W. Chang, R. Hill, E. Wasserman, *J. Am. Chem. Soc.* **1967**, *89*, 1112.

5. M. Saunders, R. Berger, A. Jaffe, J. M. McBride, J. O'Neill, R. Breslow, J. M. Hoffman, Jr., C. Perchonock, E. Wasserman, R. S. Hutton, V. J. Kuck, *J. Am. Chem. Soc.* **1973**, *95*, 3017.

6. P. v. R. Schleyer, C. Maerker, A. Dransfeld, H. Jiao, N. J. R. v. E. Hommes, *J. Am. Chem. Soc.* **1996**, *118*, 6317.

7. Z. Chen, C. S. Wannere, C. Corminboeuf, R. Puchta, P. v. R. Schleyer, *Chem. Rev.* **2005**, *105*, 3842.

8. D. Geuenich, K. Hess, F. Köhler, R. Herges, *Chem. Rev.* **2005**, *105*, 3758.

9. T. M. Krygowski, M. K. Cyranski, *Chem. Rev.* **2001**, *101*, 1385.

10. T. Kawase, T. Fujikawa, C. Kitamura, A. Konishi, Y. Hirao, K. Matsumoto, H. Kurata, T. Kubo, S. Shinamura, H. Mori, E. Miyazaki, K. Takimiya, *Angew. Chem. Int. Ed.* **2010**, *49*, 7728.

11. D. T. Chase, A. G. Fix, S. J. Kang, B. D. Rose, C. D. Weber, Y. Zhong, L. N. Zakharov, M. C. Lonergan, C. Nuckolls, M. M. Haley, *J. Am. Chem. Soc.* **2012**, *134*, 10349.

12. T. Nishinaga, T. Ohmae, K. Aita, M. Takase, M. Iyoda, T. Arai, Y. Kunugi, *Chem. Commun.* **2013**, *49*, 5354.

13. M. Nakano, I. Osaka, K. Takimiya, T. Koganezawa, *J. Mater. Chem. C* **2014**, *2*, 64.

14. J. L. Marshall, K. Uchida, C. K. Frederickson, C. Schütt, A. M. Zeidell, K. P. Goetz, T. W. Finn, K. Jarolimek, L. N. Zakharov, C. Risko, R. Herges, O. D. Jurchescu, M. M. Haley, *Chem. Sci.* **2016**, *7*, 5547.

15. L. Watts, J. D. Fitzpatrick, R. Pettit, *J. Am. Chem. Soc.* **1965**, *87*, 3253.

16. T. Bally, S. Chai, M. Neuenschwander, Z. Zhu, *J. Am. Chem. Soc.* **1997**, *119*, 1869.

17. T. Nishinaga, T. Uto, R. Inoue, A. Matsuura, N. Treitel, M. Rabinovitz, K. Komatsu, *Chem. Eur. J.* **2008**. *14*, 2067.

18. C. Fan, L. G. Mercier, W. E. Piers, H. M. Tuononen, M. Parvez, *J. Am. Chem. Soc.* **2010**, *132*, 9604.

19. A. Y. Houghton, V. A. Karttunen, C. Fan, W. E. Piers, H. M. Tuononen, *J. Am. Chem. Soc.* **2013**, *135*, 941.

20. W. Kaim, *J. Am. Chem. Soc.* **1983**, *105*, 707.

21. T. Saito, H. Nishiyama, H. Tanahashi, K. Kawakita, H. Tsurugi, K. Mashima, *J. Am. Chem. Soc.* **2014**, *136*, 5161.

22. T. Yurino, Y. Ueda, Y. Shimizu, S. Tanaka, H. Nishiyama, H. Tsurugi, K. Sato, K. Mashima, *Angew. Chem. Int. Ed.* **2015**, *54*, 14437.

23. M. Rosenberg, C. Dahlstrand, K. Kilså, H. Ottosson, *Chem. Rev.* **2014**, *114*, 5349.

24. R. Papadakis, H. Li, J. Bergman, A. Lundstedt, K. Jorner, R. Ayub, S. Halder, B. O. Jahn, A. Denisova, B. Zietz, R. Lindh, B. Sanyal, H. Grennberg, K. Leifer, H. Ottosson, *Nat. Commun.* **2016**, *7*, 12962.

25. M. Ueda, K. Jorner, Y. M. Sung, T. Mori, Q. Xiao, D. Kim, H. Ottosson, T. Aida, Y. Itoh, *Nat. Commun.* **2017**, *8*, 346.

26. S. Hiroto, H. Shinokubo, in *Handbook of Porphyrin Science*, *Vol. 37* (Eds.: K. M. Kadish, K. M. Smith, R. Guilard) World Scientific, Singapore, **2016**, pp 233-302.

27. S. Saito, A. Osuka, *Angew. Chem. Int. Ed.* **2011**, *50*, 4342.

28. M. Pawlicki, L. Latos-Grażyński, *Chem. Asian J.* **2015**, *10*, 1438.

29. B. K. Reddy, A. Basavarajappa, M. D. Ambhore, V. G. Anand, *Chem. Rev.* **2017**, *117*, 3420.

30. Y. Yamamoto, A. Yamamoto, S. Furuta, M. Horie, M. Kodama, W. Sato, K. Akiba, S. Tsuzuki, T. Uchimaru, D. Hashizume, F. Iwasaki, *J. Am. Chem. Soc.* **2005**, *127*, 14540.

31. T. Kakui, S. Sugawara, Y. Hirata, S. Kojima, Y. Yamamoto, *Chem. Eur. J.* **2011**, *17*, 7768.

32. S. Sugawara, Y. Hirata, S. Kojima, Y. Yamamoto, E. Miyazaki, K. Takimiya, S. Matsukawa, D. Hashizume, J. Mack, N. Kobayashi, Z. Fu., K. M. Kadish, Y. M. Sung, K. S. Kim, D. Kim, *Chem. Eur. J.* **2012**, *18*, 3566.

33. J. A. Cissell, T. P. Vaid, G. P. A. Yap, *Org. Lett.* **2006**, *8*, 2401.

34. J. A. Cissell, T. P. Vaid, A. L. Rheingold, *J. Am. Chem. Soc.* **2005**, *127*, 12212.

35. T. P. Vaid, *J. Am. Chem. Soc.* **2011**, *133*, 15838.

36. A, Weiss, M. C. Hodgson, P. D. W. Boyd, W. Siebert, P. J. Brothers, *Chem. Eur. J.* **2007**, *13*, 5982.

37. J. S. Reddy, V. G. Anand, *J. Am. Chem. Soc.* **2008**, *130*, 3718.

38. T. Satoh, M. Minoura, H. Nakano, K. Furukawa, Y. Matano, *Angew. Chem. Int. Ed.* **2016**, *55*, 2235.

39. A. Yamaji, H. Tsurugi, Y. Miyake, K. Mashima, H. Shinokubo, *Chem. Eur. J.* **2016**, *22*, 3956.

40. J.-Y. Shin, K. S. Kim, M.-C. Yoon, J. M. Lim, Z. S. Yoon, A. Osuka, D. Kim, *Chem. Soc. Rev.* **2010**, *39*, 2751.

41. S. Mori, A. Osuka, *J. Am. Chem. Soc.* **2005**, *127*, 8030.

42. A. Muranaka, O. Matsushita, K. Yoshida, S. Mori, M, Suzuki, T. Furuyama, M. Uchiyama, A. Osuka, N. Kobayashi, *Chem. Eur. J.* **2009**, *15*, 3744.

43. M.-C. Yoon, S. Cho, M, Suzuki, A. Osuka, D. Kim, *J. Am. Chem. Soc.* **2009**, *131*, 7360.

44. T. Higashino, J. M. Lim, T. Miura, S. Saito, J.-Y. Shin, D. Kim, A. Osuka, *Angew. Chem. Int. Ed.* **2010**, *49*, 4950.

45. T. Higashino, B. S. Lee, J. M. Lim, D. Kim, A. Osuka, *Angew. Chem. Int. Ed.* **2012**, *51*, 13105.

46. Y. M. Sung, M.-C. Yoon, J. M. Lim, H. Rath, K. Naoda, A. Osuka, D. Kim, *Nat. Chem.* **2015**, *7*, 418.

47. J. S. Reddy, S. Mandal, V. G. Anand, *Org. Lett.* **2006**, *8*, 5541.

48. T. Yoneda, Y. M. Sung, J. M. Lim, D. Kim, A. Osuka, *Angew. Chem. Int. Ed.* **2014**, *53*, 13169.

49. M. Bröring, S. Köhler, C. Kleeberg, *Angew. Chem. Int. Ed.* **2008**, *47*, 5658.

50. T. Ito, Y. Hayashi, S. Shimizu, J.-Y. Shin, N. Kobayashi, H. Shinokubo, *Angew. Chem. Int. Ed.* **2012**, *51*, 8542.

51. H. Kido, J.-Y. Shin, H. Shinokubo, *Angew. Chem. Int. Ed.* **2013**, *52*, 13727.

52. J.-Y. Shin, T. Yamada, H. Yoshikawa, K. Awaga, H. Shinokubo, *Angew. Chem. Int. Ed.* **2014**, *53*, 3096.

53. T. Fukuoka, K. Uchida, Y. M. Sung, J.-Y. Shin, S. Ishida, J. M. Lim, S. Hiroto, K. Furukawa, D. Kim, T.

Iwamoto, H. Shinokubo, *Angew. Chem. Int. Ed.* **2014**, *53*, 1505.

54. B. Liu, X. Li, M. Stępień, P. J. Chmielewski, *Chem. Eur. J.* **2015**, *21*, 7790.

55. R. Nozawa, K. Yamamoto, I. Hisaki, J.-Y. Shin, H. Shinokubo, *Chem. Commun.* **2016**, *52*, 7106.

56. R. Nozawa, K. Yamamoto, J.-Y. Shin, S. Hiroto, H. Shinokubo, *Angew. Chem. Int. Ed.* **2015**, *54*, 8454.

57. Z. Deng, X. Li, M. Stępień, P. J. Chmielewski, *Chem. Eur. J.* **2016**, *22*, 4231.

58. H. Kawashima, S. Hiroto, H. Shinokubo, *J. Org. Chem.* **2017**, *82*, 10425.

59. R. Nozawa, H. Tanaka, W.-Y. Cha, Y. Hong, I. Hisaki, S. Shimizu, J.-Y. Shin, T. Kowalczyk, S. Irle, D. Kim, H. Shinokubo, *Nat. Commun.* **2016**, *7*, 13620.

60. C. Corminboeuf, P. V. R. Schleyer, P. Warner, *Org. Lett.* **2007**, *9*, 3263.

61. D. E. Bean, P. W. Flower, *Org. Lett.* **2008**, *10*, 5573.

62. T. Yonezawa, S. A. Shafie, S. Hiroto, H. Shinokubo, *Angew. Chem. Int. Ed.* **2017**, *56*, 11822.

Chapter 2

Modulation of the Absorption Band and Charge Mobility of Norcorroles by Effects of *meso*-Substituents

Takuya Yoshida, Daisuke Sakamaki, Shu Seki, Hiroshi Shinokubo,

Contents

2-1. Introduction

Narrow HOMO–LUMO gaps are particularly attractive to achieve effective near IR (NIR) absorbing organic dyes.[1-5] Unfortunately, however, antiaromatic compounds inherently exhibit very weak low-energy absorption due to their forbidden HOMO–LUMO transitions.[6] This feature limits their utility as functional dyes for optical application. It is highly desirable to establish a strategy to enhance their low-energy absorbing property. In addition, narrow HOMO–LUMO gaps also allows the design of novel ambipolar semiconductor materials on the basis of $4n\pi$-electron systems.[7,8] Nevertheless, systematic fine-tuning of optical and electronic properties of antiaromatic compounds has been a challenging issue because of their inherent instability associated with antiaromatic destabilization.
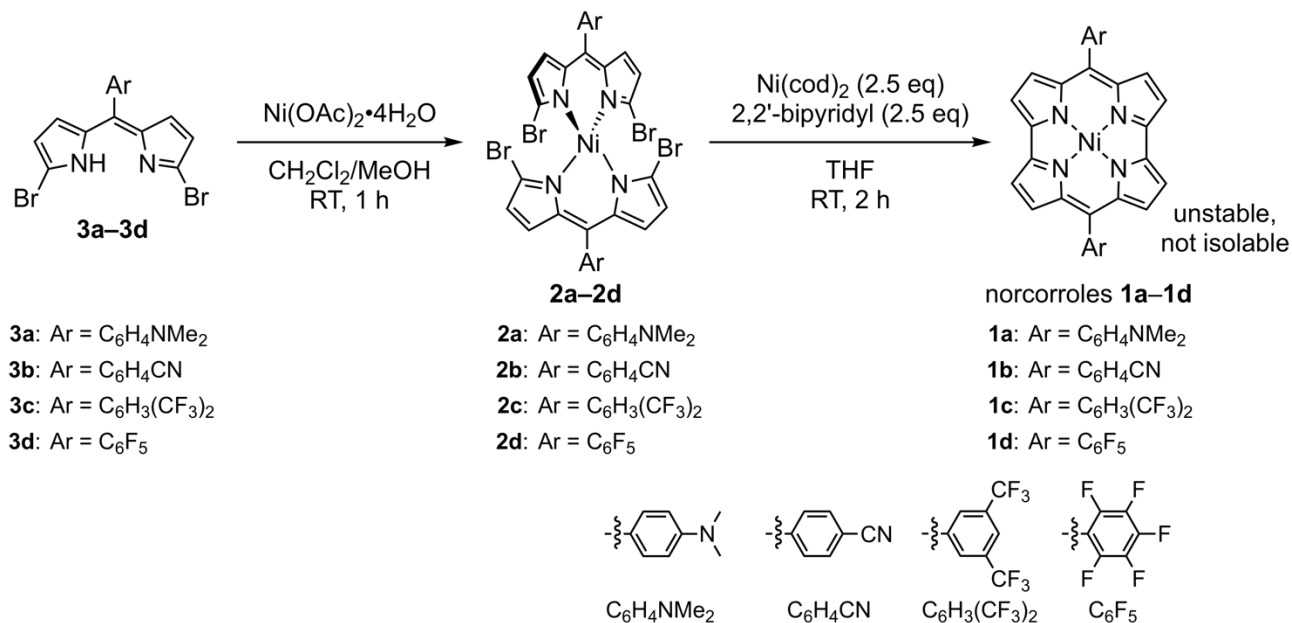
The modification of the electronic nature of *meso*-substituents is a conventional but effective approach to alter properties of porphyrinoids.[9-16] However, the substituent effect at *meso*-positions of antiaromatic porphyrinoids has not been explored in detail. In the case of Ni^{II} norcorroles, *meso*-aryl groups have been limited only to mesityl and phenyl groups in contrast to the variety of pyrrole-modified Ni^{II} norcorroles (see Chapter 1). Consequently, Ni^{II} norcorroles with various aryl groups were synthesized to investigate the structural and electronic effects of *meso*-aryl groups of antiaromatic norcorroles. Furthermore, the author demonstrated that intramolecular charge transfer interactions are effective to improve the low-energy absorbing feature of antiaromatic porphyrinoids.

2-2. Synthesis of Ni^{II} norcorroles with various aryl groups at *meso*-positions

Synthesis of norcorroles **1a–1d** with several aryl groups in a symmetrical manner was initially attempted (Scheme 2-1). Electron-donating 4-dimethylaminophenyl and electron-withdrawing 4-cyanophenyl, 3,5-bistrifluorophenyl and pentafluorophenyl groups were selected as substituents to be introduced at the *meso*-positions. α,α'-Dibromodipyrrin Ni^{II} complexes **2a–2d** were prepared by dimerization of α,α'-dibromodipyrrin **3a–3d** in the presence of Ni^{II} acetate. Ni^{0}-Mediated reductive homo-coupling reactions were performed for **2a–2d** to obtain **1a–1d**. However, all attempts to isolate symmetrically substituted norcorroles **1a–1d** resulted in failure due to their instability under ambient conditions.

The instability of norcorroles **1a–1d** could be attributed to the change in energy levels of frontier orbitals by substituents. The antiaromatic norcorrole system has inherently high HOMO and low LUMO energy levels, and the former is further destabilized by electron-donating substituents and the latter is further stabilized by electron-withdrawing substituents, thus increasing the instability of norcorroles. This prediction was supported by DFT calculation, which estimated fairly high HOMO level of **1a** (–4.23 eV) induced by 4-dimethylamino-phenyl groups and fairly low LUMO level of **1d** (–3.69 eV) induced by pentafluorophenyl groups, as compared with those of **NiNc** and Ni^{II} diphenylnorcorrole **Ph-NiNc**[17] (Figure 2-1). On the basis of this consideration, two different aryl groups were introduced to norcorrole to reduce electron-donating or -withdrawing substituent effects for frontier orbitals (Scheme 2-2). Dissymmetric bisdipyrrin complexes **2e–2i** were prepared by

treatment of two different α,α'-dibromodipyrrins with Ni^{II} acetate followed by silica-gel column separation. The homo-coupling reaction of **2e–2i** afforded dissymmetrical norcorroles **1e–1i** with an electron-donating 4-dimethylaminophenyl group on one side (Ar^1), and mesityl, phenyl and three electron-withdrawing substituents on the other side (Ar^2). The stability of **1e–1i** were enhanced as compared with **1a–1d**, and **1e–1i** could be isolated in 15–45% yields by silica-gel column purification under ambient conditions. Consequently, the dissymmetric substitution strategy is effective to obtain various antiaromatic and stable norcorroles.

3a: Ar = C$_6$H$_4$NMe$_2$
3b: Ar = C$_6$H$_4$CN
3c: Ar = C$_6$H$_3$(CF$_3$)$_2$
3d: Ar = C$_6$F$_5$

2a: Ar = C$_6$H$_4$NMe$_2$
2b: Ar = C$_6$H$_4$CN
2c: Ar = C$_6$H$_3$(CF$_3$)$_2$
2d: Ar = C$_6$F$_5$

1a: Ar = C$_6$H$_4$NMe$_2$
1b: Ar = C$_6$H$_4$CN
1c: Ar = C$_6$H$_3$(CF$_3$)$_2$
1d: Ar = C$_6$F$_5$

C$_6$H$_4$NMe$_2$ C$_6$H$_4$CN   C$_6$H$_3$(CF$_3$)$_2$ C$_6$F$_5$

Scheme 2-1. Synthesis of norcorroles **1a-1d**.
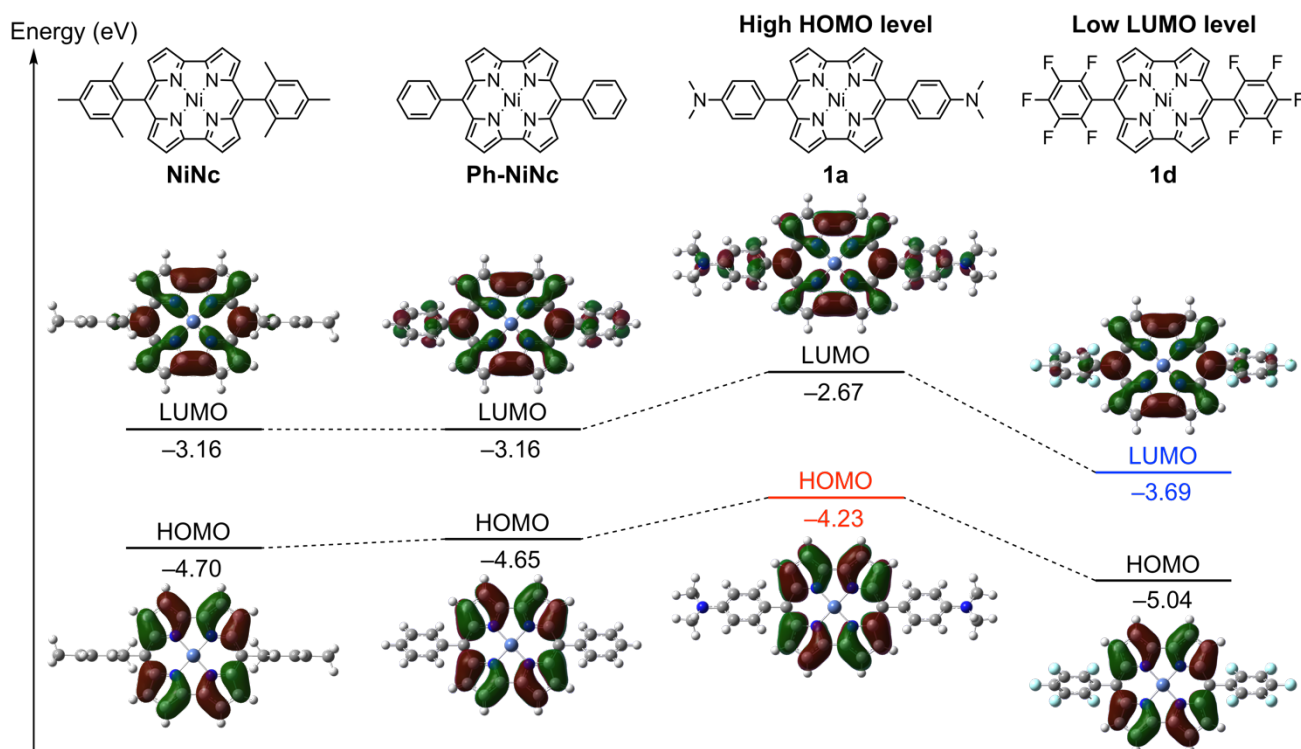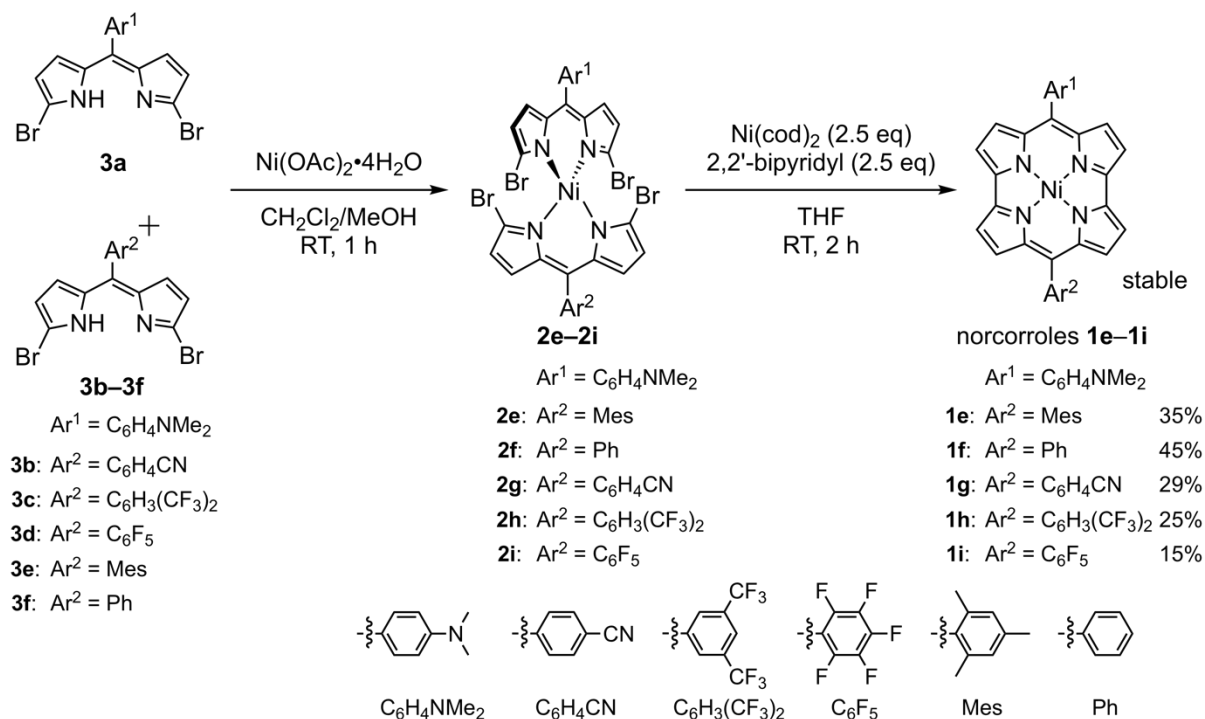

Figure 2-1. MO diagrams for **NiNc**, **Ph-NiNc**, **1a**, and **1d** calculated at the B3LYP/6-31G(d)+SDD level.

Scheme 2-2. Synthesis of dissymmetric norcorroles **1e–1f**.

^{1}H NMR spectra of **1e–1i** in CDCl$_3$ exhibited their pyrroles protons in the high-field region (3–2 ppm) due to the paratropic ring current effect, supporting distinct antiaromatic character with 16π-electron systems. Interestingly, the spectrum of **1h** showed concentration dependence, in which the pyrrole protons signals were down-field shifted and significantly broadened at higher concentration of the solution, suggesting its aggregation behavior (Figure 2-2).
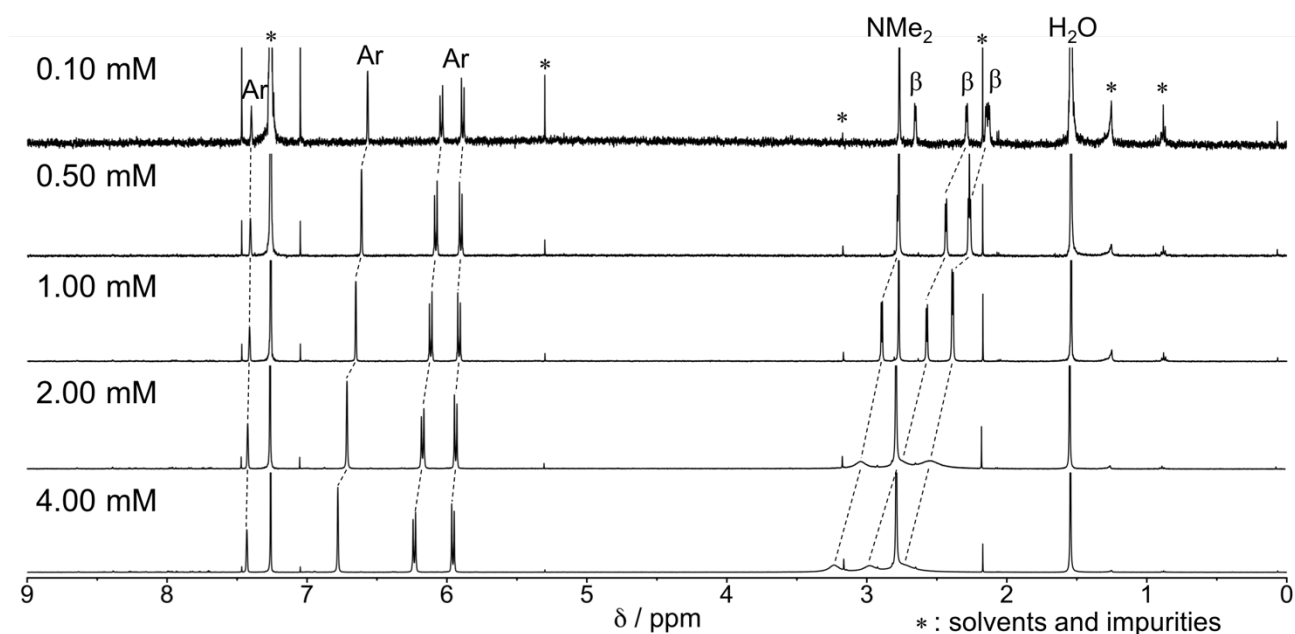
Figure 2-2. Concentration dependent ^{1}H NMR spectra (500 MHz) of **1h** in CDCl$_3$.

2-3. Structural analyses

The structures of all dissymmetric norcorroles Ni^{II} complexes **1e–1i** were unambiguously elucidated by X-ray structural analyses. Interestingly, their packing modes varied significantly depending on the subtle change of substituents (Figure 2-3). In the cases of **1e** and **1f**, the norcorrole macrocycles are located separately without π-stacking due to dominance of CH–π interactions. On the other hand, π–π stacking between norcorrole planes was observed in the packing structures of **1g–1i**, which contain electron-withdrawing groups. Norcorrole planes of **1g** and **1i** show slipped π-stacking with mean plane distances of 3.29 and 3.34 Å between norcorroles, respectively. Interestingly, **1g** formed an infinite π–π stacking structure in the crystal, while packing of **1i** composed of stacked dimeric units. Furthermore, **1h** formed triple-decker stacking structure with a distance of 3.10 Å between Ni atoms, reflecting aggregation behavior of **1h** observed in the ^{1}H NMR measurement. The two outer norcorroles are slightly distorted but the inner norcorrole maintained planar conformation. A similar triple stacking was also observed in the crystal structure of **Ph-NiNc**.[17] Dihedral angles between central norcorrole planes and peripheral aryl groups were evaluated, because they are an important factor to determine the magnitude of the substituent effect. Norcorrole **1e–1i** showed relatively small dihedral angles in the crystal structures except the case of the bulky mesityl group of **1e** (Table 2-1).
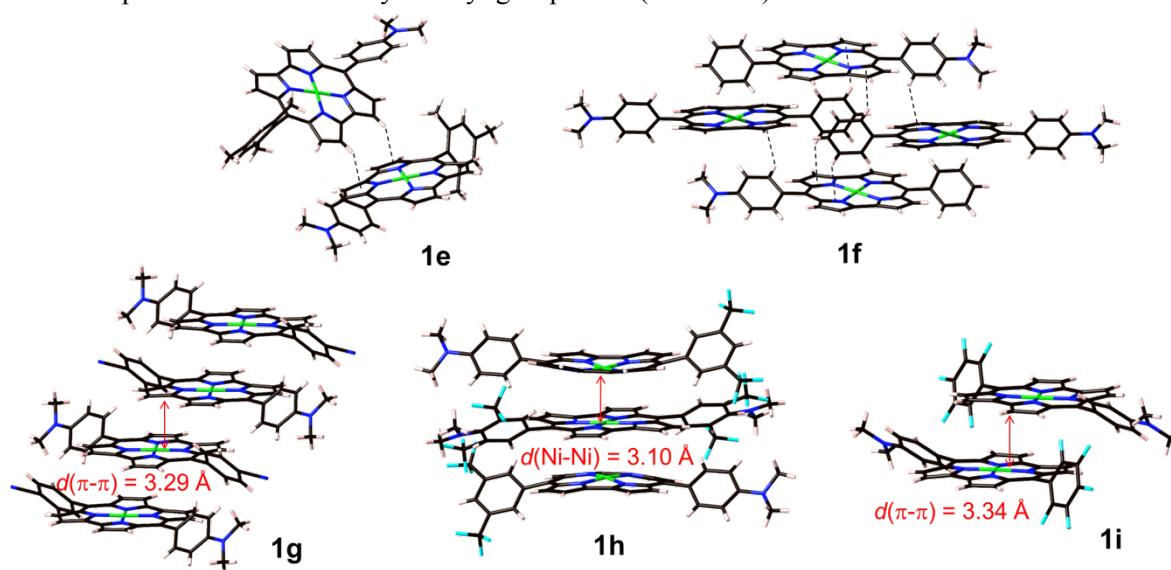

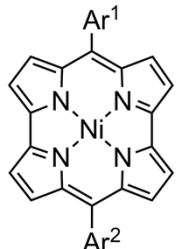
Figure 2-3. Packing structures of norcorroles **1e–1i**.

Compounds	Norcorrole-Ar^1 (4-dimethylaminophenyl)	Norcorrole-Ar^2
1e	38.3	78.9
1f	34.5	43.3
1g	49.8	47.8
1h (center, edge)	38.5, 47.0	38.5, 49.0
1i	40.5	69.6

Ar^1 = C$_6$H$_4$NMe$_2$
Ar^2 = Mes (**1e**)
Ar^2 = Ph (**1f**)
Ar^2 = C$_6$H$_4$CN (**1g**)
Ar^2 = C$_6$H$_3$(CF$_3$)$_2$ (**1h**)
Ar^2 = C$_6$F$_5$ (**1i**)

norcorroles **1e–1i**

Table 2-1. Dihedral angles between norcorrole cores and Ar^1 or Ar^2 in the X-ray structures of **1e–1i**.

2-4. Optical properties and theoretical studies

UV-vis-NIR absorption spectra of norcorroles **1e–1i** and **NiNc** in CH$_2$Cl$_2$ were shown in Figure 2-4. In contrast to the absorption spectrum of **NiNc**, dissymmetric norcorroles **1e–1i** exhibit characteristic intense absorption bands around 650 nm. These bands were further bathochromically shifted by the introduction of electron-withdrawing groups. Meanwhile, the absorption envelope and intensity of **1e–1i** are similar to that of **NiNc** except for the bands around 650 nm. These results clearly demonstrated that the use of the substituent effect is effective to enhance the low-energy absorption band of norcorrole.
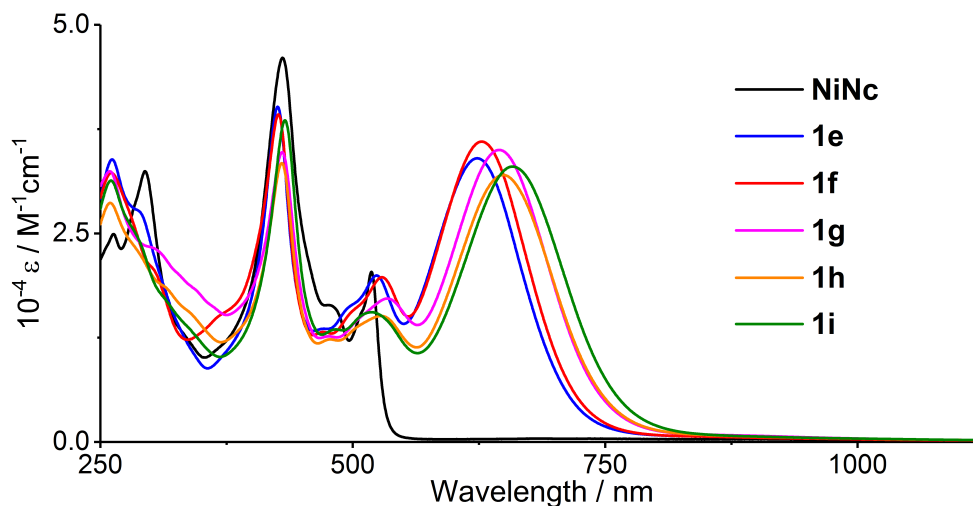

Figure 2-4. UV-vis-NIR absorption spectra of **NiNc** and **1e–1i** in CH$_2$Cl$_2$.

To investigate the unusual absorption bands of **1e–1i**, time-dependent (TD)-density functional theory (DFT) calculations were performed for **1e** and **1i** at the B3LYP/6-31G(d)+SDD level (Figure 2-5, 2-6). The result clearly demonstrates that the absorption around 650 nm should be assigned to the transition from HOMO–3 to LUMO, which have significant intermolecular charge transfer character from the electron-donating 4-dimethylaminophenyl group to the norcorrole core (Table 2-2). It also should be noted that the CT absorption band of **1i** appeared in a lower energy region than that of **1e**. This tendency was well-reproduced by the TD-DFT calculations, which indicated that the red-shifted CT absorption band of **1i** resulted from the lowered LUMO level due to the electron-withdrawing pentafluorophenyl group. The CT character of this absorption band was experimentally confirmed by absorption spectra of **1e** measured in various solvents, in which wavelength of the CT-like band is considerably affected by effects of solvents, compared with those of other absorption bands (Figure 2-7). Furthermore, the CT-like absorption band of **1e** was significantly decreased upon an addition of an acid and was returned to the nearly initial intensity upon an addition of base (Figure 2-8). This spectral change also supports the CT interactions from the 4-dimethylaminophenyl group to the norcorrole core, because the acid should reduce the electron-donating nature of the sp^3 nitrogen atom in the amino group. These spectroscopic and theoretical studies conclude that the norcorrole macrocycle behaves as an electron-accepting unit when coupled with electron-donating *meso*-substituents.
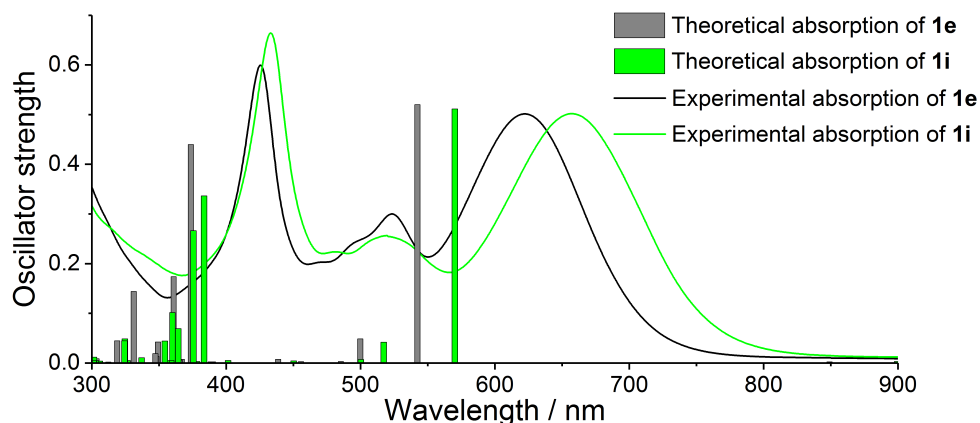
Figure 2-5. Theoretical absorption spectra of **1e** and **1i** calculated at the B3LYP/6-31G(d)+SDD level (sticks) and their experimental absorption spectra in CH$_2$Cl$_2$ (solid lines).
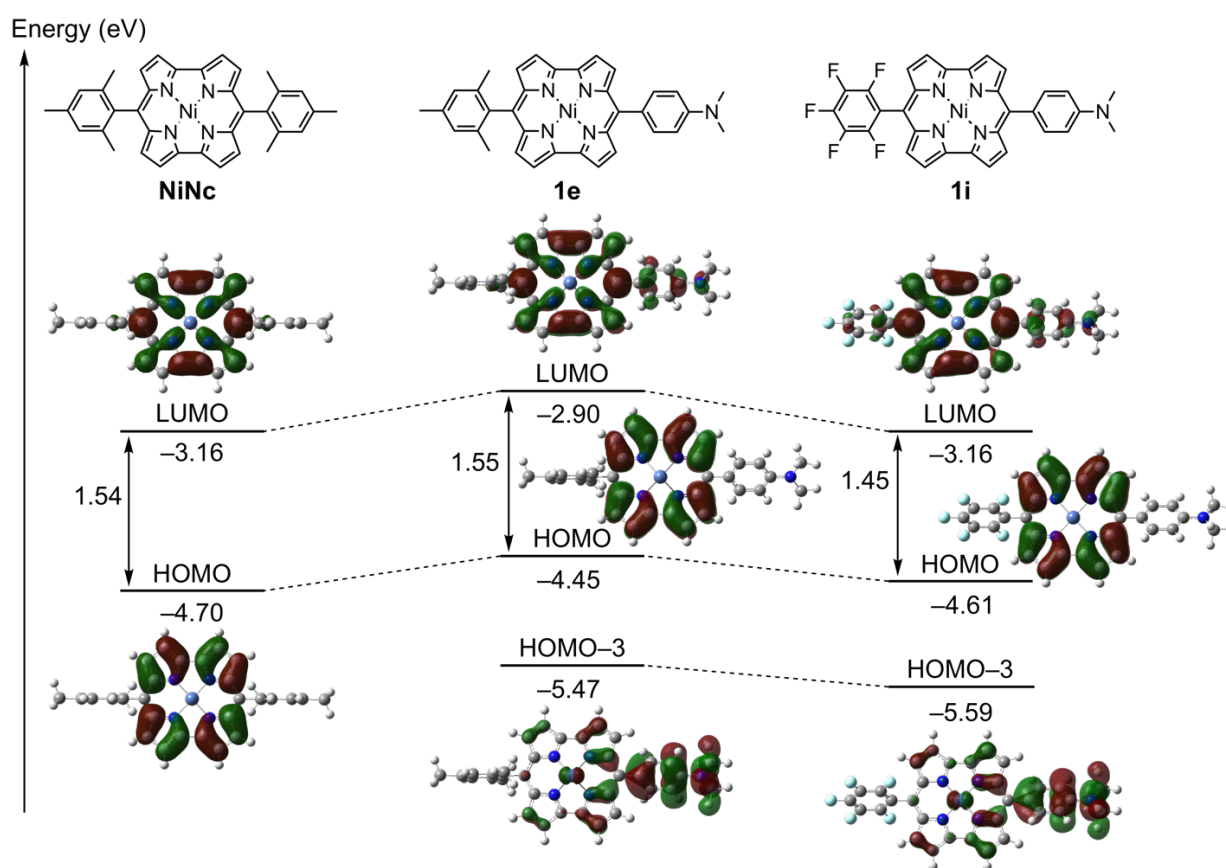

Figure 2-6. MO diagrams for **NiNc**, **1e**, and **1i** calculated at the B3LYP/6-31G(d)+SDD levels.

Table 2-2. Calculated exited wavelengths (λ) and oscillator strengths (f) of selected transitions of **1e** and **1i**.

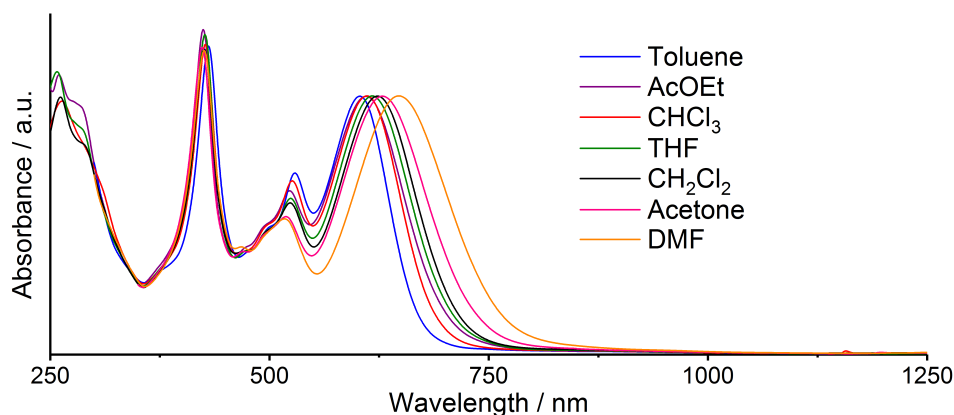| Compound	λ (nm)	f	Composition (%)	Assignment
1e	1424	0.0000	HOMO→LUMO (100%)	forbidden transition
	542	0.5200	HOMO−3→LUMO (94%)	CT
1i	1573	0.0003	HOMO→LUMO (100%)	forbidden transition
	570	0.5113	HOMO−3→LUMO (92%)	CT

Figure 2-7. UV-vis-NIR absorption spectra of **1e** in various solvents.
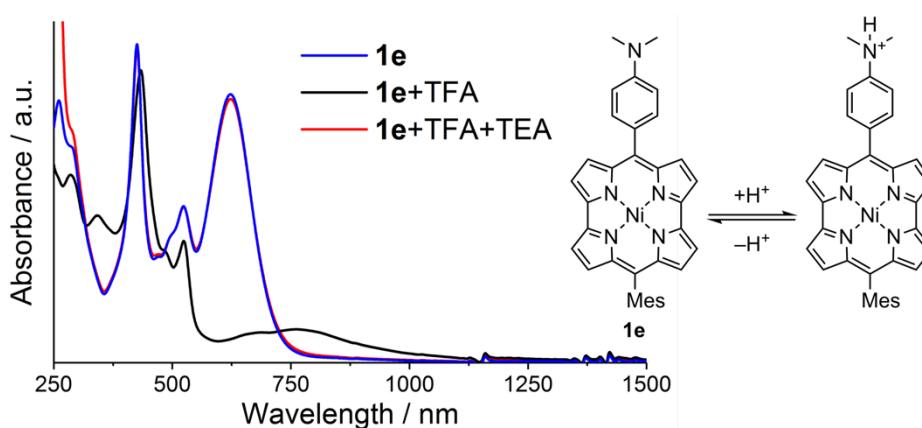

Figure 2-8. Spectral change in the solution of **1e** in CH$_2$Cl$_2$ upon the addition of trifluoroacetic acid (TFA) as an acid and triethylamine (TEA) as a base.

Oxidation reaction of **1e** with *m*CPBA was conducted to obtain corresponding 10-oxacorrole **4**, which has aromaticity due to its 18 π-electron system (Figure 2-9a).[18] Interestingly, oxacorrole **4** showed Q- and Soret-like bands, which are characteristics of aromatic porphyrinoids, but showed no CT-like absorption band (Figure 2-9b). TD-DFT calculations also predicted no CT-like transition of **4**. The absence of the CT band in the absorption spectrum of **4** suggested that the electron-accepting character of the norcorrole originated from its antiaromaticity is crucial for the emergence of the CT transition from the electron-donating group.
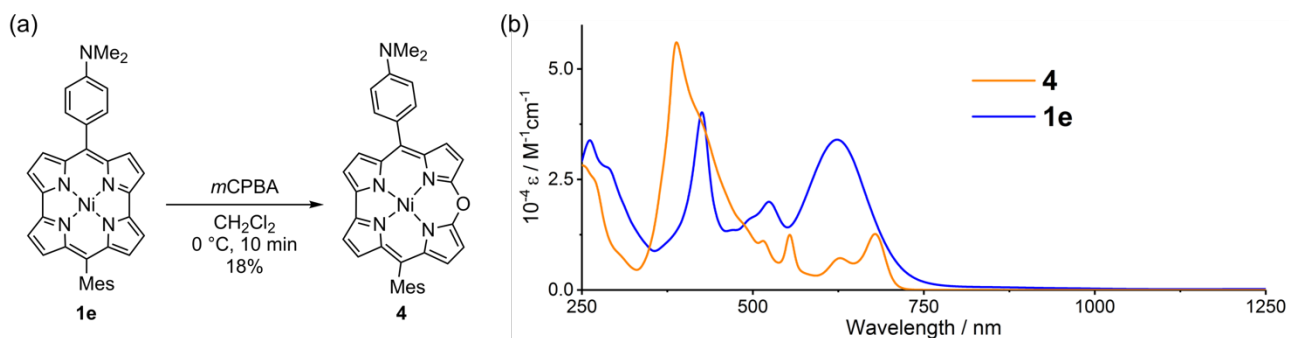

Figure 2-9. (a) Synthesis of oxacorrole **4** and (b) UV-vis-NIR absorption spectra of **4** and **1e** in CH$_2$Cl$_2$.

28

2-5. Electrochemical measurements

The substituent effect was further evaluated by electrochemistry of dissymmetric norcorroles **1e–1i** using cyclic voltammetry measurements (Figure 2-10). All norcorroles exhibit several reversible oxidation and reduction waves. The first oxidation potentials of all dissymmetric norcorroles **1e–1i** exhibited marked cathodic shifts as compared with that of **NiNc** due to the strong electron-donating nature of the 4-dimethylaminophenyl group, while anodic shifts of the first reduction potentials were observed in norcorroles **1g–1i** by their electron-withdrawing groups. In addition to electronic properties of substituents, their structural feature also affects the electrochemistry: the first oxidation processes of **1f** and **1h** split into two waves. **1f** and **1h** have Ar^2 groups without *ortho*-substituents, in which whose dihedral angles with the norcorrole cores are smaller than those of **1e** and **1i** (Table 2-1). The oxidation wave of structurally similar **1g** was not split but broad. These twin waves of **1f** and **1h** should be considered as one-electron oxidation process, which is split by intermolecular interaction during the oxidation. This interpretation was supported by spectroelectrochemical analyses of **1e** and **1h**, because the spectral change during the E_{ox1} process of **1e** by the single wave was almost the same as E_{ox1} process of **1h**, which consists of split waves (Figure 2-11). These splits resulted in the considerably low oxidation potential of **1f** and **1h** (–0.11 and –0.07, respectively).
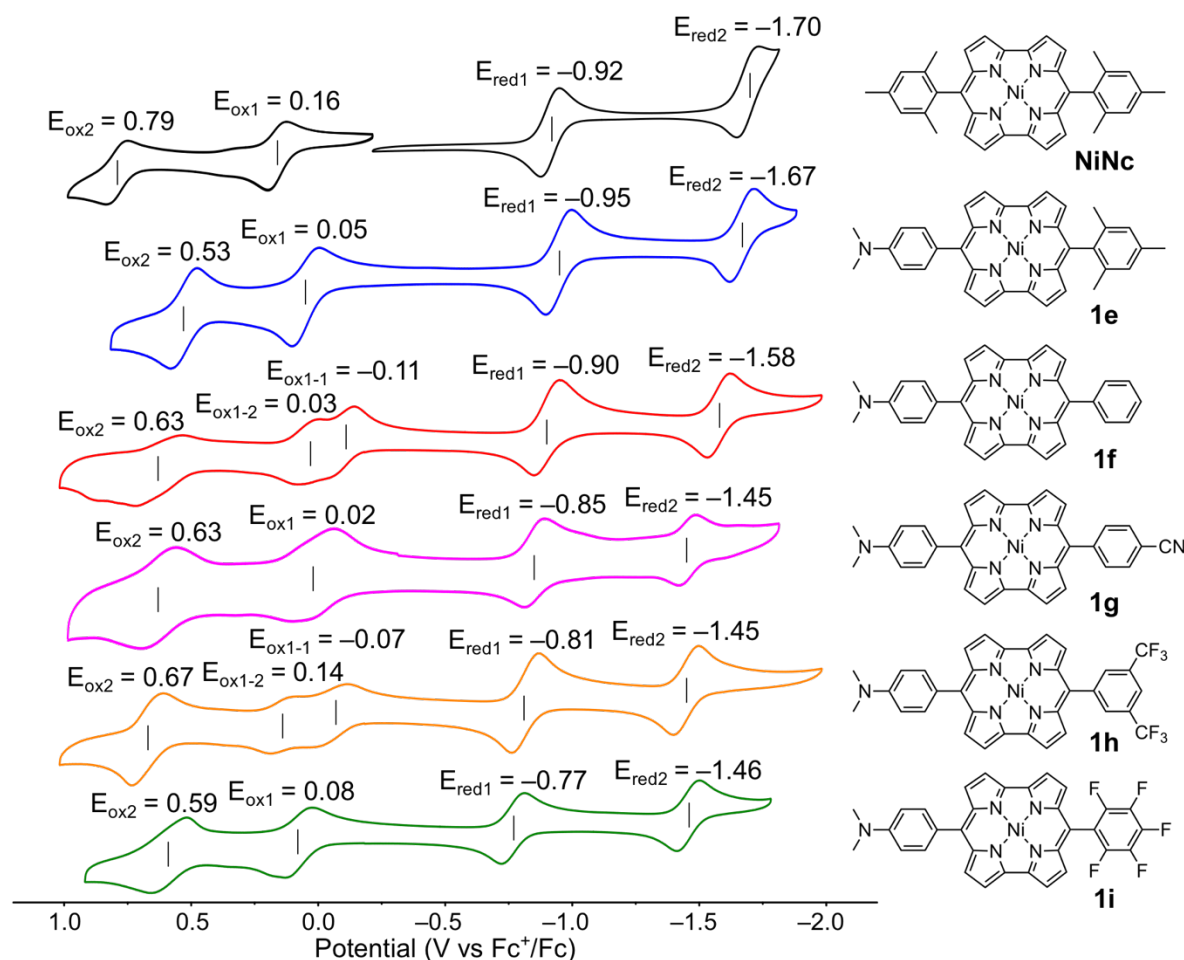

Figure 2-10. Cyclic voltammograms (0.1 V•s^{-1}) of **NiNc** and **1e–1i** in CH$_2$Cl$_2$ (0.1 M TBAPF$_6$). Working electrode: grass carbon, counter electrode: Pt, reference electrode: Ag/AgClO$_4$.
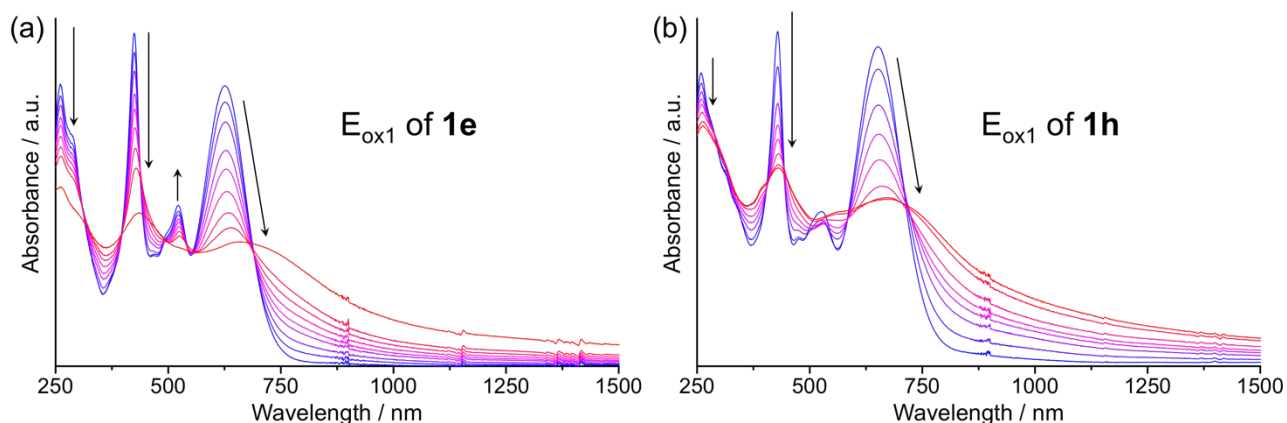
Figure 2-11. Spectral change of (a) **1e** and (b) **1h** in CH_2Cl_2 during electrochemical oxidation upon applying 0 V to 0.6 V (blue line to red line). analyte: 0.3 mM, electrolyte: 0.1 M of tetrabutylammonium tetrafluoroborate, working electrode: Pt, counter electrode: Pt, reference electrode: Ag^+/Ag.

2-6. Carrier conductivities

The charge carrier conductivities of **1e**–**1i** were evaluated using flash-photolysis time-resolved microwave conductivity (FP-TRMC) technique,[19] since a difference of intermolecular interactions significantly affect conductivity of materials. The maximum transient conductivities of ($\phi\Sigma\mu$) **1e**–**1i** were summarized in Figure 2-12. Norcorroles **1g**–**1i** with π–π stacking structures in their crystals exhibited larger conductivities than **1e** and **1f**, which have none of such interactions (Figure 2-3). The relatively lower $\phi\Sigma\mu$ value of **1g** than those of **1h** and **1i** would attribute to lower crystallinity of the powder sample of **1g**. The result suggests that existence of π–π stacking between norcorrole units should be important to attain higher $\phi\Sigma\mu$ values. Nevertheless, the absolute $\phi\Sigma\mu$ values of **1h** and **1i** are still low. Consequently, improvements in crystallinity and stacked structures of norcorroles are necessary to achieve much higher carrier conductivities.
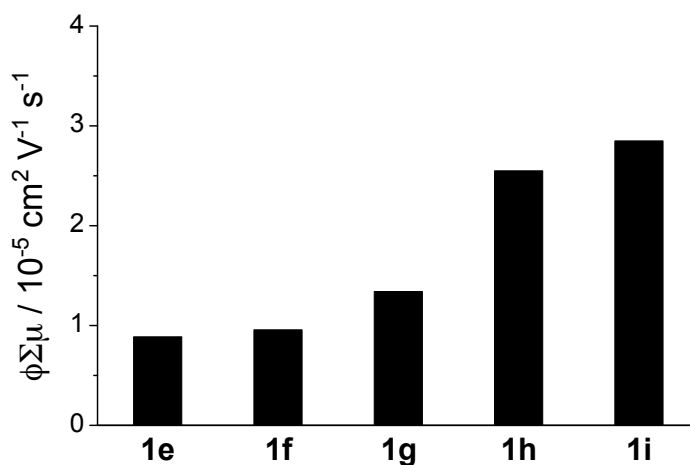

Figure 2-12. The maximum transient conductivities ($\phi\Sigma\mu$) of 1e–1i observed upon excitation with a 355 nm laser pulse.

2-7. Summary of Chapter 2

In summary, the author has found that dissymmetrical substitution on *meso*-positions enables fine-tuning of properties of norcorroles with maintaining their stability. The optical and electrochemical properties of dissymmetrical norcorrole Ni^{II} complexes were considerably altered in comparison to dimesitylnorcorrole Ni^{II} complex (**NiNc**) by substituent effects. Furthermore, novel norcorroles showed various packing structures in crystal depending on the subtle structural change of aryl groups. The effect of packing structures on carrier mobilities of dissymmetric norcorroles was examined using TRMC technique. The conductivities correlated with the presence or absence of π–π stacking structures between norcorrole moieties. The present study has demonstrated that manipulation of *meso*-substituents of Ni^{II} norcorroles is effective to improve their low-energy absorption property as well as modulate their charge carrier mobility. These insights provided by the modification of norcorroles should promote further development of optical and electronic materials based on antiaromatic porphyrinoids.

2-8. References

1. N. G. Pschirer, C. Kohl, F. Nolde, J. Qu, K. Müllen, *Angew. Chem. Int. Ed.* **2006**, *45*, 1401.

2. A. Muranaka, M. Yonehara, M. Uchiyama, *J. Am. Chem. Soc.* **2010**, *132*, 7844.

3. Y. Kubo, K. Watanabe, R. Nishiyabu, R. Hata, A. Murakami, T. Shoda, H. Ota, *Org. Lett.* **2011**, *13*, 4574.

4. T. Okujima, C. Ando, J. Mack, S. Mori, I. Hisaki, T. Nakae, H. Yamada, K. Ohara, N. Kobayashi, H. Uno, *Chem. Eur. J.* **2013**, *19*, 13970.

5. T. Furuyama, K. Satoh, T. Kushiya, N. Kobayashi. *J. Am. Chem. Soc.* **2014**, *136*, 765.

6. S. Cho, Z. S. Yoon, K. S. Kim, M.-C. Yoon, D.-G. Cho, J. L. Sessler, D. Kim, *J. Phys. Chem. Lett.* **2010**, *1*, 895.

7. D. T. Chase, A. G. Fix, S. J. Kang, B. D. Rose, C. D. Weber, Y. Zhong, L. N. Zakharov, M. C. Lonergan, C. Nuckolls, M. M. Haley, *J. Am. Chem. Soc.* **2012**, *134*, 10349.

8. T. Nishinaga, T. Ohmae, K. Aita, M. Takase, M. Iyoda, T. Arai, Y. Kunugi, *Chem. Commun.* **2013**, *49*, 5354.

9. S. M. LeCours, S. G. DiMango, M. J. Therien, *J. Am. Chem. Soc.* **1996**, *118*, 11854.

10. S. Okada, H. Segawa, *J. Am. Chem. Soc.* **2003**, *125*, 1792.

11. Y. Inokuma, Z. S. Yoon, D. Kim, A. Osuka, *J. Am. Chem. Soc.* **2007**, *129*, 4747.

12. S. Easwaramoorthi, J.-Y. Shin, S. Cho, P. Kim, Y. Inokuma, E. Tsurumaki, A. Osuka, D. Kim, *Chem. Eur. J.* **2009**, *15*, 12005.

13. C.-P. Hsieh, H.-P. Lu, C.-L. Chiu, C.-W. Lee, S.-H. Chuang, C.-L. Mai, W.-N. Yen, S.-J. Hsu, E. W.-G. Diau, C.-Y. Yeh, *J. Mater. Chem.* **2010**, *20*, 1127.

14. K. Yoshida, H. Mori, T. Tanaka, T. Mori, A. Osuka, *Eur. J. Org. Chem.* **2014**, 3997.

15. H. Mori, M. Suzuki, W. Kim, J. M. Lim, D. Kim, A. Osuka, *Chem. Sci.* **2015**, *6*, 1696.

16. D. Shimizu, J. Oh, K. Furukawa, D. Kim, A. Osuka, *J. Am. Chem. Soc.* **2015**, *137*, 15584.

17. R. Nozawa, H. Tanaka, W.-Y. Cha, Y. Hong, I. Hisaki, S. Shimizu, J.-Y. Shin, T. Kowalczyk, S. Irle, D. Kim, H. Shinokubo, *Nat. Commun.* **2016**, *7*, 13620.

18. T. Ito, Y. Hayashi, S. Shimizu, J.-Y. Shin, N. Kobayashi, H. Shinokubo, *Angew. Chem. Int. Ed.* **2012**, *51*, 8542.

19. S. Seki, A. Saeki, T. Sakurai, D. Sakamaki, *Phys. Chem. Chem. Phys.* **2014**, *16*, 11093.

Chapter 3

Facile Direct Amination of Norcorrole
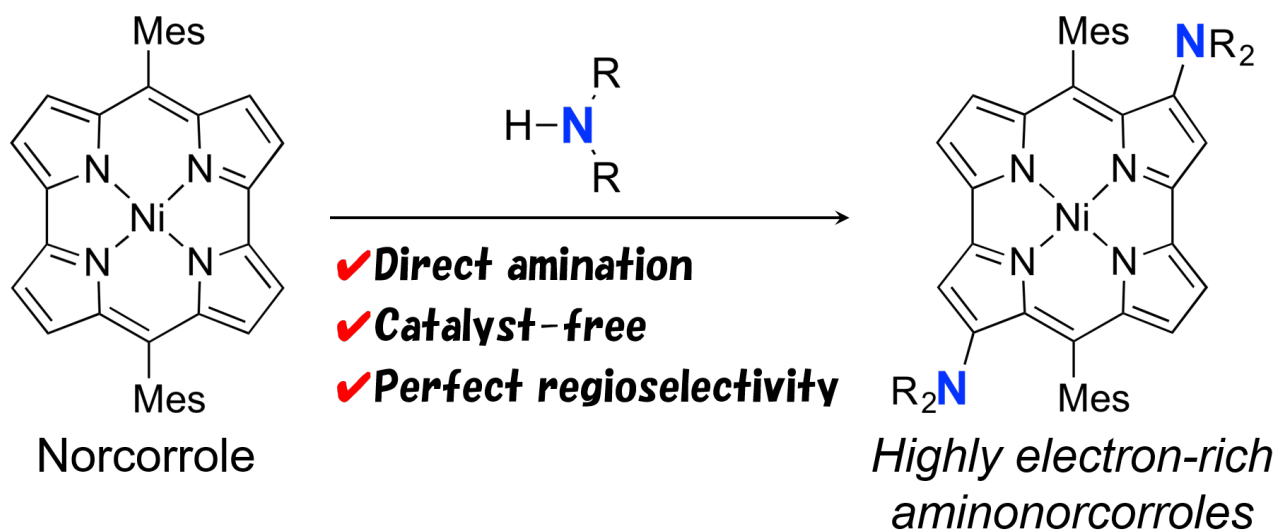
Takuya Yoshida, Hiroshi Shinokubo,
Mater. Chem. Front. **2017**, *1*, 1583.

Contents

3-1. Introduction

Antiaromatic compounds sometimes exhibit unique and enhanced reactivity because of their inherently unstable 4nπ-electron systems.[1-4] Such high reactivity is potentially useful for selective functionalization of antiaromatic compounds toward further manipulation of their physical properties, which should be important for future applications.

Although various types of antiaromatic porphyrinoids have been reported to date, their reactivity have rarely been investigated.[5,6] From this point of view, reactivity of norcorrole have been explored using various types of reagents (see Chapter 1). In particular, direct nucleophilic substitution reactions at pyrrole β-positions achieved easy access to functionalized norcorroles, which exhibited modulated optical and electrochemical properties.[7] The nucleophilic substitution reaction also enabled to design and synthesis a tethered norcorrole dimer, which experimentally demonstrated the emergence of three-dimensional aromaticity in π-stacked antiaromatic compounds.[8] In the present work, direct amination reactions of Ni[II] dimesitylnorcorrle **NiNc** with several amines have been investigated for the further development of the facile and regioselective nucleophilic functionalization method for norcorrole. It should be noted that recently Chmielewski *et al.* also reported the amination of norcorrole in different manners.[9,10]

3-2. Amination of norcorrole

Initially, it was found that amination of **NiNc** proceeded upon simple heating of a solution of **NiNc** in butylamine (Scheme 3-1, entry 1). On the basis of ^{1}H NMR and MS analyses, a bisamination product was obtained in 48% yield as a single regioisomer. X-ray structural analysis unambiguously identified the bisamination compound as **5b**, in which two butylamino groups were introduced at the diagonal 3- and 12-positions of **NiNc** (Figure 3-1). Notably, the present direct amination reaction of **NiNc** requires only butylamine: neither addition of any catalysts nor pre-functionalization of the norcorrole skeleton is necessary. In entry 2, the use of degassed butylamine resulted in decrease in the yield of **5a** to 26% and monoamino product **5a** was isolated in 23% yield. This result suggested that a trace amount of dioxygen in butylamine was crucial in the amination process. Consequently, the amination reaction of **NiNc** was attempted under air. In the presence of dioxygen, **NiNc** was totally consumed within 1 h at room temperatureto afford **5a** and **5b** in 45% and 52% yields, respectively (entry 3). The amination under air at 80 °C provided **5b** selectively in 82% yield in 20 min (entry 4).

Besides primary alkylamines, secondary alkylamines and primary arylamines could be employed as the reaction partner in the amination: The reaction with dibutylamine at 80 °C afforded monoamino product **6a** in 70% yield, while the yield of bisamino product **6b** was low (entry 5). The reaction with piperidine at room temperature only furnished **7b** as a major product (80%) with a trace amount of monoamino product **7a** (entry 6). These results suggest that nucleophilicity of amines is critical in this amination reaction. The amination of **NiNc** with aniline also provided only monoamino product **8a** in 55% yield (entry 7). In this case, an addition of

tributylamine as a base enhanced the reactivity to provide bisamino product **8b** along with **8a** after stirring for 10 h (entry 8). Unfortunately, none of amination products were obtained in the reaction of **NiNc** with diphenylamine probably due to its low nucleophilic character. In all entries, norcorroles substituted with three or four amino groups were not detected.
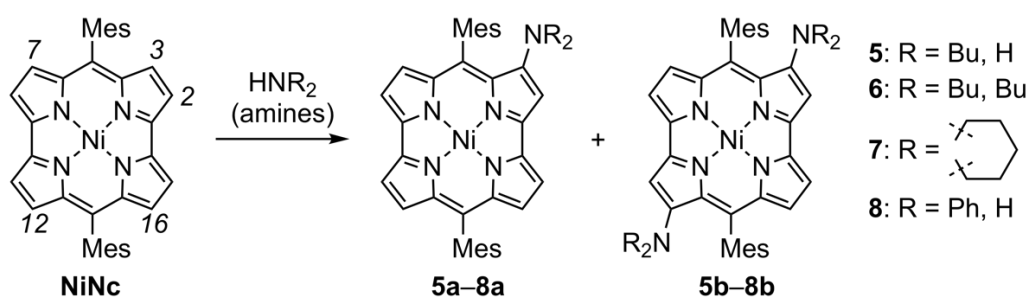
entry	amines	temp. (°C)	time	condition	products (yields %)	
1	butylamine	80	6 h	$N_2{}^a$		**5b** (48%)
2	butylamine	80	6 h	$N_2{}^b$	**5a** (23%)	**5b** (26%)
3	butylamine	RT	1 h	air	**5a** (45%)	**5b** (52%)
4	butylamine	80	20 min	air		**5b** (82%)
5	dibutylamine	80	2 h	air	**6a** (70%)	**6b** (trace)
6	piperidine	RT	1 h	air	**7a** (trace)	**7b** (80%)
7	aniline	80	6 h	air	**8a** (55%)	
8^c	aniline	80	10 h	air	**8a** (72%)	**8b** (17%)

Scheme 3-1. Synthesis of the mono- and bisaminonorcorroles. ^{a}The reaction was conducted under a N_2 atmosphere. ^{b}The reaction was conducted under N_2 atmosphere with degassed butylamine. ^{c}A drop of tributylamine was added as a base.
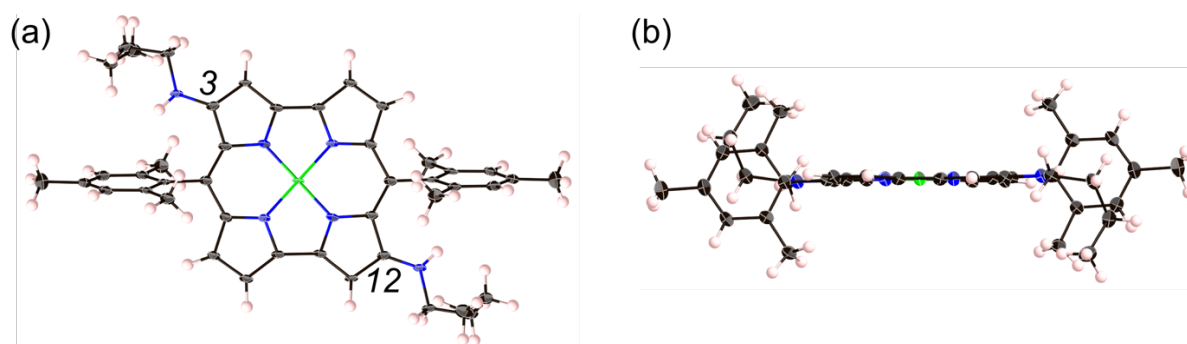

Figure 3-1. (a) Top view (b) side view of the X-ray crystal structure of bisaminonorcorrole **5b**. Atomic displacement parameters set at 50% probability.

3-3. Mechanism and selectivity of the amination

Although the reaction mechanism is not still completely understood at this moment, the plausible reaction mechanism is proposed in Scheme 3-2. The nucleophilic addition of an amine to **NiNc** provides an anionic

intermediate **A**. Then proton migration from the amine nitrogen to the anionic carbon atom yields a chlorin-type intermediate **B**, which is oxidized to aminonorcorrole **C** by atmospheric oxygen to restore the cyclic π-conjugation of norcorrole. Air oxidation of a chlorin-type dihydronorcorrole to norcorrole has been disclosed.[11]
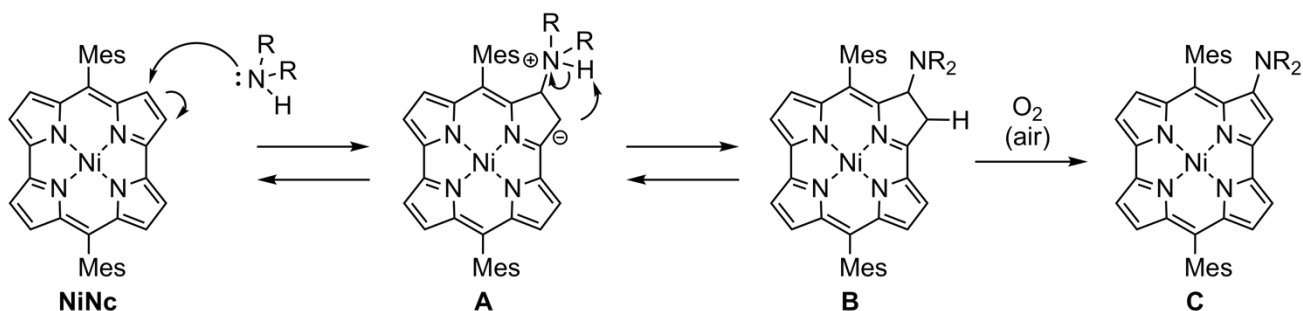
Scheme 3-2. Plausible reaction mechanism for the amination of **NiNc**.

To elucidate the origin of the observed regioselectivity, theoretical calculations were conducted by the density functional theory (DFT) method at the B3LYP/6-31G(d)+SDD level. To reduce the calculation costs, the butylamino groups in **5a** and **5b** were replaced with methylamino groups in model compounds **5a'** and **5b'**. The regioselectivity of the present amination reaction is clearly accounted for by distribution of LUMOs of norcorroles **NiNc**, **5a'** and **5b'** (Figure 3-2). The LUMO of **NiNc** suggests that the initial nucleophilic attack of the amine should occur at one of four β-positions near to the *meso*-aryl substituents (3-, 7-, 12-, and 16-positions) to afford **5a**, because the orbital is substantially distributed at 3-, 7-, 12-, and 16-positions. In the LUMO of **5a'**, a larger orbital coefficient lies on at the 12-position than other unsubstituted β-positions. This anisotropic distribution is the reason why the second amine attacks at the diagonal site to form **5b** as the dominant bisamino product. Furthermore, **5b** is no longer reactive to amines, because remained β-positions have fairly small orbital coefficients on the LUMO of **5b'**. Strong electron-donating effects of two amino groups also reduces the reactivity of **5b**.
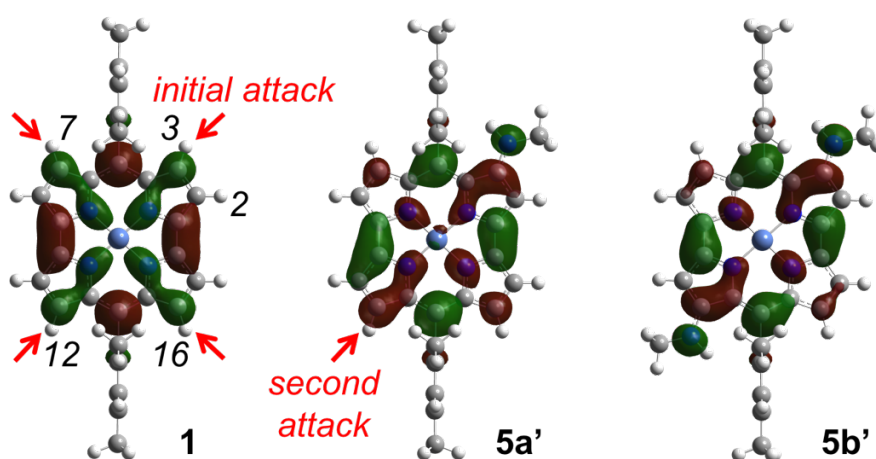

Figure 3-2. LUMOs of norcorroles **NiNc**, **5a'**, and **5b'** calculated at B3LYP/6-31G(d)+SDD level. The red arrows indicate the reactive positions.

3-4. Electrochemical properties

In order to evaluate effects of introduced amino groups for norcorrole, electrochemical properties of aminonorcorroles was investigated using cyclic voltammetry. The voltummograms of **5–8** in CH_2Cl_2 aredisplayed in Figure 3-3 along with those of **NiNc**. Both **NiNc** and aminonorcorroles show reversible reduction and oxidation waves. All potentials are cathodically shifted with the introduction of amino groups. Aminonorcorroles consequently exhibit significantly low first oxidation potentials (0.02 to –0.17 V) due to the inherent low oxidation potential of the antiaromatic norcorrole core as well as the electron-donating effect of amines. This result demonstrates that the present amination method is useful to create electron-rich motifs on the basis of norcorroles. The energy gap between the first oxidation and reduction potentials (ΔE) was increased in the cases of bisaminonorcorroles **5b**, **7b**, and **8b** (1.28, 1.16 and 1.20 V, respectively), because of the cathodic shift in the first reduction potentials. This tendency was matched well with the results of computational studies, in which the LUMO of **5b'** is particularly destabilized by the electron-donating effect of the amino group to increase the HOMO–LUMO gap (Figure 3-4).
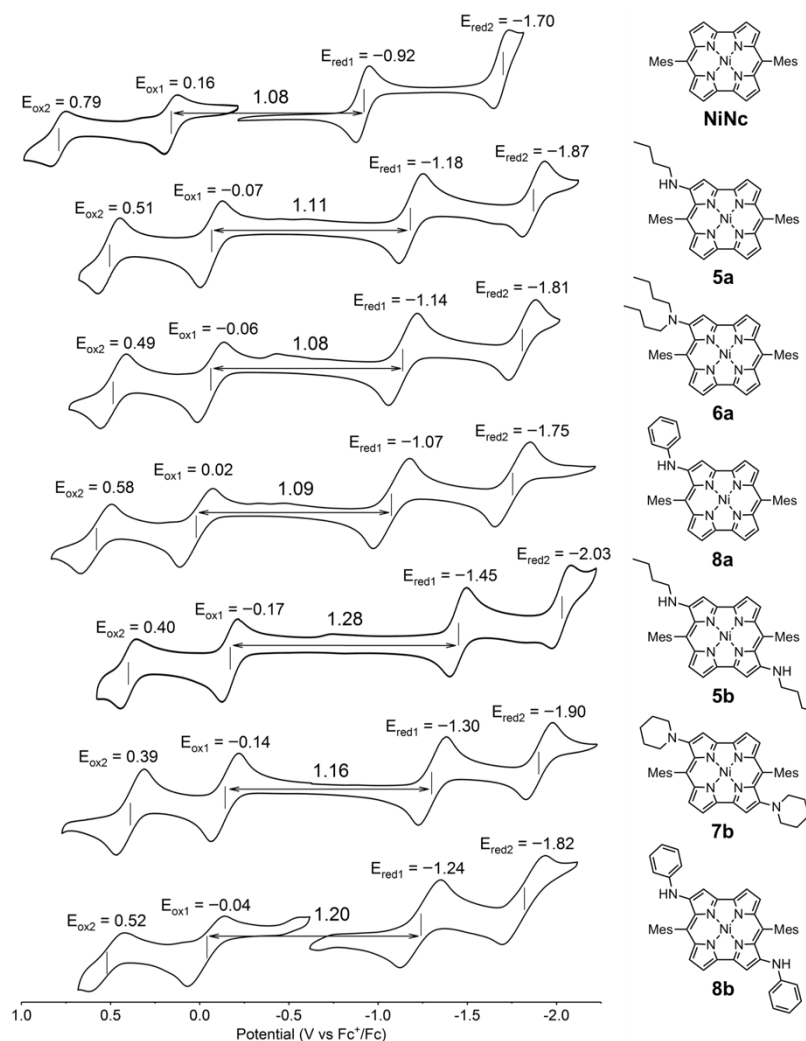

Figure 3-3. Cyclic voltammograms (0.1 V•s^{-1}) of **NiNc** and **5–8** in CH_2Cl_2 (0.1 M TBAPF$_6$). Working electrode: grass carbon, counter electrode: Pt, reference electrode: Ag/AgClO$_4$.
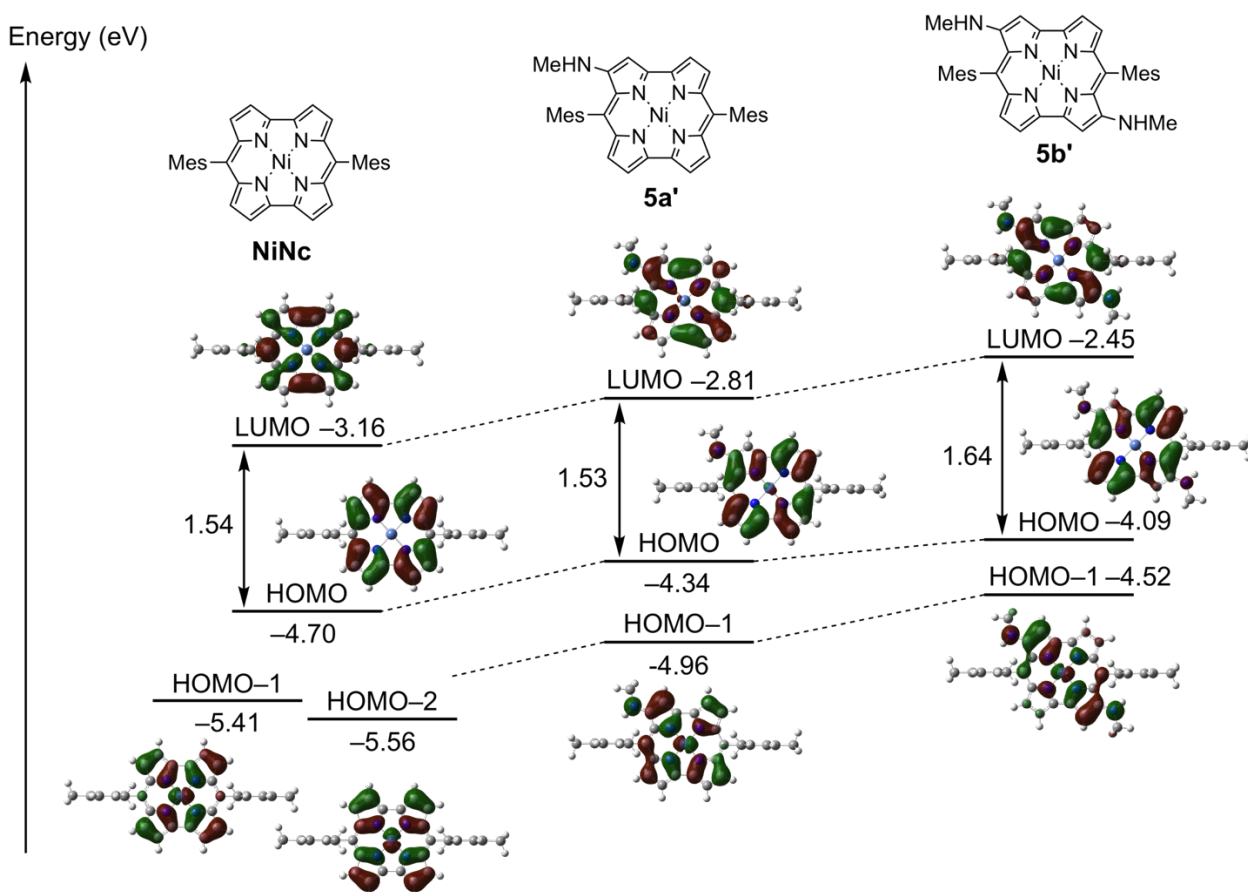
Figure 3-4. MO diagrams for norcorroles **NiNc**, **5a'** and **5b'** calculated at the B3LYP/6-31G(d)+SDD level.

3-5. Optical properties

The UV-vis-NIR absorption spectra of these norcorroles in CH_2Cl_2 were displayed in Figure 3-5. The whole absorption envelopes are distinctly depending on the number of amino groups attached to the norcorrole core: monoaminonorcorroles **5a**, **6a** and **8a** exhibit broaden and relatively weak absorption bands, while bisaminonorcorroles **5b**, **7b** and **8b** show sharp absorption bands similarly to **NiNc**.[12] Furthermore, **5b**, **7b** and **8b** have increased absorption bands in the NIR region as compared with that of **NiNc**. TD-DFT calculations for **5a'** and **5b'** were performed to obtain their theoretical absorption bands (Figure 3-6). The theoretical absorption spectra of **5a'** shows complex feature with many transitions, which is in good agreement with the broadened experimental absorption spectra of **5a**, **6a** and **8a**. The lower symmetric structure of monoaminonorcorrole **2a'** increases the number of its transition bands. The absorption of **5b'** is composed of fewer transitions because of its C_2-symmetric structure, and thus **5b**, **7b** and **8b** exhibit relatively simple absorption bands. The theoretical spectrum of **5b'** also suggested that the bear IR absorption bands of bisaminonorcorroles can be assigned to the transition from HOMO–1 to LUMO, which are significantly intensified after the introduction of amino groups (Table 3-1). On the other hand, the HOMO–LUMO transition of both mono- and bisaminonorcorroles remain forbidden.
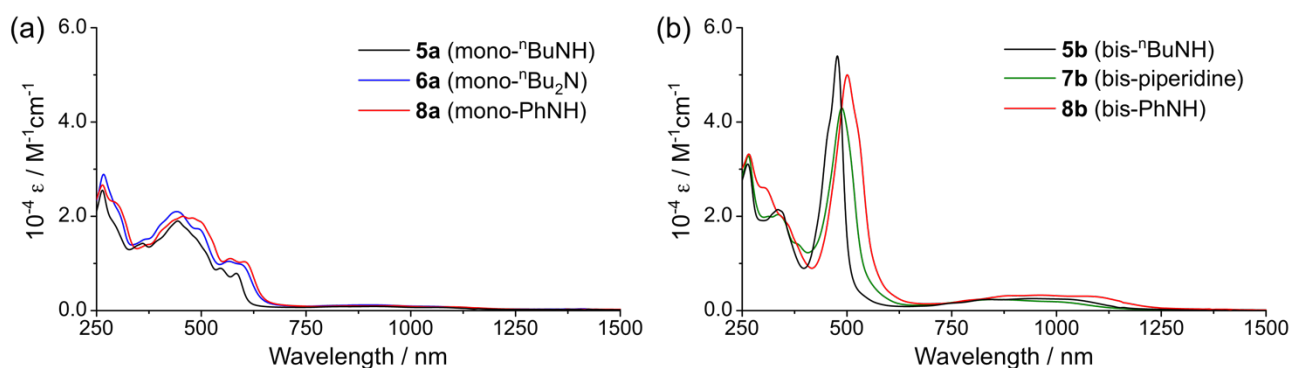
Figure 3-5. UV-vis-NIR absorption spectra of (a) mono- and (b) bisaminonorcorroles in CH_2Cl_2.
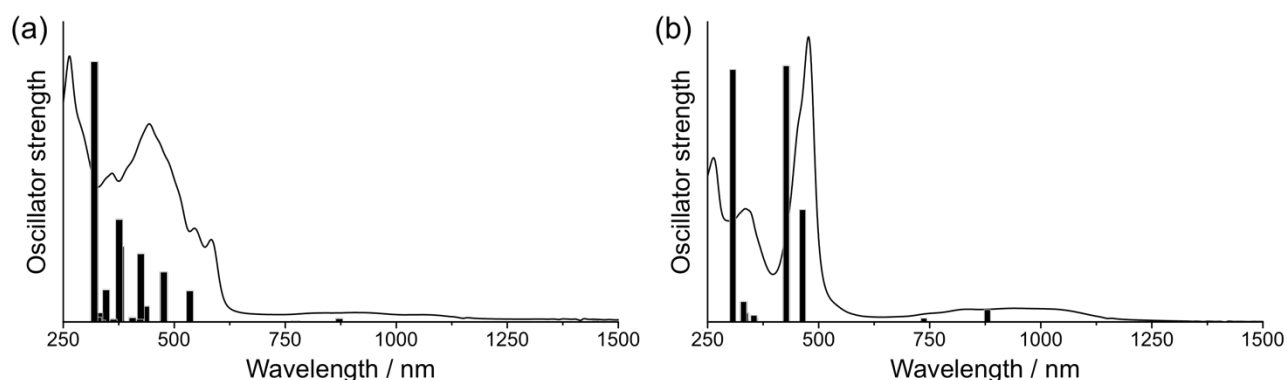

Figure 3-6. Theoretical absorption bands of (a) **5a'** and (b) **5b'** calculated at the B3LYP/6-31G(d)+SDD (sticks) with experimental spectra of (a) **5a** and (b) **5b** (solid lines).

Table 3-1. Calculated exited wavelengths (λ) and oscillator strengths (*f*) of selected transitions of **5a'** and **5b'**.

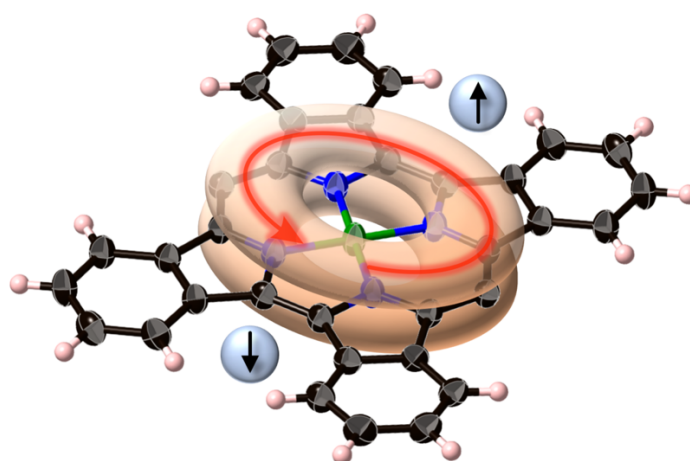| Compound	λ (nm)	*f*	Composition (%)
5a'	1448	0.0022	HOMO→LUMO (100%)
	872	0.0060	HOMO−1→LUMO (100%)
5b'	1315	0.0000	HOMO→LUMO (100%)
	880	0.0244	HOMO−1→LUMO (97%)

3-6. Summary of Chapter 3

In conclusion, the catalyst-free amination reaction of norcorrole successfully afforded mono- and bis-aminonorcorroles with perfect regioselectivity. The reaction only requires atmospheric oxygen as an oxidant besides an amine. This functionalization procedure represents the high reactivity of antiaromatic porphyrinoids induced by their unstable electronic structure. Aminonorcorroles exhibited highly electron-rich character and considerably altered optical properties because of strong electronic perturbation by the introduced amino groups. This facile functionalization methodology enables to design various novel norcorroles, which would be useful for device applications.

3-7. References

1. L. Watts, J. D. Fitzpatrick, R. Pettit, *J. Am. Chem. Soc.* **1965**, *87*, 3253.

2. T. Bally, S. Chai, M. Neuenschwander, Z. Zhu, *J. Am. Chem. Soc.* **1997**, *119*, 1869.

3. T. Nishinaga, T. Uto, R. Inoue, A. Matsuura, N. Treitel, M. Rabinovitz, K. Komatsu, *Chem. Eur. J.* **2008**. *14*, 2067.

4. C. Fan, L. G. Mercier, W. E. Piers, H. M. Tuononen, M. Parvez, *J. Am. Chem. Soc.* **2010**, *132*, 9604.

5. C. Liu, D.-M. Shen, Q.-Y. Chen, *J. Am. Chem. Soc.* **2007**, *129*, 5814.

6. V. L. Mishra, T. Furuyama, N. Kobayashi, K. Goto, T. Miyazaki, J.-S. Yang, T. Shinmyozu, *Chem. Eur. J.* **2016**, *22*, 9190.

7. R. Nozawa, K. Yamamoto, J.-Y. Shin, S. Hiroto, H. Shinokubo, *Angew. Chem. Int. Ed.* **2015**, *54*, 8454.

8. R. Nozawa, H. Tanaka, W.-Y. Cha, Y. Hong, I. Hisaki, S. Shimizu, J.-Y. Shin, T. Kowalczyk, S. Irle, D. Kim, H. Shinokubo, *Nat. Commun.* **2016**, *7*, 13620.

9. B. Liu, T. Yoshida, X. Li, M. Stępień, H. Shinokubo, P. J. Chmielewski, *Angew. Chem. Int. Ed.* **2016**, *55*, 13142.

10. X. Li, Y. Meng, P. Yi, M. Stępień, P. J. Chmielewski, *Angew. Chem. Int. Ed.* **2017**, *56*, 10810.

11. R. Nozawa, K. Yamamoto, I. Hisaki, J.-Y. Shin, H. Shinokubo, *Chem. Commun.* **2016**, *52*, 7106.

12. T. Ito, Y. Hayashi, S. Shimizu, J.-Y. Shin, N. Kobayashi, H. Shinokubo, *Angew. Chem. Int. Ed.* **2012**, *51*, 8542.

Chapter 4

Synthesis of Benzonorcorroles Showing Strong Antiaromaticity and the Emergence of Singlet Diradical Character

Takuya Yoshida, Kohtaro Takahashi, Yuki Ide, Jun-ya Fujiyoshi, Sangsu Lee, Yuya Hiraoka,
Donghо Kim, Masayoshi Nakano, Takahisa Ikeue, Hiroko Yamada, Hiroshi Shinokubo

Contents

4-1. Introduction

Expanding π-conjugation systems by the fusion of benzene rings is one of the most conventional and powerful way to alter their physical properties. In the cases of antiaromatic compounds, the expansion of π-conjugation by benzo-fusion is an effective strategy to enhance their stability, which has enabled isolation and easy handling of a number of 4n π-electron systems. However, the introduction of the fused benzo rings in antiaromatic compounds usually counterbalances the antiaromatic nature, as the strong local aromaticity of the benzene ring disturbs the contribution of the macrocyclic 4n π-conjugation system (Figure 4-1). For instance, while *s*-indacene is an unstable 12π antiaromatic polycyclic hydrocarbon, its dibenzo-fused analogue, indenofluorene, is stable due to a significant reduction of antiaromaticity.[1,2] Dibenzoborrole also shows attenuated antiaromaticity relative to that of the distinctly antiaromatic pristine borrole.[3,4]
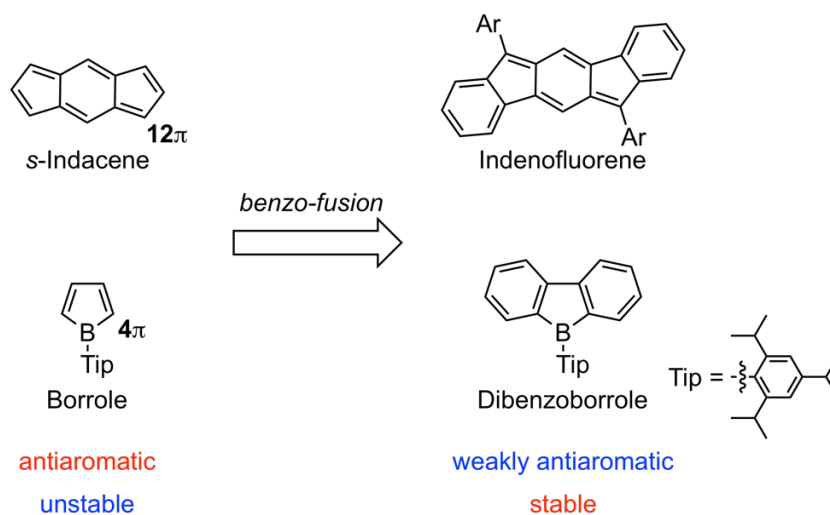

Figure 4-1. Indenofluorene and dibenzoborrole as examples of benzo-fused antiaromatic compounds.[1-4]

While antiaromatic porphyrinoids have been explored extensively, benzo-fused antiaromatic porphyrinoids are still limited to several examples (Figure 4-2).[5-10] Furthermore, the effect of benzo-fusion on their antiaromaticity has not been understood sufficiently, because of difficulty in preparing both an antiaromatic porphyrinoid and its benzo-fused derivative to investigate the difference in their properties depending on absence or presence of benzene rings.

In this study, the author has synthesized tetrabenzonorcorrole **NiTBNc** and dibenzonorcorrole **NiDBNc** to reveal the effect of benzo-fusion on the properties of norcorroles (Figure 4-3). The present work particularly focused on the change in the ring current effect by the benzene rings. A systematic comparison among these Ni[II] norcorroles allowed to conclude that benzo-fusion significantly decreases their HOMO–LUMO gaps and increases their paratropic ring current. Moreover, the author discovered that benzo-fusion induces singlet diradical character. Since singlet diradical character is associated with nonlinear optical properties and singlet fission processes,[11-15] delocalized singlet diradicals have received much attention.[16-23]
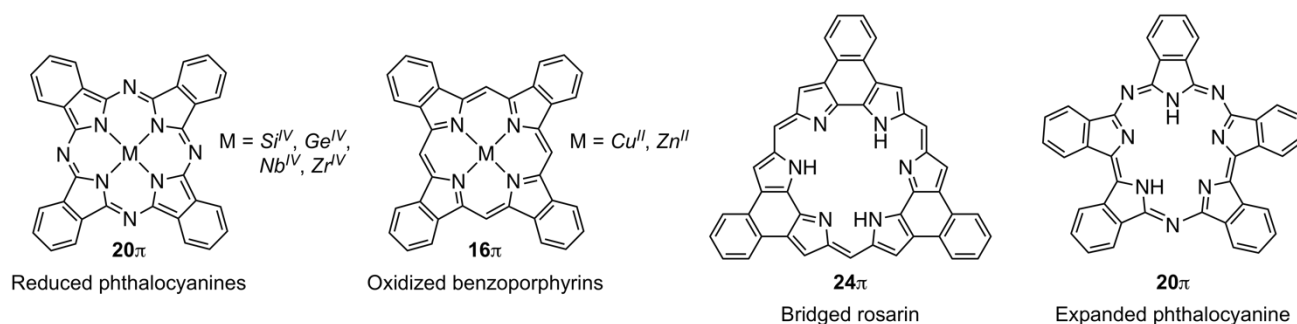
Figure 4-2. Antiaromatic porphyrinoids bearing fused benzene rings.
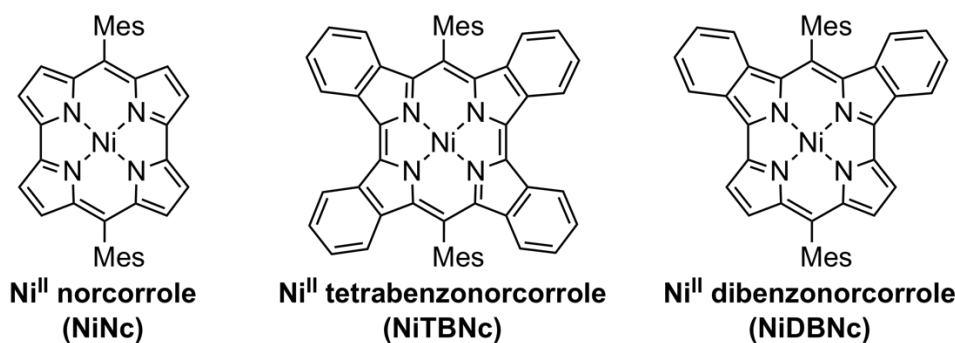

Figure 4-3. Structures of **NiNc**, and benzonorcorroles **NiTBNc** and **NiDBNc**.

4-2. Synthesis and characterization of Ni^{II} benzonorcorroles

The synthesis of benzonorcorroles **NiTBNc** and **NiDBNc** was conducted on the basis of the preparation of benzoporphyrins,[24] in which a retro-Diels–Alder reaction converts the bicyclo[2,2,2]octadiene (BCOD) moieties into the benzo units (Scheme 4-1 and 4-2). BCOD-fused α,α'-dibromodipyrrin **10** was synthesized through several steps from BCOD-fused pyrrole **9**. Treatment of **10** with Ni(OAc)$_2$ provided Ni^{II} complex **11a**, which was converted to tetraBCOD-fused norcorrole **12a** by the Ni^0-mediated intramolecular coupling reaction. **NiTBNc** was obtained from a retro-Diels–Alder reaction of **12a** at 200 °C under reduced pressure. Complexation of a mixture of **10** and **10'**, followed by chromatographic separation, afforded unsymmetrical Ni^{II} complex **11b**. The following coupling reaction provided bisBCOD-fused norcorrole **12b**, from which **NiDBNc** was prepared in a same manner. As **NiTBNc** and **NiDBNc** were gradually oxidized in solution, these complexes were isolated in a glovebox via repeated recrystallization. Since Ni^{II} norcorrole **NiNc** is stable under air at room temperature, the benzo-fusion clearly resulted in destabilization of the π-system of norcorrole.

X-ray diffraction analyses of **NiTBNc** and **NiDBNc** unambiguously determined their structures (Figure 4-4). In the crystal, **NiTBNc** exhibits a perfectly planer structure. π–π Stacking was not observed in the crystal of **NiTBNc**. The crystal structure of **NiDBNc** contains two independent stacked molecules per unit cell (structure 1 and structure 2). **NiDBNc** maintains rather flat conformation in structure 1, while structure 2 is distorted. Interestingly, **NiTBNc** exhibits a different type of the bond length-alternation (BLA) than **NiNc** and **NiDBNc** (Figure 4-5). The difference in BLA particularly appeared at the C–C bond lengths between the pyrrole α-

carbons (C_α–C_α bond). The C_α–C_α bonds in **NiNc** (1.491(2) Å) and **NiDBNc** (1.478(7) Å) are relatively long, while that in **NiTBNc** exhibits a clear double bond character (1.392(2) Å). The BLA in the crystal structures of Ni^{II} norcorroles were quantified on the basis of the harmonic oscillator model of aromaticity (HOMA)[25] values (Table 4-1). The HOMA value of **NiTBNc** (0.81) was much higher than those of **NiDBNc** (0.50, 0.38) and **NiNc** (0.43), reflecting the change in the BLA of **NiTBNc**. This difference in HOMA values was nicely reproduced by optimized structures of these norcorroles.
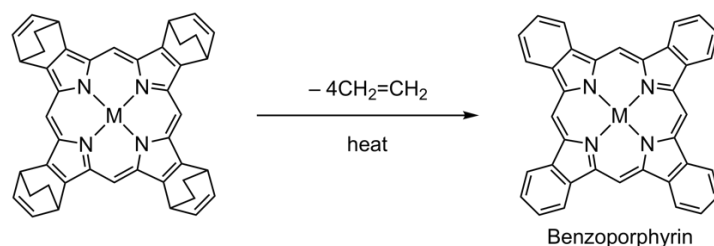
Scheme 4-1. Synthesis of benzoporphyrin by a retro-Diels–Alder reaction.
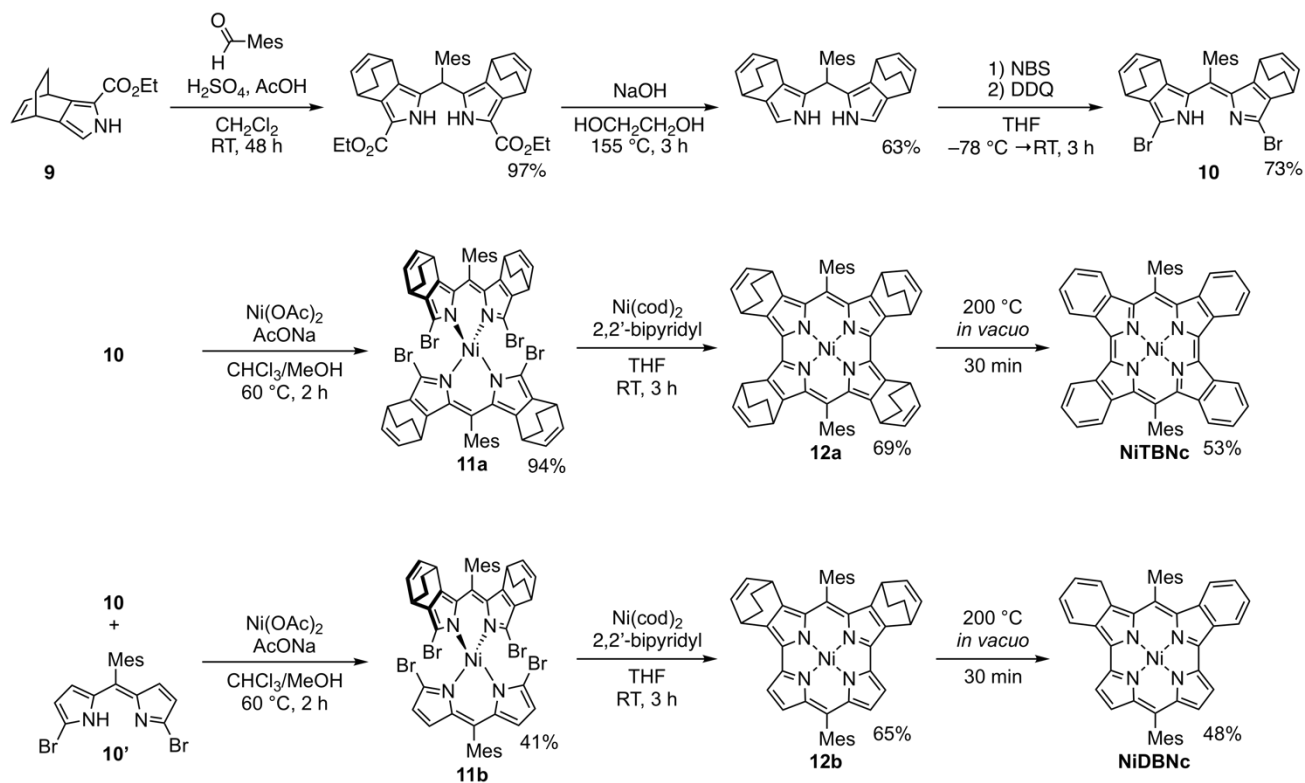
Scheme 4-2. Synthetic routes to **NiTBNc** and **NiDBN**c.
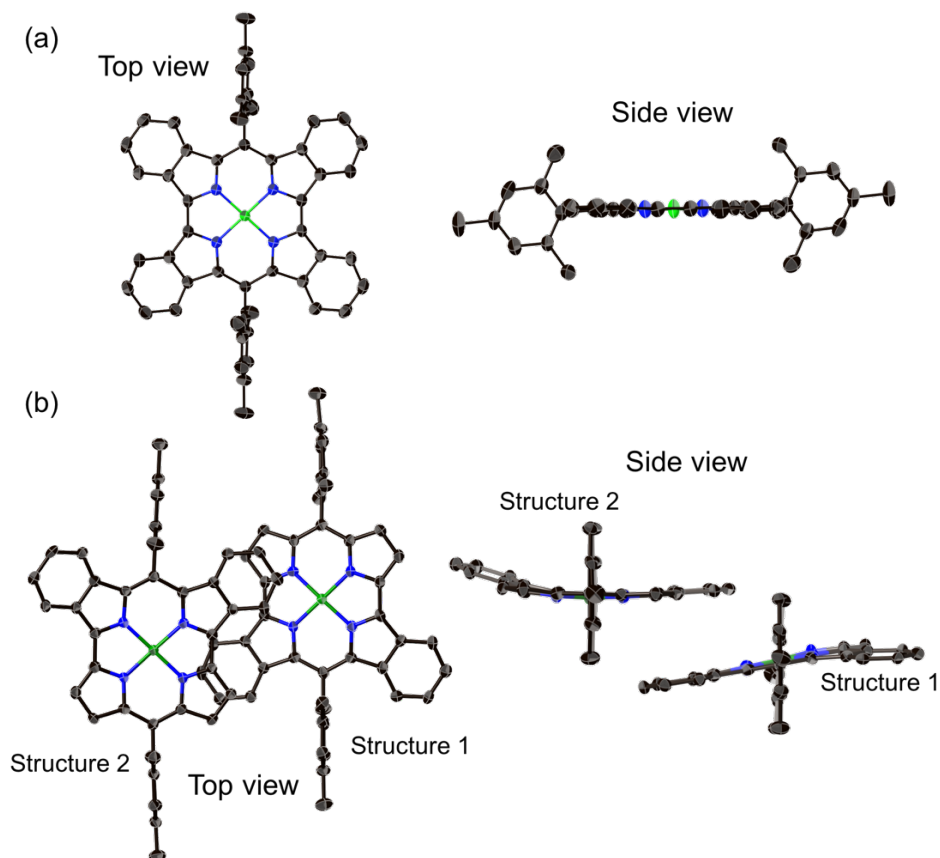
Figure 4-4. X-ray crystal structures of (a) **NiTBNc** and (b) **NiDBNc**. Atomic displacement parameters set at 50% probability and hydrogen atoms are omitted for clarity.
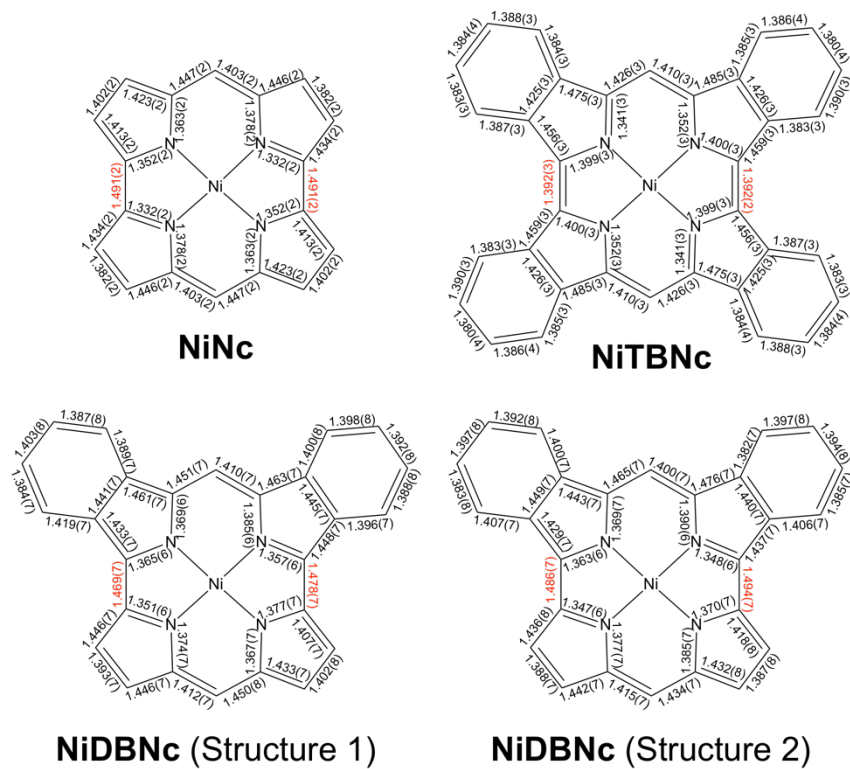

Figure 4-5. Bond lengths in crystal structures of **NiNc**, **NiTBNc**, and **NiDBNc**. C–C bond lengths between the pyrrole α-carbons (C$_\alpha$–C$_\alpha$ bond) bonds are shown as red values.

Table 4-1. Summary of HOMA values of Ni^{II} norcorroles calculated based on inner conjugation circuits of norcorroles consisted of 6 C–C bonds and 8 C–N bonds (right).

Compound	X-ray structure	Optimized structure (RB3LYP/ 6-31G(d)+SDD)
NiNc	0.43	0.35
NiDBNc (Structure 1)	0.50	0.43
NiDBNc (Structure 2)	0.38	
NiTBNc	0.81	0.74
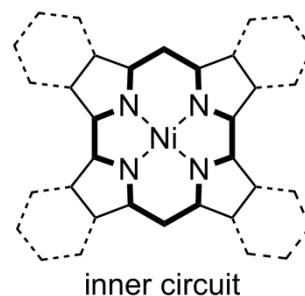
The ^{1}H NMR spectra of **NiTBNc** and **NiDBNc** in toluene-d_8 displayed broad signals at room temperature (Figure 4-6). The protons on the benzene rings (H_B) and protons on the pyrrole-β positions (H_β) are particularly broad in comparison to the mesityl protons. It is moreover highly remarkable that the H_B of **NiTBNc** and **NiDBNc** appear at δ = 3.0 and 0.5 ppm, suggesting that the strong paratropic ring current of **NiTBNc** and **NiDBNc** overrides the inherent diatropic ring current of the benzene rings. Furthermore, **NiDBNc** displays significantly high-filed shifted H_β (δ = −2.79 and −3.91 ppm) compared to those of **NiNc** (δ = 1.44 and 1.22 ppm). These observed chemical shifts verify a dramatic increase in the antiaromatic ring current effect by the benzo-fusion.
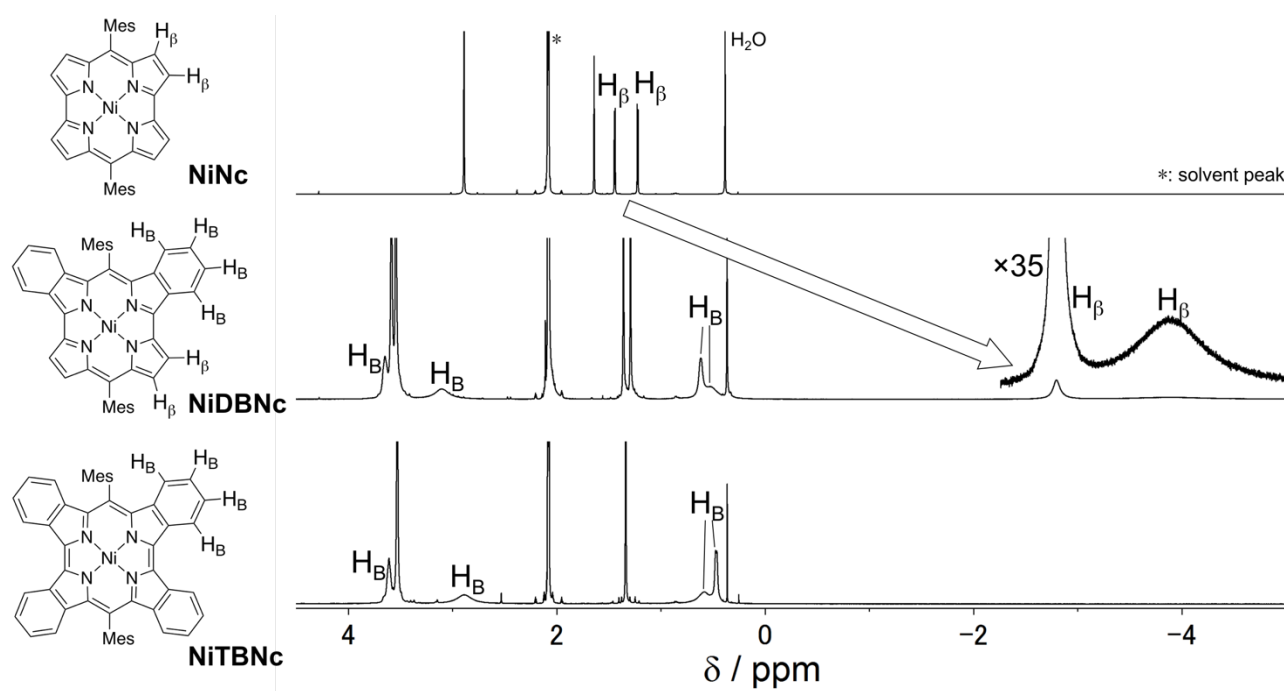

Figure 4-6. ^{1}H NMR (500 MHz) spectra of **NiNc** (top), **NiDBNc** (middle), and **NiTBNc** (bottom) in toluene-d_8. H_β: protons on the pyrrole-β positions. H_B: protons on the benzene rings.

4-3. Electrochemical and optical properties

The cyclic voltammograms of **NiNc**, **NiDBNc**, and **NiTBNc** measured in CH_2Cl_2 exhibited four reversible waves (Figure 4-7). The first oxidation processes of **NiDBNc** (–0.12 V) and **NiTBNc** (–0.28 V) are shifted to low potentials in comparison to that of **NiNc** (0.16 V), while their first reduction processes are not affected by the benzo-fusion. The decrease in stability of benzonorcorroles should be due to the fairly low oxidation potentials. Given the cathodic shifts of the first oxidation potentials, the electrochemically determined HOMO–LUMO gaps (ΔE) for **NiDBNc** (0.79 V) and **NiTBNc** (0.75 V) are substantially narrow.
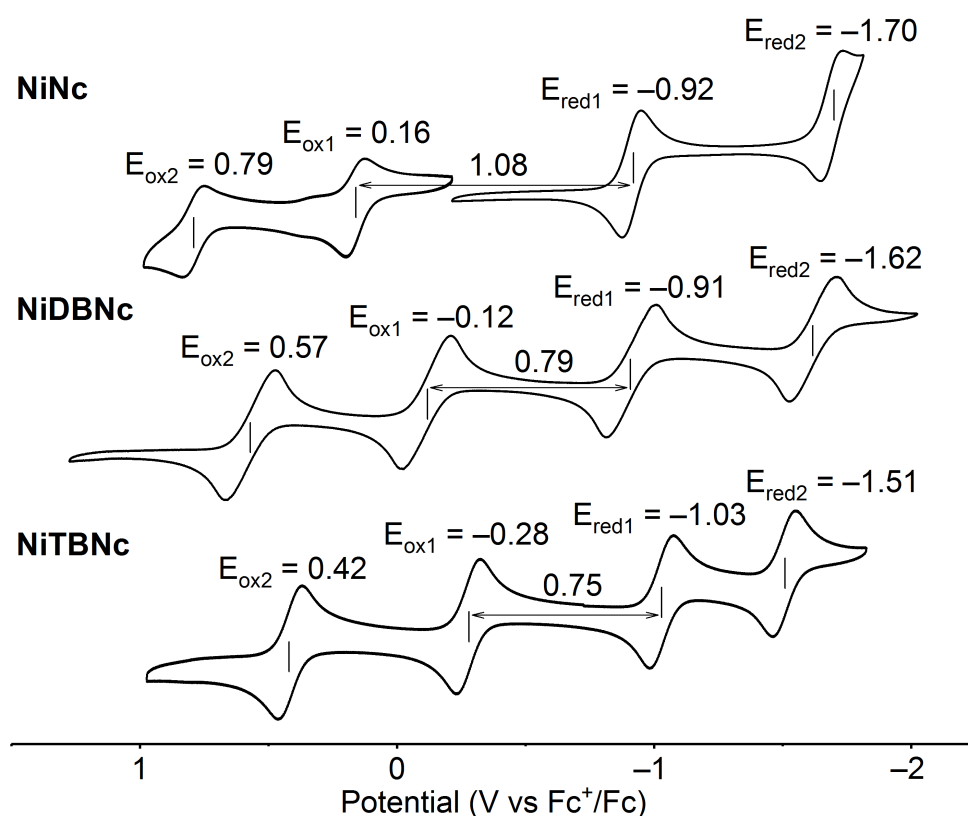

Figure 4-7. Cyclic voltammograms (0.1 V•s^{-1}) of **NiNc**, **NiDBNc**, and **NiTBNc** in CH_2Cl_2 (0.1 M TBAPF$_6$). Working electrode: grass carbon, counter electrode: Pt, reference electrode: Ag/AgClO$_4$.

The UV-Vis-NIR absorption spectra of **NiNc**, **NiDBNc** and **NiTBNc** are displayed in Figure 4-8a. Benzonorcorroles **NiTBNc** and **NiDBNc** show weak and broad absorption bands at 1500–2500 nm. These transition energies are much smaller than that of **NiNc** (~1000 nm). These electrochemical and optical measurements suggest the significantly narrowed HOMO–LUMO gaps in benzonorcorroles. Interestingly, the lowest transition band is clearly observable in the spectrum of **NiDBNc**, despite its inherently forbidden character. The lower symmetric structure of **NiDBNc** would partly dissolve the forbidden nature of the HOMO–LUMO transition of the norcorrole system. This prediction is supported by the TD-DFT calculations, in which non-zero oscillator strength of the lowest transition is estimated only for **NiDBNc** (Figure4-8b and Table 4-2).
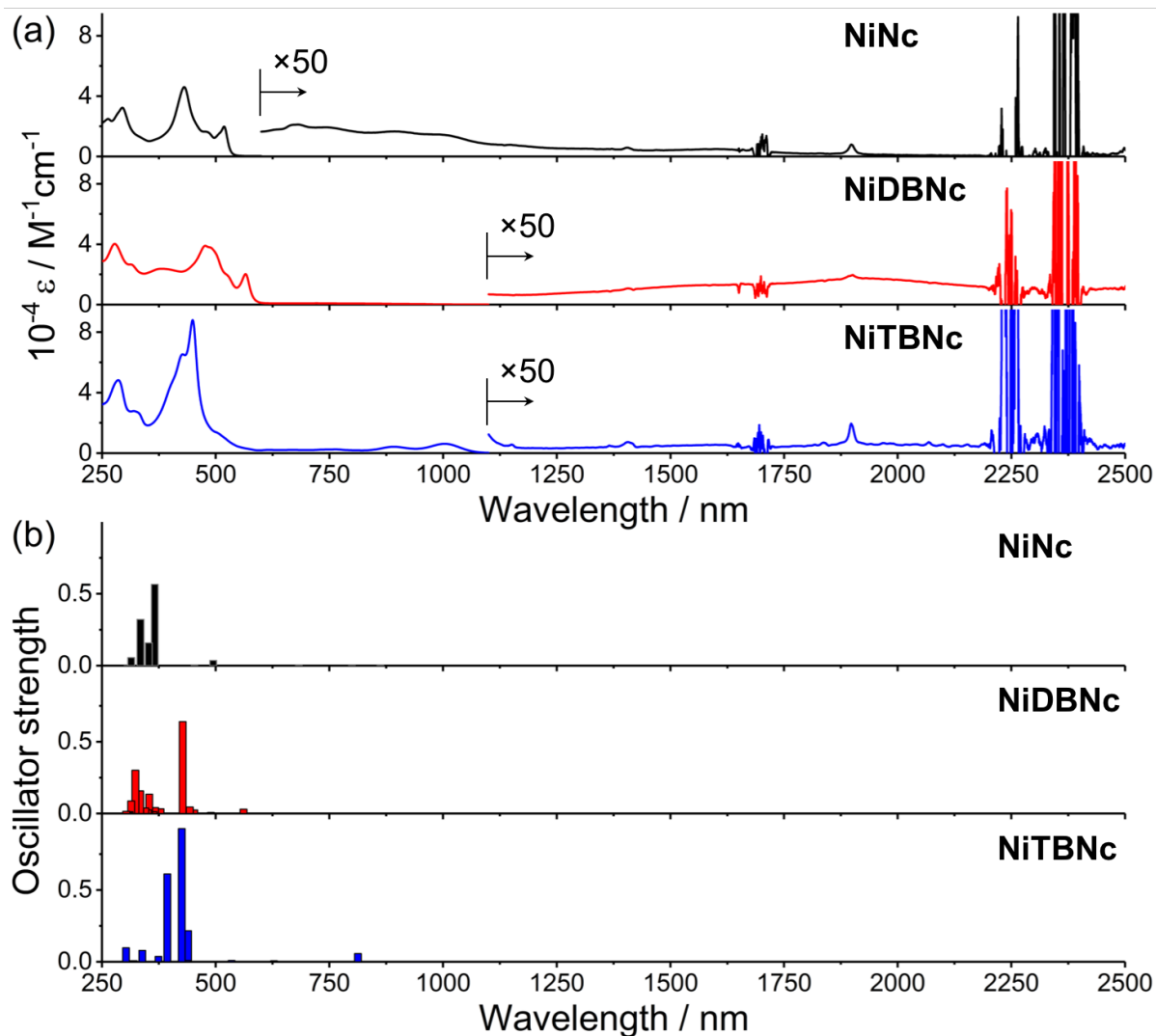
Figure 4-8. (a) UV-vis-NIR absorption spectra of **NiNc** (top), **NiDBNc** (middle), and **NiTBNc** (bottom) in CH_2Cl_2 and (b) their theoretical absorption bands calculated at the RB3LYP/6-31G(d)+SDD level.

Table 4-2. Calculated exited wavelengths (λ) and oscillator strengths (*f*) of low-energy transitions of **NiNc**, **NiDBNc**, and **NiTBNc**.

Compound	λ (nm)	*f*	Composition (%)
NiNc	1469.26	0.0000	HOMO→LUMO (100%)
	862.16	0.0005	HOMO−1→LUMO (100%)
NiDBNc	2604.77	0.0016	HOMO→LUMO (100%)
	783.23	0.0005	HOMO−1→LUMO (100%)
NiTBNc	3166.16	0.0000	HOMO→LUMO (100%)
	812.74	0.0578	HOMO−1→LUMO (100%)

4-4. Molecular orbitals

To confirm the narrow HOMO–LUMO gaps of **NiTBNc** and **NiDBNc**, molecular orbitals of Ni^{II} norcorroles were analyzed by using the DFT calculations at the RB3LYP/6-31G(d)+SDD level (Figure 4-9). The HOMO and LUMO of **NiNc** can be assigned to *a*-symmetric and *b*-symmetric orbitals, respectively. Comparing the orbitals of **NiDBNc** with those of **NiNc**, the *a*-symmetric HOMO of **NiDBNc** is destabilized by antibonding interactions between two benzo rings and the norcorrole core. In the case of **NiTBNc**, the *a*-symmetric orbital is further destabilized to become the LUMO, while the *b*-symmetric orbital concomitantly becomes the HOMO. The orbital inversion affects the structures of **NiTBNc**, which exhibits a much shorter C_α–C_α bond length between the two pyrrole units than **NiNc** or **NiDBNc**, as the *b*-symmetric orbital exhibits bonding character between the two C_α carbons. Although there is little orbital interaction in the *b*-symmetric orbitals associated with benzo-fusion, the *b*-symmetric orbital of **NiTBNc** is considerably stabilized because of the structural change in **NiTBNc**. As a result of these orbital interactions, **NiTBNc** and **NiDBNc** show significantly narrow HOMO–LUMO gaps (1.13 and 1.09 eV, respectively). The destabilized HOMOs and reduced HOMO–LUMO gaps are in good accordance with the electrochemical analysis and absorption spectra. Since previously reported theoretical studies have predicted a correlation between the paratropic ring current effect and small HOMO–LUMO energy gap,[26,27] the author presumes that the strong antiaromaticity (paratropic ring current) of benzonorcorroles is attributed to their narrow HOMO–LUMO gaps.
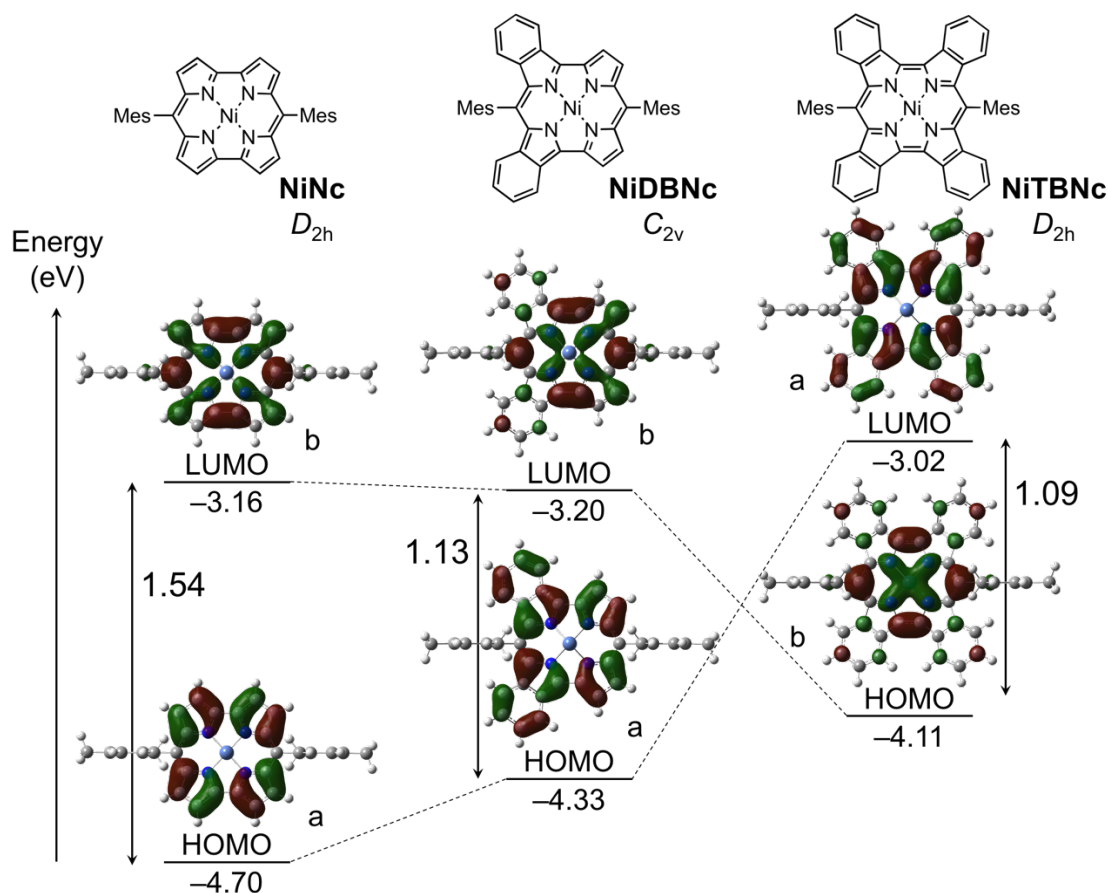

Figure 4-9. MO diagrams for **NiNc**, **NiDBNc**, and **NiTBNc** calculated at the RB3LYP/6-31G(d)+SDD level.

4-5. Open shell characters

To reveal the origin of their broad NMR spectra, variable-temperature (VT) ^{1}H NMR spectra of **NiTBNc** and **NiDBNc** were recorded from –80 °C to 100 °C in toluene-d_8 (Figure 4-10 and 4-11). The proton signals were further broadened at higher temperatures. Conversely, the peaks sharpened at lower temperatures, which allowed identifying proton couplings. This temperature-dependence implied an open-shell character for **NiTBNc** and **NiDBNc**. The temperature-dependent magnetic susceptibility ($\chi_p T$) of **TBNc** was measured by a superconducting quantum-interference device (SQUID) (Figure 4-12a). In addition, the $\chi_p T$ was also evaluated by the Evans method (Figure 4-12b).[28] Both measurements provide essentially the same temperature dependence. The magnetic susceptibility gradually increased at T > 200 K. This behavior is typical for singlet diradicaloids, whose triplet state is populated by the thermal excitation from the open-shell singlet ground state (Figure 4-13). The least-square curve fitting of the $\chi_p T$ values using the Bleaney–Bowers equation afforded $J_{S–T}$ values (a singlet triplet energy gap $\Delta E_{S–T} = E_S – E_T = J_{S–T}$) of –1.76 kcal mol^{-1} (SQUID) and –1.40 kcal mol^{-1} (Evans). Nevertheless, the contribution of open-shell character is not predominant, because obtained $\chi_p T$ were substantially smaller than that in S = 1.
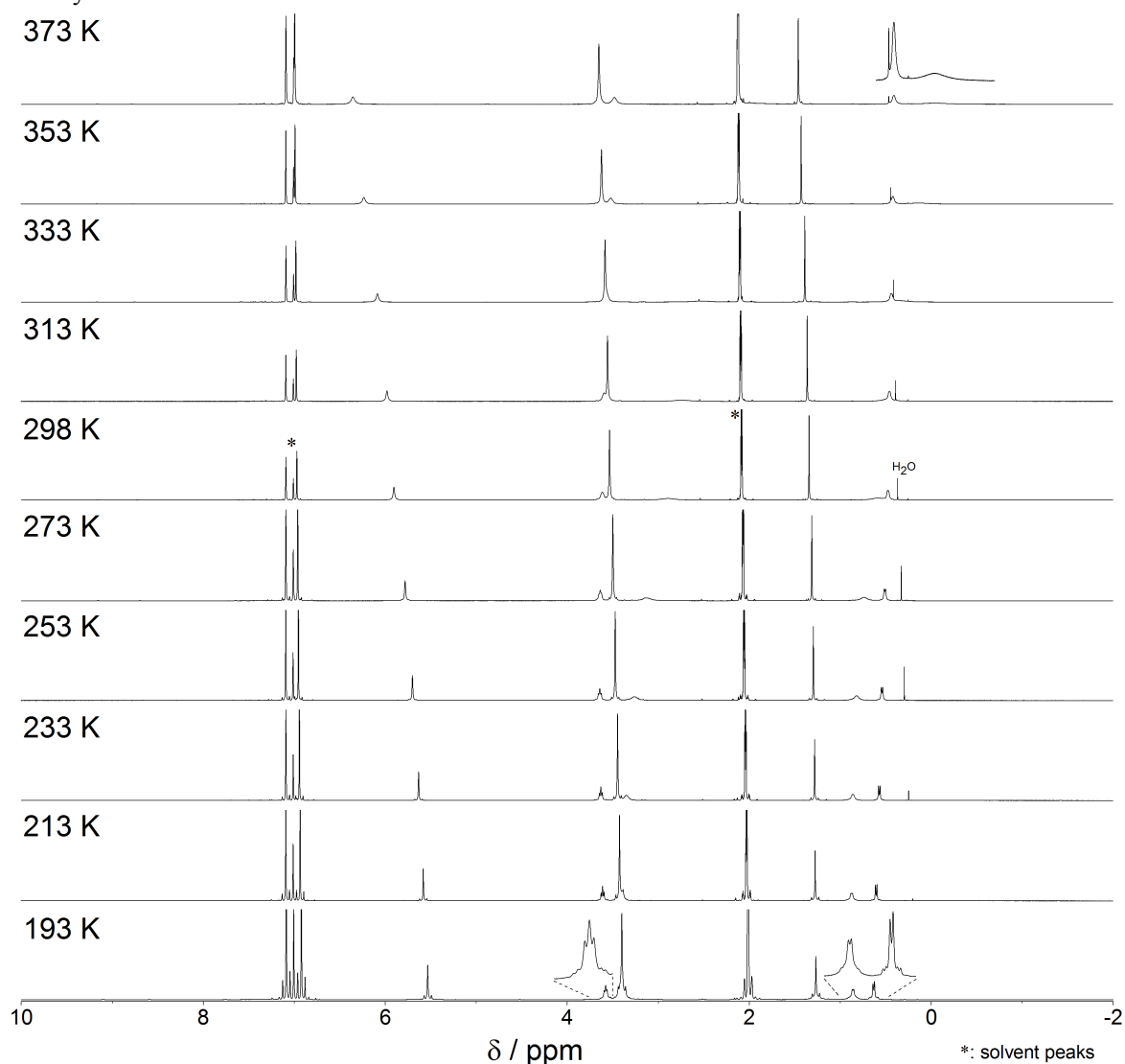

Figure 4-10. Variable temperature ^{1}H NMR (500 MHz) spectra of **NiTBNc** in toluene-d_8.
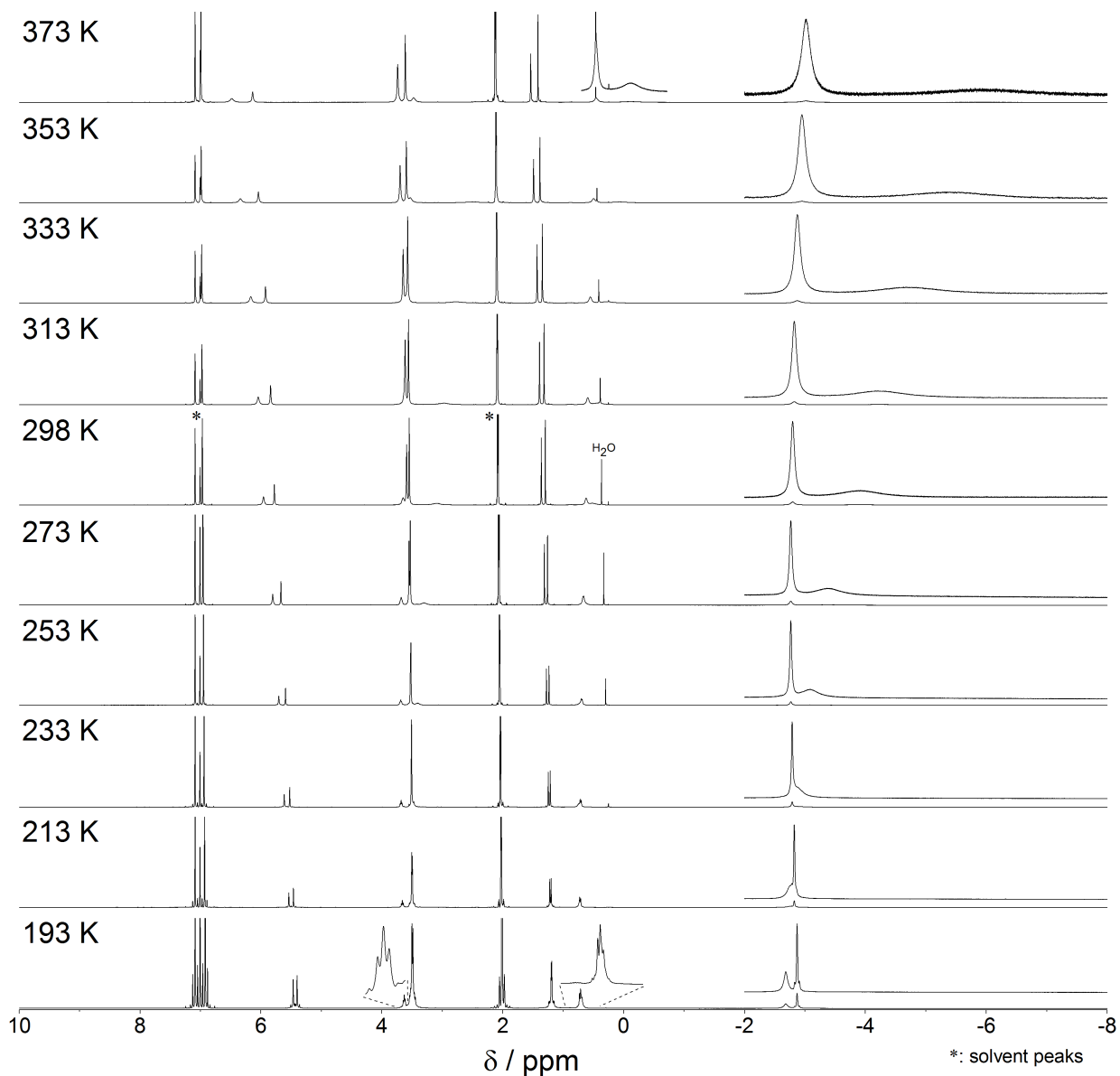
Figure 4-11. Variable temperature ^{1}H NMR (500 MHz) spectra of **NiDBNc** in toluene-d_8.
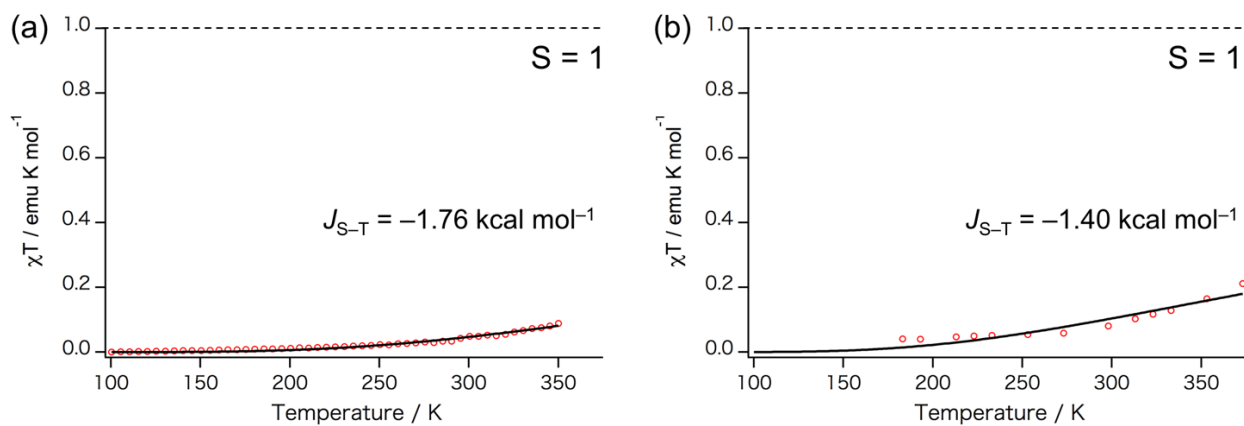

Figure 4-12. Temperature-dependent magnetic susceptibility of **NiTBNc** measured by (a) SQUID and (b) Evans method.
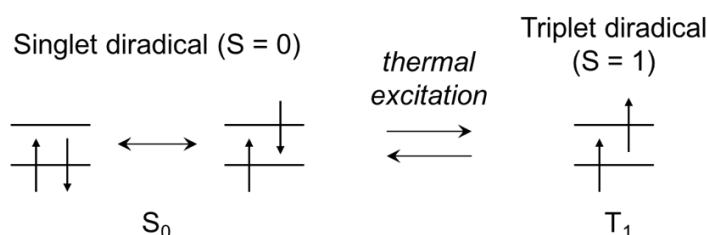
Figure 4-13. Schematic illustration of a thermally accessible triplet state from an open-shell singlet ground state.

The singlet diradical character of **NiTBNc** and **NiDBNc** was supported by quantum calculations. The energy levels of closed-shell singlet, open-shell singlet, and open-shell triplet configurations of **NiTBNc** and **NiDBNc** were calculated based on their crystal structures (Table 4-3). The open-shell singlet state was obtained by the symmetry-broken (BS) method. J_{S-T} values were estimated using Yamaguchi's equation.[29] The results revealed that the open-shell singlet states are the most stable states for both **NiTBNc** and **NiDBNc**. In addition, the calculated J_{S-T} value was in good agreement with the experimental values. The diradical character, y, was inferred from the occupation number of the lowest unoccupied natural orbital calculated at the LC-UBLYP(BS)/6-31G(d)+SDD level.[30] As the calculated diradical indexes, y, of **NiDBNc** (0.34) and **NiTBNc** (0.39) are much higher than that of **NiNc** (0.06), it was concluded that the benzo-fusion of the norcorrole system enhances its diradical character (Table 4-4 and 4-5). The highly delocalized spin density of benzonorcorroles were estimated by the calculations at the UB3LYP/6-31G(d)+SDD level, both in open-shell singlet and triplet states. (Figure 4-14).

Table 4-3. Calculated total energies (hartree) of singlet and triplet states of **NiTBNc** and **NiDBNc**, as well as J_{S-T} values (kcal mol^{-1}).^{a}

Compound	Closed-shell singlet	Open-shell singlet	Open-shell triplet	J_{S-T}
NiTBNc	−2393.99496251	−2393.99574407 (0.4568)^b	−2393.98870191 (2.0098)^b	−2.85
NiDBNc (Structure 1)	−2086.7623644	−2086.76342058 (0.5148)^b	−2086.75751944 (2.0098)^b	−2.48
NiDBNc (Structure 2)	−2086.76429212	−2086.76469583 (0.3294)^b	−2086.75683416 (2.0099)^b	−2.94

^{a}Calcuations were performed at the B3LYP/6-31G(d)+SDD level. ^{b}Values in parenthesis represent $<S^2>$ values.

Table 4-4. HOMO–LUMO gaps and diradical characters y calculated using RB3LYP/6-31G(d)+SDD optimized structures.

Compound	Energy gap by CV (V)	RB3LYP HOMO–LUMO gap (eV)	RHF HOMO–LUMO gap (eV)	PUHF y	LC-UBLYP y
NiNc	1.08	1.53	5.82	0.52	0.06
NiDBNc	0.79	1.13	5.14	0.72	0.34
NiTBNc	0.75	1.09	5.51	0.56	0.39

Table 4-5. HOMO–LUMO gaps and diradical characters *y* calculated using X-ray crystallographic structures.

Compound	RB3LYP HOMO–LUMO gap (eV)	RHF HOMO–LUMO gap (eV)	PUHF *y*	LC-UBLYP *y*
NiNc	1.55	5.91	0.41	0.01
NiDBNc (Structure 1)	1.02	5.02	0.75	0.45
NiDBNc (Structure 2)	1.09	5.12	0.65	0.37
NiTBNc	1.06	5.45	0.52	0.43

(a) NiTBNc NiDBNc (b) NiTBNc NiDBNc
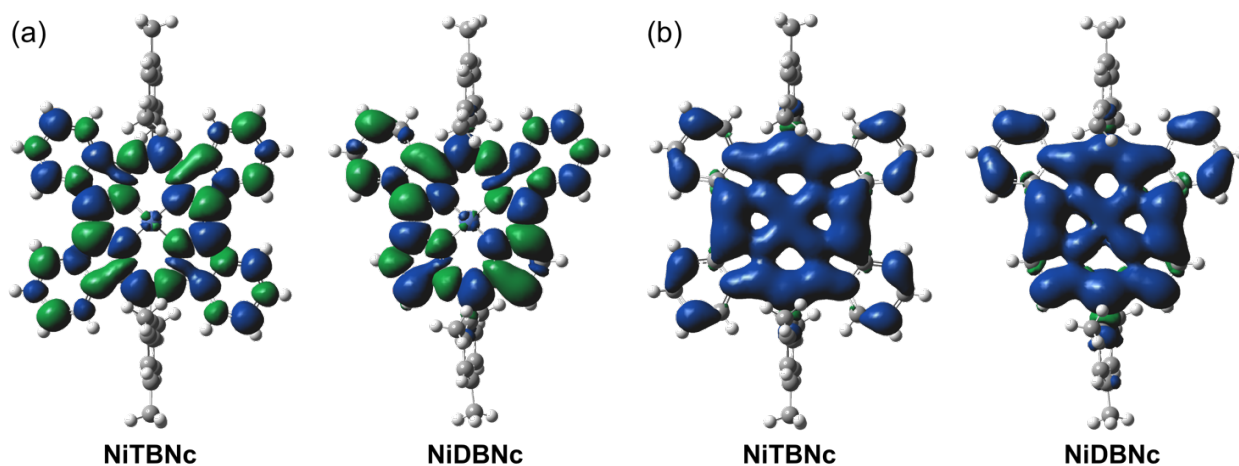
Figure 4-14. Spin density maps of **NiTBNc** and **NiDBNc** in (a) open-shell singlet states and (b) triplet states calculated at UB3LYP/6-31G(d)+SDD level. using X-ray crystal geometries (Structure 1 was used for the calculation of **NiDBNc**).

4-6. Evaluation of the ring currents effects

In order to evaluate the ring current effect, nucleus-independent chemical shift (NICS) values were calculated based on both crystal and DFT optimized structures.[31] To include the influence by the open-shell contribution, the BS method was used for calculations (Figure 4-15a). The NICS(1) values for **NiNc** (~35 ppm) are substantially smaller than those for **NiTBNc** and **NiDBNc** (52–68 ppm). Calculations in the closed-shell singlet states afforded considerably large NICS(1) values for **NiTBNc** and **NiDBNc** (93–117 ppm), whereas those for **NiNc** were identical to values in the open-shell singlet states (Figure 4-15b). The NICS(1) values in closed-shell singlet states of **NiTBNc** and **NiDBNc** were overestimated, because their open-shell contribution should suppress paratropic ring current according to the Baird's rule.[32] In addition, calculations using DFT optimized geometries nicely reproduced experimental ^{1}H NMR chemical shift values and supported enhanced paratropic ring current in benzonorcorroles (Table 4-6 to 4-11). The ring currents of the Ni[II] norcorroles, visualized using the anisotropy of the induced current density (ACID) method,[33] also supported the presence of an enhanced anticlockwise paratropic ring current in **NiTBNc** and **NiDBNc** (Figure 4-16). On the basis of these theoretical analyses in combination with the experimental results (high-field shifted proton signals and reduced stability), the author concluded that Ni[II] benzonorcorroles exhibit increased antiaromaticity.
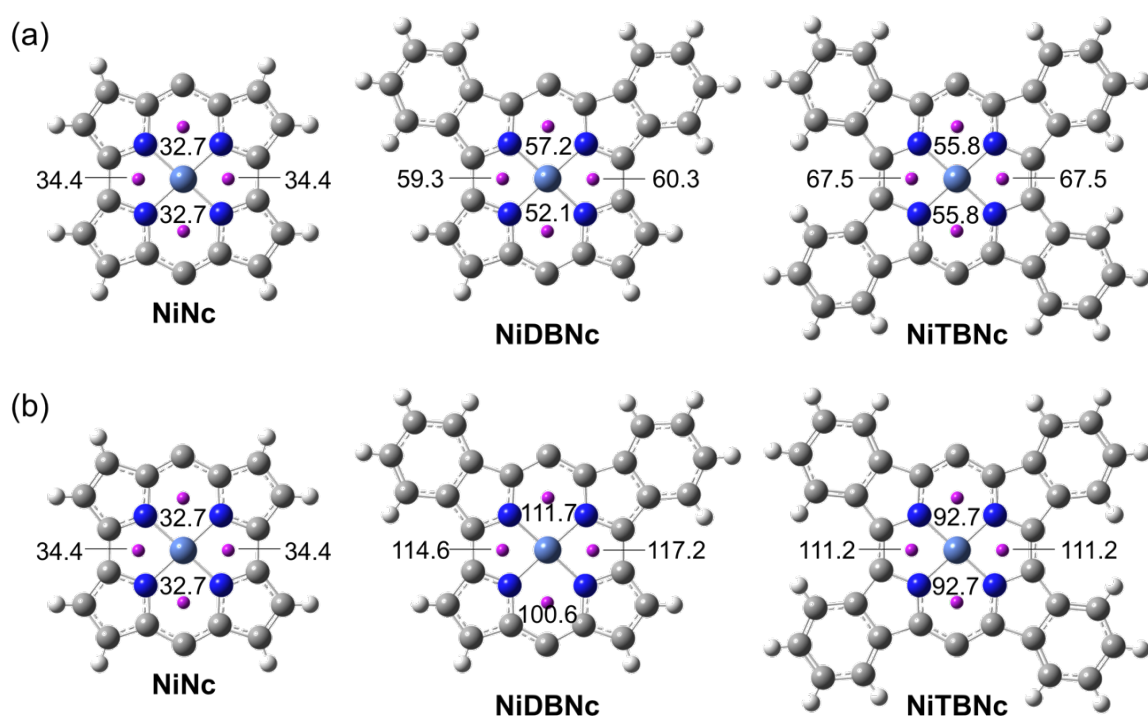
Figure 4-15. NICS(1) values (ppm) for **NiNc**, **NiDBNc** and **NiTBNc** calculated at the (a) UB3LYP(BS)/6-31G(d)+SDD and (b) RB3LYP/6-31G(d)+SDD level of theory using X-ray crystal geometries (Structure 1 was used for the calculation of **NiDBNc**).

Figure 4-16. ACID-derived induced-ring-current maps for **NiNc**, **NiDBNc**, and **NiTBNc** calculated at the UB3LYP/6-31G(d)+SDD level of theory using X-ray crystal geometries (Structure 1 was used for the calculation of **NiDBNc**). Red arrows indicate the overall directions of ring currents.

Table 4-6. Comparison of theoretical and experimental ^{1}H NMR chemical shifts for selected H atoms of **NiNc** (ppm) along with the numbering of atoms.

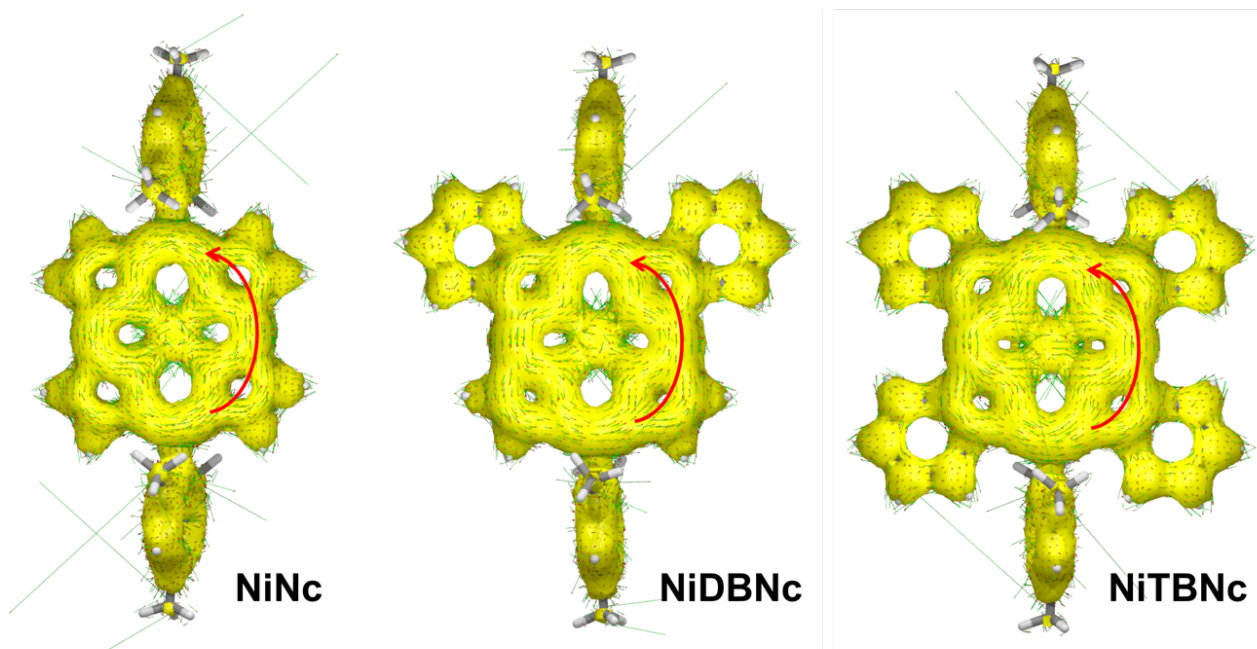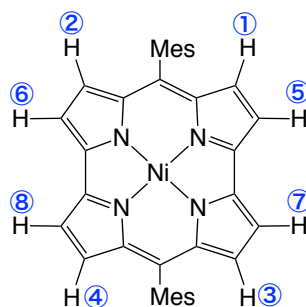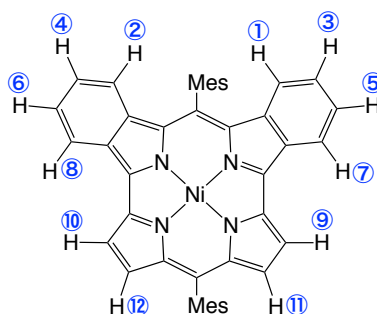| Position	RB3LYP/6-31G(d,p)+SDD [a]	UB3LYP/6-31G(d,p)+SDD [ab]	Expt. peak position
1, 2, 3, 4	1.8	1.8	1.44, 1.22
5, 6, 7, 8	1.4	1.4	

[a] RB3LYP/6-31G(d)+SDD optimized geometry is used. Absolute shielding value for standard TMS (31.79 ppm) is evaluated at the RB3LYP/6-31G(d,p)//RB3LYP/6-311G(d,p) level. Calculations are performed in gas phase. [b] UB3LYP solution is reduced to the RB3LYP solution.

Table 4-7. Comparison of theoretical and experimental ^{1}H NMR chemical shifts for selected H atoms of **NiDBNc** (ppm) along with the numbering of atoms.

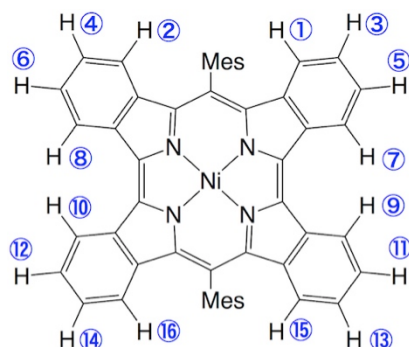| Position	RB3LYP/6-31G(d,p)+SDD [a]	UB3LYP/6-31G(d,p)+SDD [a]	Expt. peak position
1, 2	–0.1, 0.0	1.1, 1.1	0.62
3, 4	3.4, 3.4	4.0, 4.0	3.11
5, 6	3.5, 3.5	4.1, 4.1	3.65
7, 8	0.5, 0.5	1.7, 1.8	0.53
9, 10	–3.3, –3.4	–1.7, –1.7	–2.79
11, 12	–3.0, –3.0	–1.3, –1.4	–3.87

[a] RB3LYP/6-31G(d)+SDD optimized geometry is used. Absolute shielding value for standard TMS (31.79 ppm) is evaluated at the RB3LYP/6-31G(d,p)//RB3LYP/6-311G(d,p) level. Calculations are performed in gas phase.

Table 4-8. Comparison of theoretical and experimental ^{1}H NMR chemical shifts for selected H atoms of **NiTBNc** (ppm) along with the numbering of atoms.
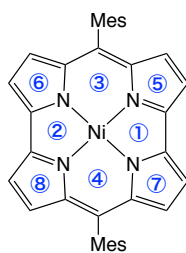

Position	RB3LYP/6-31G(d,p)+SDD ^{a}	UB3LYP/6-31G(d,p)+SDD ^{a}	Expt. peak position
1	−1.5	1.1	0.48
2	−1.6	1.1	
3	2.6	4.1	2.91
4	2.6	4.0	
5	2.8	4.3	3.62
6	2.8	4.3	
7	−0.9	1.9	
8	−0.9	1.9	0.61
9	−0.9	1.9	
10	−0.9	1.9	
11	2.8	4.3	3.62
12	2.8	4.3	
13	2.6	4.0	2.91
14	2.6	4.1	
15	−1.6	1.1	0.48
16	−1.5	1.1	

^{a} RB3LYP/6-31G(d)+SDD optimized geometry is used. Absolute shielding value for standard TMS (31.79 ppm) is evaluated at the RB3LYP/6-31G(d,p)//RB3LYP/6-311G(d,p) level. Calculations are performed in gas phase.

Table 4-9. NICS(0) values of **NiNc** (ppm) along with the numbering of the positions.

Position	RB3LYP/6-31G(d)+SDD [a]	UB3LYP/6-31G(d)+SDD [ab]
1, 2	39.6, 39.8	39.6, 39.8
3, 4	39,4, 39.2	39,4, 39.2
5, 6, 7, 8	5.9, 5.7, 6.0, 5.7	5.9, 5.7, 6.0, 5.7

[a] X-ray crystallographic structure is used.   NICS calculation is performed in gas phase.   [b] UB3LYP solution is reduced to the RB3LYP solution.

Table 4-10. NICS(0) values of **NiDBNc** (ppm) along with the numbering of the positions.
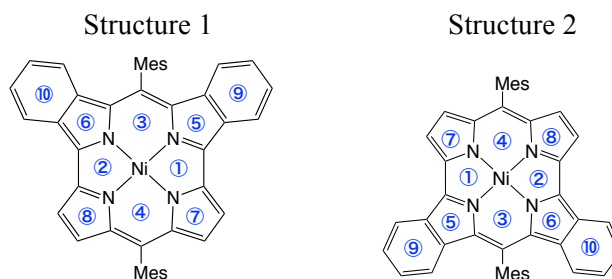
Position	RB3LYP/6-31G(d)+SDD [a]	UB3LYP/6-31G(d)+SDD [a]
	Structure 1 / Structure 2	Structure 1 / Structure 2
1	136.6 / 100.8	69.4 / 69.6
2	134.1 / 96.0	68.7 / 66.7
3	132.7 / 100.8	67.9 / 67.8
4	120.1 / 97.5	62.3 / 62.1
5	5.6 / 5.1	1.5 / 2.6
6	7.2 / 4.8	3.2 / 2.8
7	23.5 / 17.9	11.9 / 12.3
8	29.3 / 19.4	13.5 / 12.5
9	2.3 / 1.2	−2.7 / −1.6
10	2.5 / −0.2	−2.4 / −2.5

[a] X-ray crystallographic structures are used.   NICS calculation is performed in gas phase.

Table 4-11. NICS(0) values of **NiTBNc** (ppm) along with the numbering of the positions.
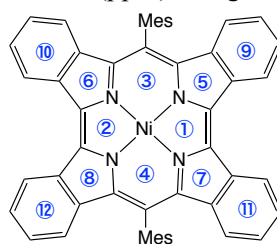
Position	RB3LYP/6-31G(d)+SDD [a]	UB3LYP/6-31G(d)+SDD [a]
1	129.2	76.9
2	129.3	77.0
3	110.7	66.8
4	110.7	66.8
5	9.4	6.3
6	10.4	6.8
7	10.3	6.7
8	9.4	6.3
9	1.0	–2.3
10	1.5	–1.9
11	1.4	–2.0
12	1.1	–2.2

[a] X-ray crystallographic structure is used.   NICS calculation is performed in gas phase.

In general, fused benzene rings to antiaromatic compounds improve their stability but attenuate their antiaromatic nature because of the strong local aromaticity of the benzene ring. For example, the core 12π-electron system of indenofluorene is disturbed by in a resonance structure in which π-electrons are used to form 6π aromatic conjugation systems of the fused benzene rings (Figure 4-17a). The present observation stands in sharp contrast to such common cases of benzo-fused antiaromatic compounds. In the case of benzonorcorroles, the 16π-conjugation systems can be considered along the inner periphery involving four nitrogen atoms and fourteen bonds to avoid the overlap with fused benzene rings (Figure 4-17b). The resonance structure based on this inner circuit is consistent with the BLA observed in the crystal structure of **NiTBNc**. **NiDBNc** also should have the contribution of this resonance structure, because the ACID plots suggest main ring currents of Ni^{II} norcorroles flow along the inner pathway. The predominance of the inner paratropic ring current is consistent with previously reported theoretical results.[34,35] If this is the case, the benzo-fusion would not disturb the 16π-conjugation of the inner circuit and the narrowed HOMO–LUMO gap by the orbital interactions would increase the paratropic ring current.
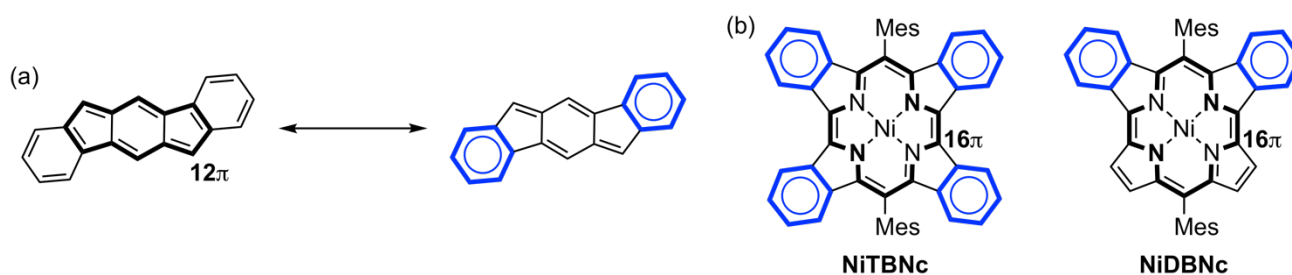

Figure 4-17. (a) Resonance structures of indenofluorene and (b) inner conjugation circuit of benzonorcorroles.

4-7. Summary of Chapter 4

In this study, Ni^{II} benzonorcorroles **NiTBNc** and **NiDBNc** have been synthesized through retro-Diels–Alder reaction and their properties have been systematically investigated along with **NiNc**. ^{1}H NMR spectra and DFT calculations revealed that the introduction of fused benzene rings unexpectedly resulted in substantial enhancement of the paratropic ring current due to their narrow HOMO–LUMO gaps. The incensement in the paratropic ring current is completely opposite to the general cases of antiaromatic compounds, in which antiaromaticity is reduced by benzo-fusion. Moreover, VT-NMR study and SQUID experiments elucidated the singlet diradical character of **NiTBNc**. Theoretical studies also supported open-shell characters of benzonorcorroles. These results demonstrate that the HOMO–LUMO manipulation by benzo-fusion can induce diradical character and strong antiaromatic ring current in 4n π-electron systems.
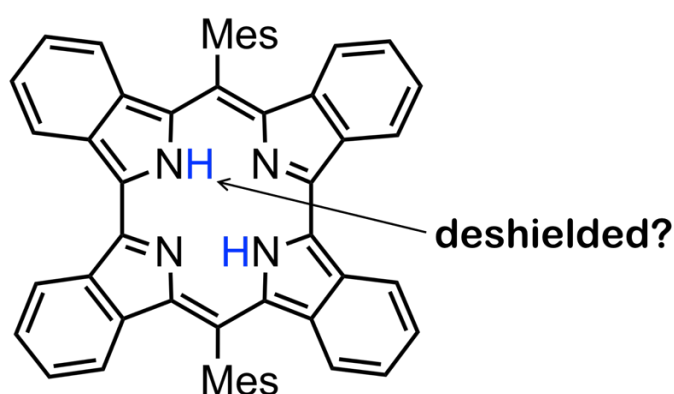
4-8. References

1. D. T. Chase, B. D. Rose, S. P. McClintock, L. N. Zakharov, M. M. Haley, *Angew. Chem. Int. Ed.* **2011**, *50*, 1127.

2. D. T. Chase, A. G. Fix, B. D. Rose, C. D. Weber, S. Nobusue, C. E. Stockwell, L. N. Zakharov, M. C. Lonergan, M. M. Haley, *Angew. Chem. Int. Ed.* **2011**, *50*, 11103.

3. A. Wakamiya, K. Mishima, K. Ekawa, S. Yamaguchi, *Chem. Commun.* **2008**, 579.

4. A. Iida, S. Yamaguchi, *J. Am. Chem. Soc.* **2011**, *133*, 6952.

5. J. A. Cissell, T. P. Vaid, A. G. DiPasquale, A. L. Rheingold, *Inorg. Chem.* **2007**, *46*, 7713.

6. E. W. Y. Wong, C. J. Walsby, T. Storr, D. B. Leznoff, *Inorg. Chem.* **2010**, *49*, 3343.

7. W. Zhou, R. H. Platel, T. T. Tasso, T. Furuyama, N. Kobayashi, D. B. Leznoff, *Dalton Trans.* **2015**, *44*, 13955.

8. S. Sugawara, Y. Hirata, S. Kojima, Y. Yamamoto, E. Miyazaki, K. Takimiya, S. Matsukawa, D. Hashizume, J. Mack, N. Kobayashi, Z. Fu., K. M. Kadish, Y. M. Sung, K. S. Kim, D. Kim, *Chem. Eur. J.* **2012**, *18*, 3566.

9. M. Ishida, S.-J. Kim, C. Preihs, K. Ohkubo, J. M. Lim, B. S. Lee, J. S. Park, V. M. Lynch, V. V. Roznyatovskiy, T. Sarma, P. K. Panda, C.-H. Lee, S. Fukuzumi, D. Kim, J. L. Sessler, *Nat. Chem.* **2013**, *5*, 15.

10. T. Furuyama, T. Sato, N. Kobayashi, *J. Am. Chem. Soc.* **2015**, *137*, 13788.

11. M. Nakano, R. Kishi, S. Ohta, H. Takahashi, T. Kubo, K. Kamada, K. Ohta, E. Botek, B. Champagne, *Phys. Rev. Lett.* **2007**, *99*, 033001.

12. M. Nakano and B. Champagne, *J. Phys. Chem. Lett.* **2015**, *6*, 3236.

13. K. Fukuda, T. Nagami, J. Fujiyoshi, M. Nakano, *J. Phys. Chem. A* **2015**, *119*, 10620.

14. T. Minami, M. Nakano, *J. Phys. Chem. Lett.* **2012**, *3*, 145.

15. S. Ito, T. Minami, M. Nakano, *J. Phys. Chem. C* **2012**, *116*, 19729.

16. Abe, M. *Chem. Rev.* **2013**, *113*, 7011.

17. Z. Sun, Z. Zeng, J. Wu, *Chem. Asian J.* **2013**, *8*, 2894.

18. C. Lambert, *Angew. Chem. Int. Ed.* **2011**, *50*, 1756.

19. Z. Sun, Q. Ye, C. Chi and J. Wu, *Chem. Soc. Rev.* **2012**, *41*, 7857.

20. T. Kubo, *Chem. Rec.* **2015**, *15*, 218.

21. A. Shimizu, R. Kishi, M. Nakano, D. Shiomi, K. Sato, T. Takui, I. Hisaki, M. Miyata, Y. Tobe, *Angew. Chem. Int. Ed.* **2013**, *52*, 6076.

22. G. E. Rudebusch, J. L. Zafra, K. Jorner, K. Fukuda, J. L. Marshall, I. Arrechea-Marcos, G. L. Espejo, R. P. Ortiz, C. J. Gómez-García, L. N. Zakharov, M. Nakano, H. Ottosson, J. Casado, M. M. Haley, *Nat. Chem.* **2016**, *8*, 753.

23. A. Konishi, Y. Okada, M. Nakano, K. Sugisaki, K. Sato, T. Takui, M. Yasuda, *J. Am. Chem. Soc.* **2017**, *139*, 15284.

24. S. Ito, T. Murashima, N. Ono, H. Uno, *Chem. Commun.* **1998**, 1661.

25. T. M. Krygowski, M. K. Cyranski, *Chem. Rev.* **2001**, *101*, 1385.

26. R. McWeeny, *Mol. Phys.* **1958**, *1*, 311.

27. J. Aihara, *Bull. Chem. Soc. Jpn.* **1985**, *58*, 1045.

28. D. F. Evans, D. Jakubovic, *J. Chem. Soc. Dalton Trans.* **1988**, 2927.

29. K. Yamaguchi, H. Fukui, T. Fueno, *Chem. Lett.* **1986**, 625.

30. K. Yamaguchi, In *Self-Consistent Field: Theory and Applications* (Eds.; R. Carbó, M. Klobukowski) Elsevier, **1990**, pp 727-828.

31. Z. Chen, C. S. Wannere, C. Corminboeuf, R. Puchta, P. v. R. Schleyer, *Chem. Rev.* **2005**, *105*, 3842.

32. M. Rosenberg, C. Dahlstrand, K. Kilså, H. Ottosson, *Chem. Rev.* **2014**, *114*, 5349.

33. D. Geuenich, K. Hess, F. Köhler, R. Herges, *Chem. Rev.* **2005**, *105*, 3758.

34. J. Aihara, *J. Phys. Chem. A* **2008**, *112*, 5305.

35. J. I. Wu, I. Fernández, P. v. R. Schleyer, *J. Am. Chem. Soc.* **2013**, *135*, 315.

Chapter 5

Synthesis of Free-Base Benzonorcorrole and Its Antiaromaticity

Contents

5-1. Introduction

Introduction of various elements into the core cavities of porphyrinoids has been widely explored.[1] Since each metal elements have different valances, electronic configuration, and ionic radius, metallation of porphyrins considerably alters their physical properties and structures depending on the natures of each metals. In this viewpoint, preparations of free-base porphyrinoids are an important subject, because they can derive a variety of metal complexes.

Another notable point of free-base porphyrinoids is the presence of inner protons, whose chemical shift in ^{1}H NMR measurement can be a reliable criterion to evaluate their (anti)aromaticity.[2-6] In Chapter 4, the enhanced antiaromaticity of Ni^{II} benzonorcorroles were demonstrated through observation of highly shielded outer protons of their macrocycles. Nevertheless, their strong deshielding effect in the core of macrocycles were evaluated only by calculations of their NICS values. Consequently, the author undertook the synthesis of free-base benzonorcorrole **H$_2$TBNc** (Figure 5-1), whose two inner NH groups should be exceptionally deshielded due to the strong antiaromaticity. Furthermore, the electrochemical properties, optical properties, molecular orbitals, and diradical character of **H$_2$TBNc** were compared with those of **NiTBNc** to examine the effects of the removal of the Ni^{II} ion from Ni^{II} benzonorcorrole.
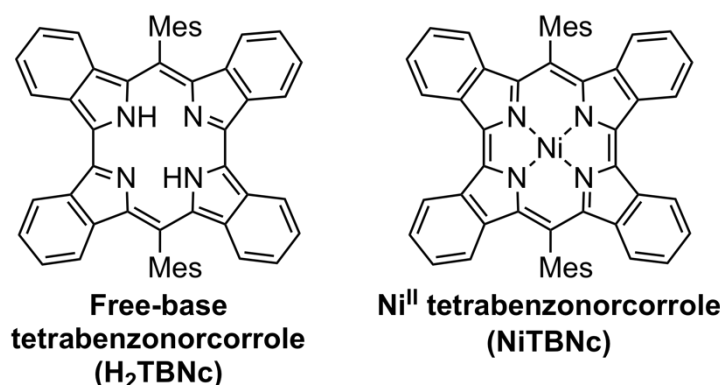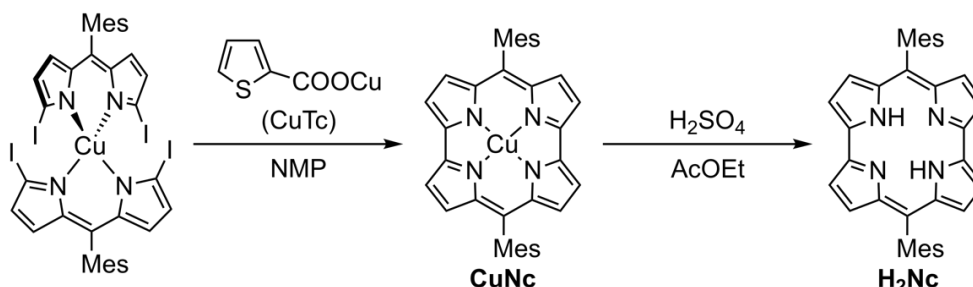

Free-base tetrabenzonorcorrole (H$_2$TBNc)

Ni^{II} tetrabenzonorcorrole (NiTBNc)

**Figure 5-1.** Structures of **H$_2$TBNc** and **NiTBNc**.

5-2. Synthesis and characterization of free-base tetrabenzonorcorrole

The synthesis of free-base norcorrole **H$_2$Nc** was previously achieved by demetallation of Cu^{II} norcorrole (**CuNc**), which was prepared by the Cu^{I}-mediated intermolecular coupling reaction of α,α'-diiododipyrrin Cu^{II} complex (Scheme 5-1).[7] This methodology was applied to the synthesis of **H$_2$TBNc**, where BCOD-fused materials were employed as precursors in the similar fashion as the synthesis of Ni^{II} benzonorcorroles (Scheme 5-2). BCOD-fused α,α'-diiododipyrrin **13** was successfully prepared by iodination and following oxidation reactions of BCOD-fused dipyrromethane. The dimerization of **13** with Cu^{II} acetate afforded the corresponding dipyrrin Cu^{II} complex **14**, which was converted to BCOD-fused Cu^{II} norcorrole **15** through intermolecular coupling with Cu^{I} 2-thiophenecarboxylate (CuTc). Crude **15** was treated with sulfuric acid to yield demetalated

BCOD-fused norcorrole **16**, which was converted to the target **H₂TBNc** by a retro-Diels–Alder reaction at 220 °C. The stability of **H₂TBNc** was lower than that of **NiTBNc**, so that **H₂TBNc** in solution was readily oxidized by atmospheric oxygen to afford 10-oxacorrole **17** and ring-opened compound **18** (Scheme 5-3). As **H₂TBNc** was stable under inert gas, the product was isolated by recrystallization in a glove box.

Scheme 5-1. Previous reported synthesis of **H₂Nc**.
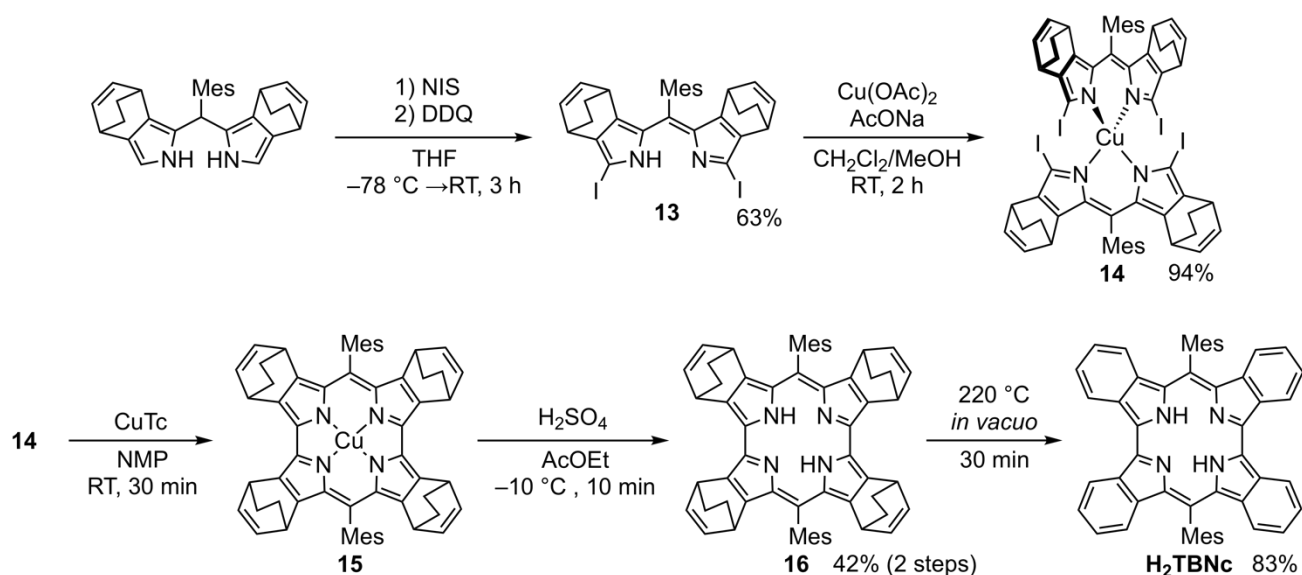
Scheme 5-2. Synthesis of free-base benzonorcorrole **H₂TBNc**.
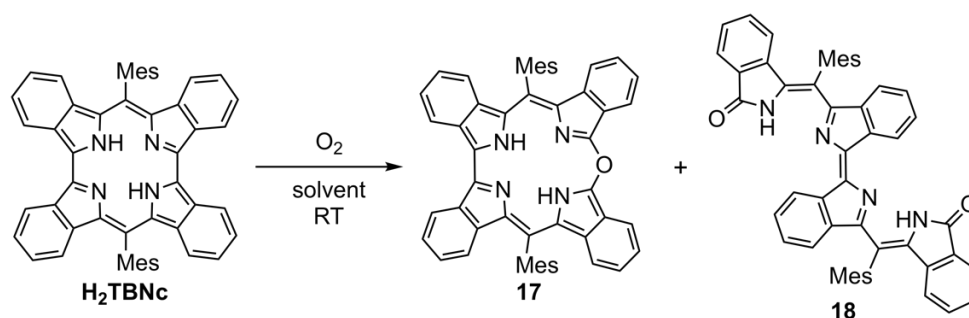
Scheme 5-3. Oxidation of **H₂TBNc** by atmospheric oxygen.

The structure of **H₂TBNc** was unambiguously elucidated by X-ray diffraction analysis (Figure 5-2). **H₂TBNc** adopts slightly distorted conformation due to the steric repulsion between inner NH groups.[7] Although **NiTBNc** exhibited a different type of BLA in which C–C bonds between pyrrole-α carbons (C_α–C_α bonds) had double bond character, such change is not found in the BLA of **H₂TBNc**. (Figure 5-3). Instead the BLA of **H₂TBNc** is similar to that of **H₂Nc**, whose C_α–C_α bonds can be regarded as single bonds. The HOMA values[8] of **H₂Nc**, **H₂TBNc**, and **NiTBNc** based on their crystal structures are summarized in Table 5-1. The value of **H₂TBNc** (0.62) is higher than that of **H₂Nc** (0.50) but is substantially smaller than that of **NiTBNc** (0.81).
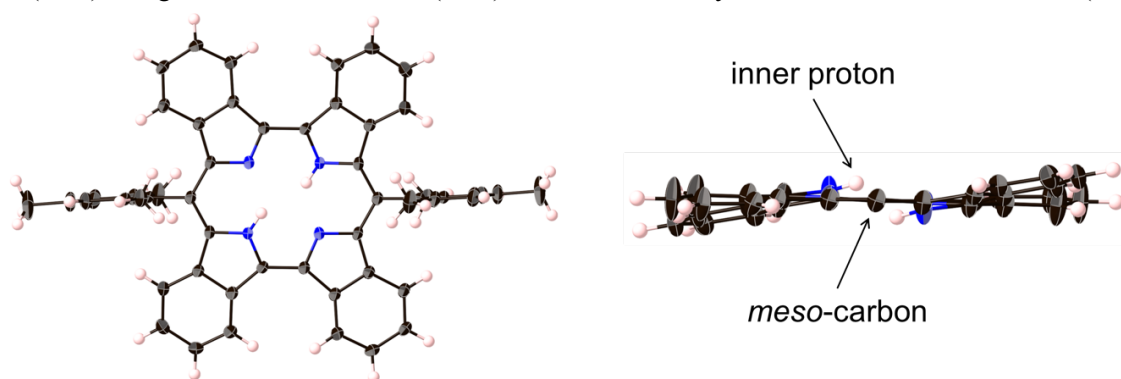

Figure 5-2. Top view (left) and side view (right) of X-ray crystal structure of **H₂TBNc**. Atomic displacement parameters set at 50% probability and mesityl groups are omitted for clarity.
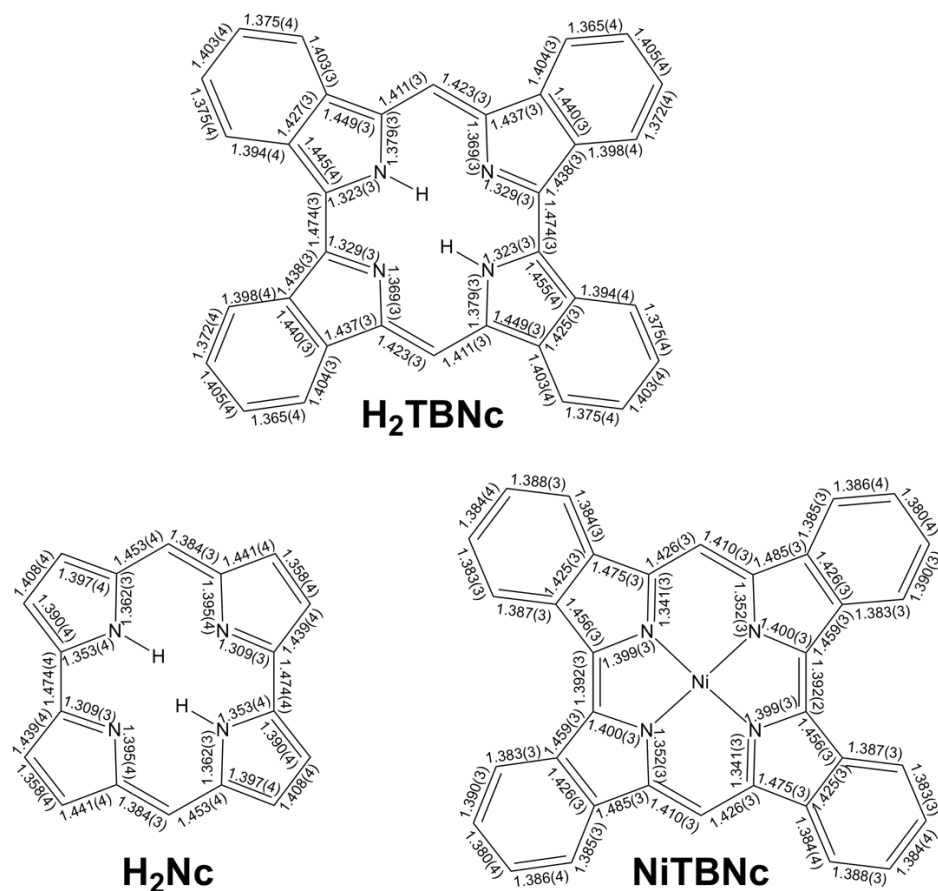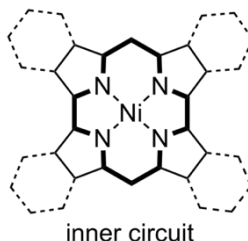

Figure 5-3. Bond lengths in crystal structures of **H₂Nc**, **H₂TBNc**, and **NiTBNc**.

Table 5-1. Summary of HOMA values of **H₂Nc**, **H₂TBNc**, and **NiTBNc** calculated based on inner conjugation circuits of norcorroles consisted of 6 C–C bonds and 8 C–N bonds (right).

Compound	X-ray structure
H₂Nc	0.50
H₂TBNc	0.62
NiTBNc	0.81

inner circuit

The ^{1}H NMR spectrum of **H₂TBNc** in toluene-d_8 is displayed in Figure 5-4. Importantly, its inner NH proton appeared around 57 ppm as a broaden signal, supporting the strong deshielding effect inside the macrocycle. Since the inner proton of **H₂Nc** was observed at 32.6 ppm in CDCl₃,[7] this highly deshielded signal of **H₂TBNc** clearly indicates its enhanced antiaromaticity by the fusion of benzene rings. As well as the inner protons, other protons of **H₂TBNc** were observed as obscure or broaden signals. The variable-temperature (VT) ^{1}H NMR spectra recorded from –80 °C to 80 °C revealed the temperature-dependence of these signals (Figure 5-5). The signals sharpened with the decrease of the temperatures but were broadened at higher temperatures. The spectrum at –80 °C allowed to observe the inner proton as a clear signal. This temperature-dependence suggests a diradical character of **H₂TBNc** as was observed in **NiTBNc**. Meanwhile, the diradical character of **H₂TBNc** would be less than that of **NiTBNc** judging from the comparison of their VT ^{1}H NMR spectra, in which the shifts of each signal of **H₂TBNc** were smaller than that of **NiTBNc** (see also Figure 4-10).
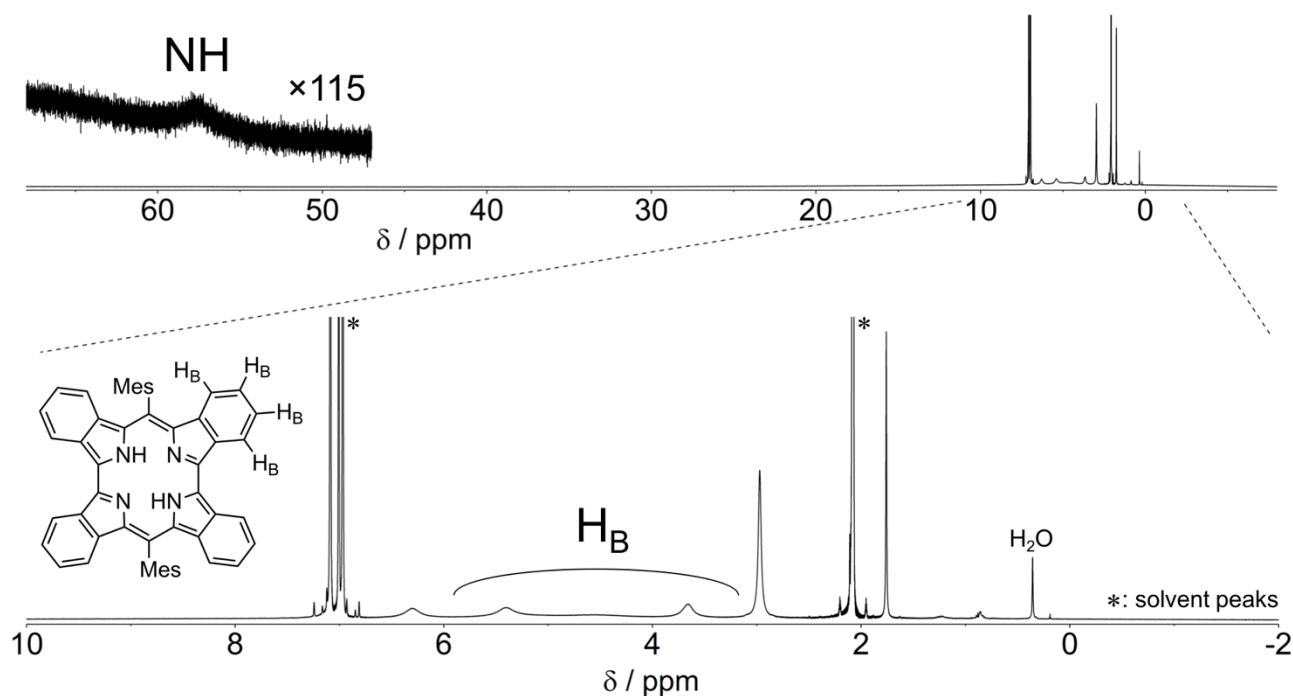
Figure 5-4. ^{1}H NMR spectrum (500 MHz) of **H₂TBNc** in toluene-d_8 at room temperature.
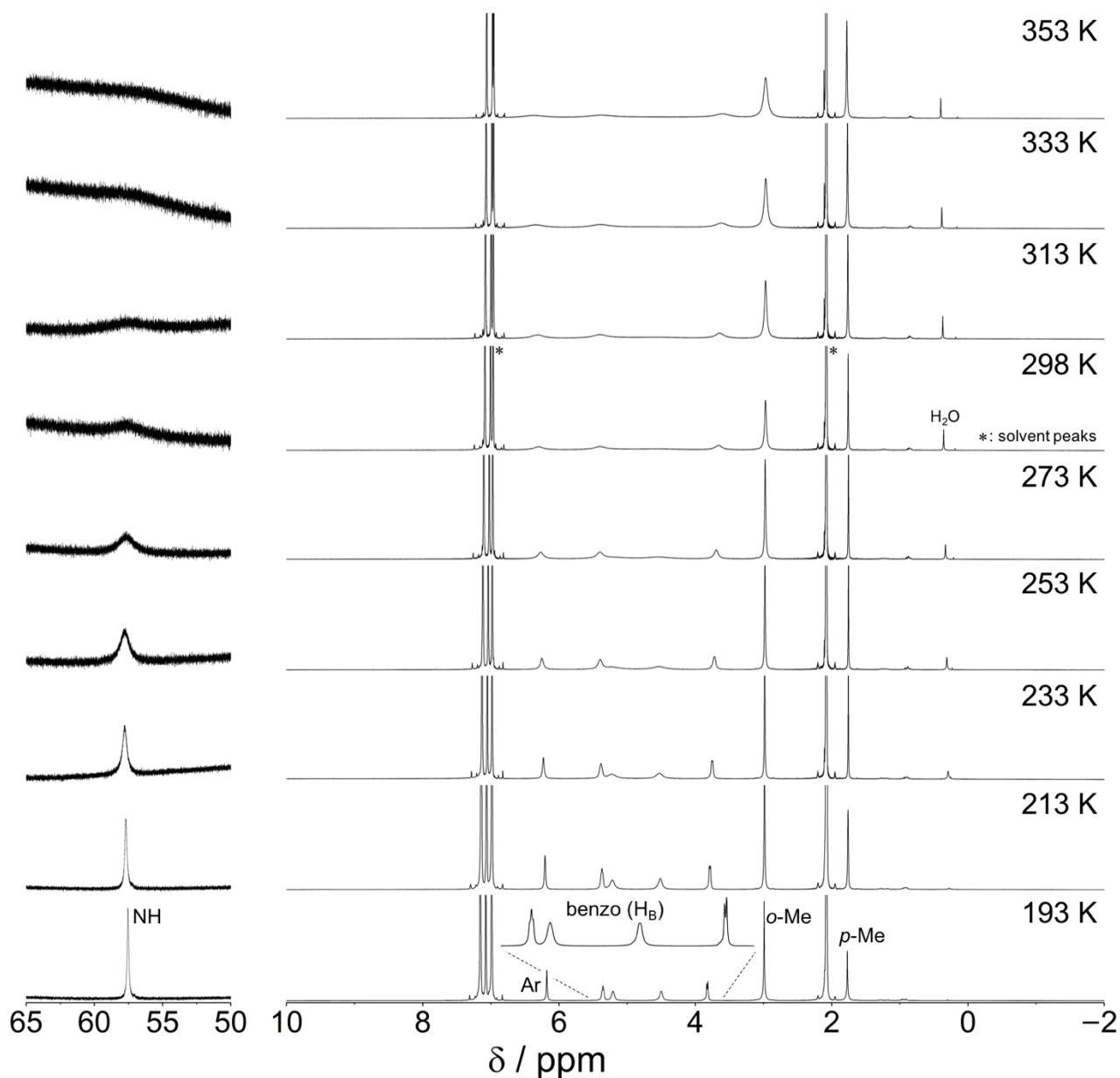
Figure 5-5. Variable temperature ^{1}H NMR (500 MHz) spectra of **H$_2$TBNc** in toluene-d_8.

5-3. Electrochemical and optical properties

Cyclic voltammogram of **H$_2$TBNc** was measured in CH$_2$Cl$_2$ and is compared with voltammograms of **H$_2$Nc** and **NiTBNc** (Figure 5-6). The cathodically shifted first oxidation potential of **H$_2$TBNc** (–0.26 V) results in the substantially smaller electrochemical energy gap **H$_2$TBNc** (0.86 V) than that of **H$_2$Nc** (1.36 V). Although the energy gap of **H$_2$TBNc** is slightly larger than that of **NiTBNc** (0.75 V), each redox process of these two benzonorcorroles is situated in similar potentials.

Figure 5-6. Cyclic voltammograms (0.1 V•s^{-1}) of **H₂Nc**, **H₂TBNc**, and **NiTBNc** in CH$_2$Cl$_2$ (0.1 M TBAPF$_6$). Working electrode: grass carbon, counter electrode: Pt, reference electrode: Ag/AgClO$_4$.

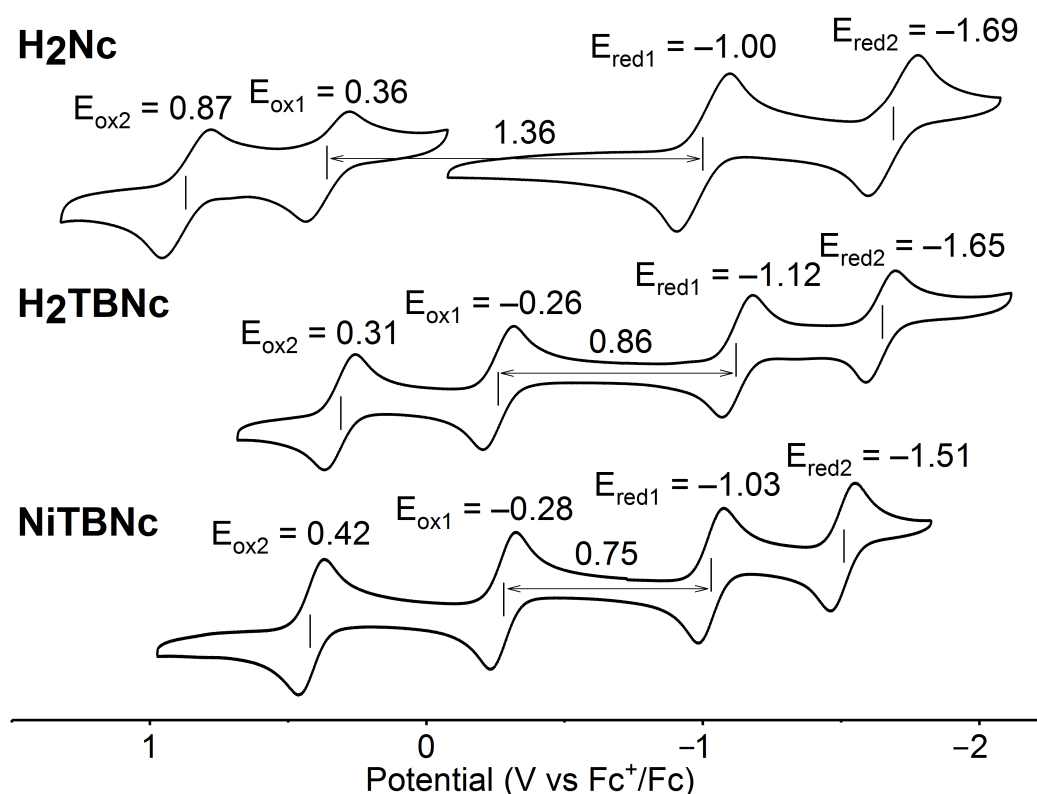The UV-vis-NIR absorption spectra in CH$_2$Cl$_2$ of **H₂Nc**, **H₂TBNc**, and **NiTBNc** are displayed in Figure 5-7a. The absorption envelope in the UV-visible region of **H₂TBNc** was broadened as compared to the sharp spectrum of **NiTBNc**, presumably due to the reduced symmetry of **H₂TBNc** by the removal of the Ni^{II} ion. The wavelength of the forbidden HOMO–LUMO transition absorption of these norcorroles are shifted to lower energy regions in the order of **H₂Nc**>**H₂TBNc**>**NiTBNc**. This order is in good accordance with the electrochemical energy gap determined in the cyclic voltammograms. TD-DFT calculations nicely predicted the absorption spectra of norcorroles (Figure 5-7b, Table 5-2). The experimental absorption band around 1000 nm in the spectrum of **NiTBNc** is disappeared in that of **H₂TBNc**. The calculation for **NiTBNc** estimated the corresponding band as a transition of HOMO–1 to LUMO, which involve a d-orbital on the central Ni^{II} ion (Figure 5-8 in next section). Consequently, the absence of this band in the spectrum of **H₂TBNc** should be caused by the removal of Ni^{II}. In fact, no transition was calculated in the NIR region of **H₂TBNc** except for the HOMO–LUMO transition estimated at 2000 nm. This situation is similar to the theoretical spectrum of **H₂Nc**.
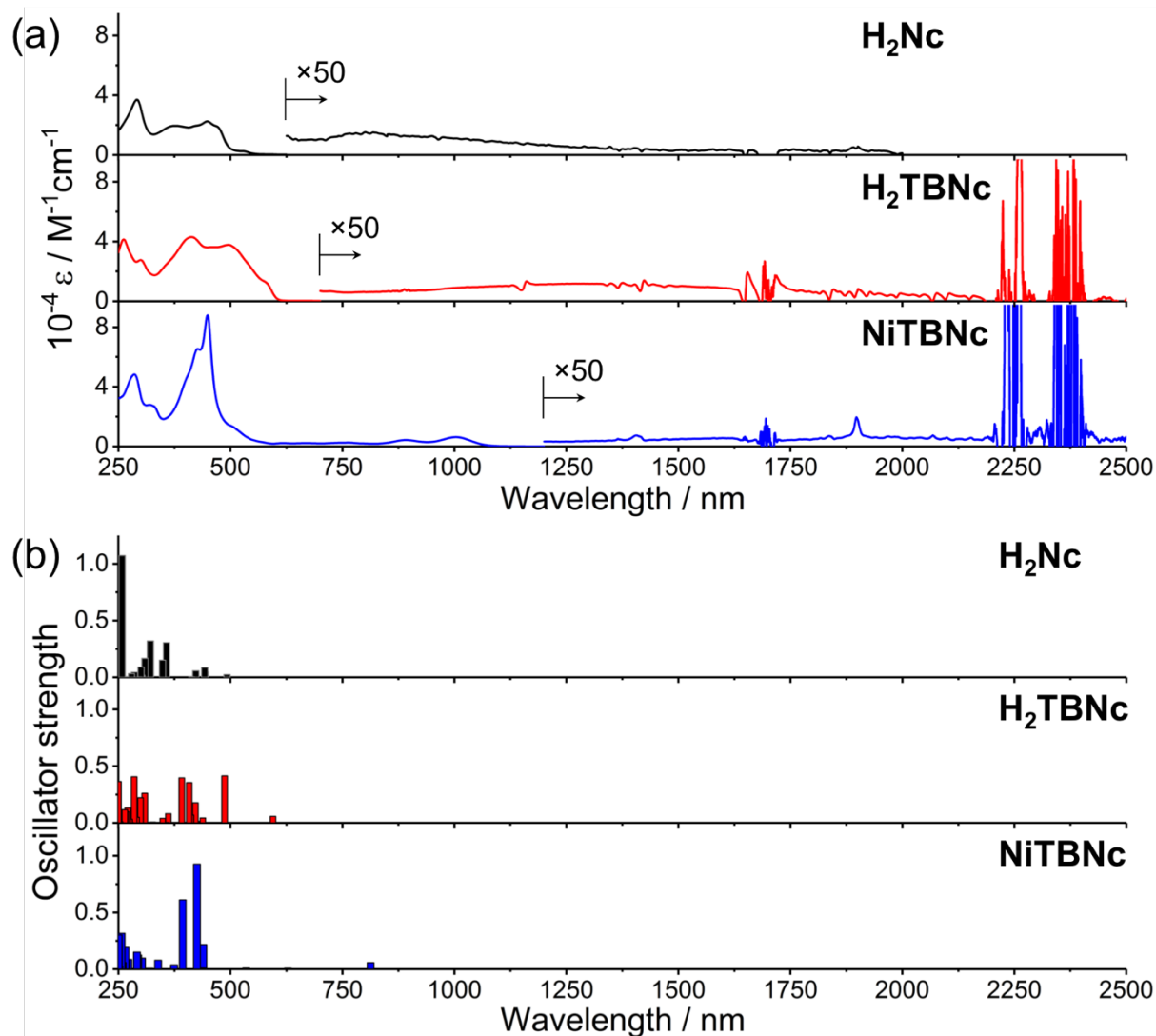
Figure 5-7. (a) UV-vis-NIR absorption spectra of **H₂Nc** (top), **H₂TBNc** (middle), and **NiTBNc** (bottom) in CH₂Cl₂ and (b) their theoretical absorption bands calculated at the RB3LYP/6-31G(d)+SDD level.

Table 5-2. Calculated exited wavelengths (λ) and oscillator strengths (*f*) of low-energy transitions of **H₂Nc**, **H₂TBNc**, and **NiTBNc**.

Compound	λ (nm)	*f*	Composition (%)
H₂Nc	1114.97	0.0000	HOMO→LUMO (100%)
	492.67	0.0249	HOMO−1→LUMO (58%)
			HOMO→LUMO+1 (42%)
H₂TBNc	2157.68	0.0000	HOMO→LUMO (100%)
	595.00	0.0580	HOMO−1→LUMO (72%)
			HOMO→LUMO+1 (28%)
NiTBNc	3166.16	0.0000	HOMO→LUMO (100%)
	812.74	0.0578	HOMO−1→LUMO (100%)

5-4. Molecular orbitals

Frontier orbitals of **H₂Nc**, **H₂TBNc**, and **NiTBNc** were compared by using DFT calculations at the RB3LYP/6-31G(d)+SDD level to evaluate the HOMO–LUMO energy gap of **H₂TBNc** (Figure 5-8). The HOMO of **H₂TBNc** (–4.17 eV) is substantially destabilized as compared with that of **H₂Nc** (–4.69 eV) due to antibonding interactions between orbitals on the core moiety and fused benzene rings, whereas the LUMO of **H₂TBNc** is not affected by the benzo-fusion. Consequently, the HOMO–LUMO energy gap of **H₂TBNc** (1.24 eV) is significantly smaller than that of **H₂Nc** (1.80 eV). As in the cases of Ni^{II} benzonorcorroles, the enhanced antiaromaticity of **H₂TBNc** should be attributed to its narrow HOMO–LUMO gap. Meanwhile, shapes of HOMO and LUMO of **H₂TBNc** are not inverted by the benzo fusion in contrast to the molecular orbitals of **NiTBNc**. The different distribution of HOMO is reflected in the BLA in the crystal structures of **H₂TBNc** and **NiTBNc**, in which C$_\alpha$–C$_\alpha$ bonds of **H₂TBNc** shows single bond character but that of **NiTBNc** shows double bond character (Figure 5-3). The calculated HOMO–LUMO energy gaps of these norcorroles are consistent with the results of electrochemical and optical measurements.
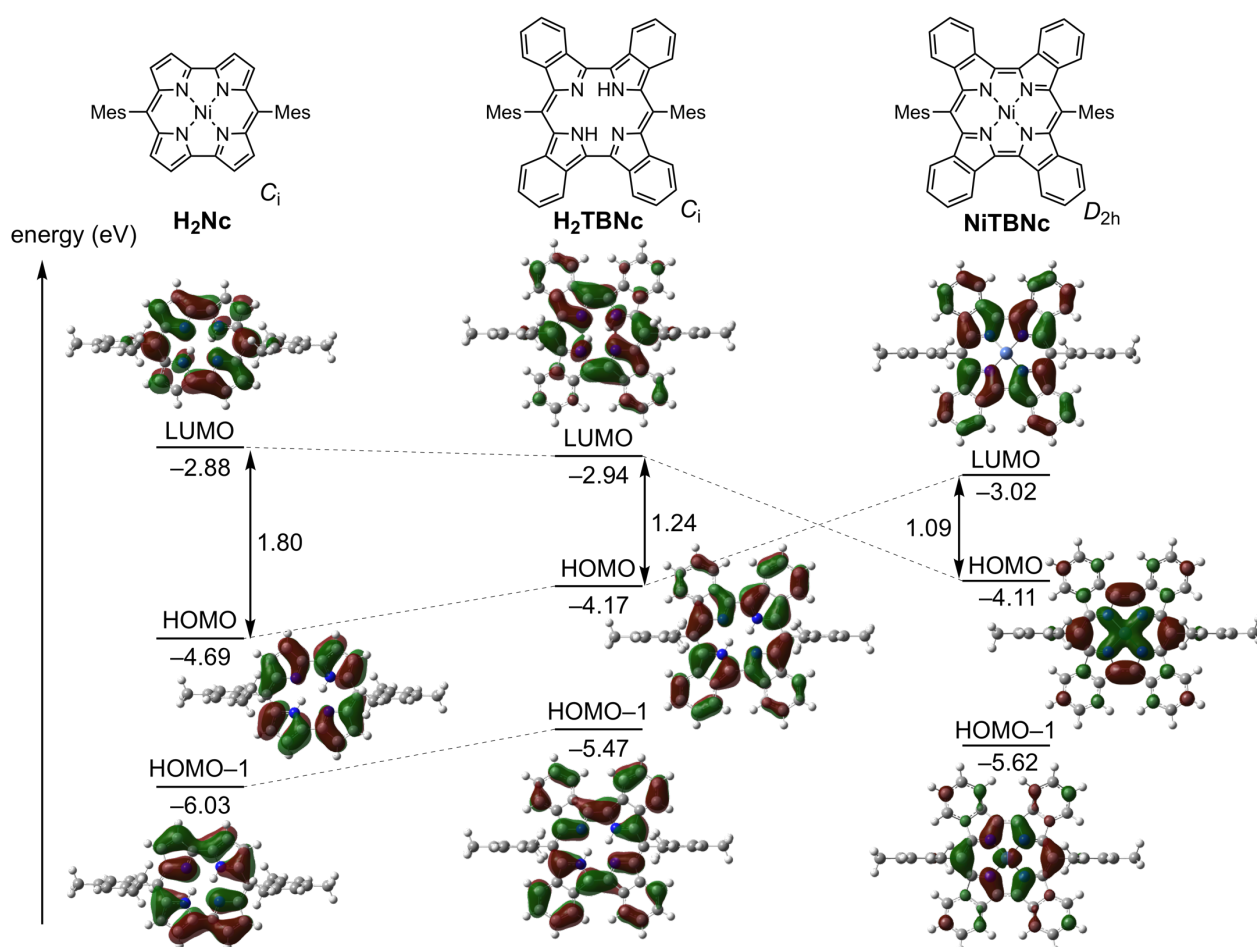

Figure 5-8. MO diagrams for **H₂Nc**, **H₂TBNc**, and **NiTBNc** calculated at the RB3LYP/6-31G(d)+SDD level.

5-5. Evaluation of antiaromaticity by computational studies

In order to evaluate the antiaromaticity in a computational approach, NICS(0)[9] of **H₂Nc** and **H₂TBNc** were calculated by the DFT method (Figure 5-9). As the diradical character of **H₂TBNc** was suggested, the calculations were performed using the unrestricted method as well as the restricted method to consider an influence of the open-shell character. Although the calculations on open- and closed-shell states afforded different NICS(0) values for **H₂TBNc**, both of the methods estimated substantially larger NICS(0) values of **H₂TBNc** at the positions of 1–3 (74–117 ppm) than those of **H₂Nc** (17–22 ppm). The reduced values in the open shell calculation of **H₂TBNc** imply a contribution of its diradical character. The antiaromaticity was also evaluated by visualizing the ring current using the ACID method (Figure 5-10)[10]. **H₂TBNc** showed the considerably large anticlockwise paratropic ring current as **NiTBNc**, which is obviously enhanced than that of **H₂Nc**. These theoretical studies clearly demonstrated the enhanced antiaromaticity (paratropic ring current) of **H₂TBNc** by the effects of the benzo-fusion.
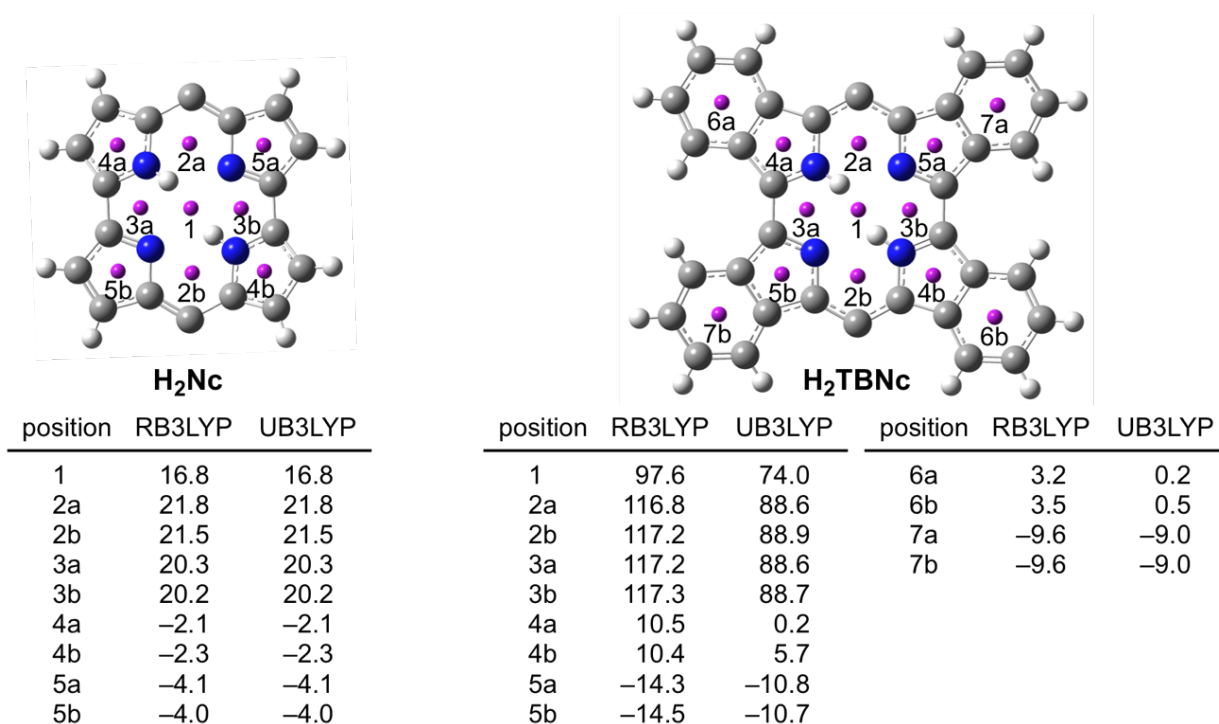

H₂Nc

position	RB3LYP	UB3LYP
1	16.8	16.8
2a	21.8	21.8
2b	21.5	21.5
3a	20.3	20.3
3b	20.2	20.2
4a	−2.1	−2.1
4b	−2.3	−2.3
5a	−4.1	−4.1
5b	−4.0	−4.0

H₂TBNc

position	RB3LYP	UB3LYP	position	RB3LYP	UB3LYP
1	97.6	74.0	6a	3.2	0.2
2a	116.8	88.6	6b	3.5	0.5
2b	117.2	88.9	7a	−9.6	−9.0
3a	117.2	88.6	7b	−9.6	−9.0
3b	117.3	88.7			
4a	10.5	0.2			
4b	10.4	5.7			
5a	−14.3	−10.8			
5b	−14.5	−10.7			

Figure 5-9. NICS(0) values of **H₂Nc** and **H₂TBNc** calculated at the B3LYP/6-31G(d)+SDD level of theory using X-ray crystal geometries.
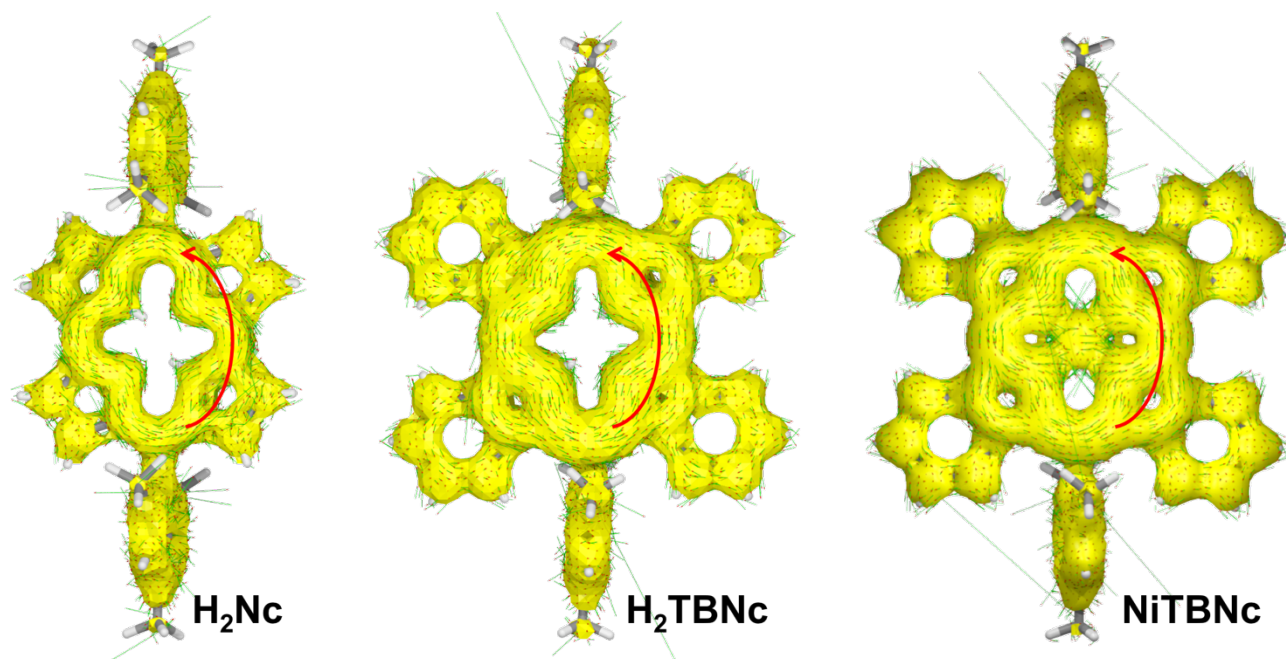
Figure 5-10. ACID-derived induced-ring-current maps for **H₂Nc**, **H₂TBNc**, and **NiTBNc** calculated at the UB3LYP/6-31G(d)+SDD level of theory using X-ray crystal geometries. Red arrows indicate the overall directions of ring currents.

5-6. Summary of Chapter 5

Free-base tetrabenzonorcorrole **H₂TBNc** was synthesized by the previously reported synthetic methodology of a free-base norcorrole combined with the retro-Diels–Alder reaction to form the fused benzene rings. **H₂TBNc** showed extremely deshielded inner protons in the ^{1}H NMR spectrum, indicating its enhanced antiaromatic character as compared with free-base norcorrole **H₂Nc**. The HOMO–LUMO energy gap of **H₂TBNc** is considerably decreased by the benzo-fusion to conclude the strong antiaromaticity is induced by the small HOMO–LUMO gap as in the case of **NiTBNc**. The computational analyses also supported the enhanced paratropic ring current of **H₂TBNc**. Further studies on properties of **H₂TBNc** and its metallation reactions to prepare various benzonorcorroles metal complexes are currently ongoing.

5-7. References

1. A. Mironov, in *Handbook of Porphyrin Science*, *Vol. 18* (Eds.: K. M. Kadish, K. M. Smith, R. Guilard) World Scientific, Singapore, **2012**, pp 303-413.

2. C. Liu, D.-M. Shen, Q.-Y. Chen, *J. Am. Chem. Soc.* **2007**, *129*, 5814.

3. M. Suzuki, A. Osuka, *J. Am. Chem. Soc.* **2007**, 129, 464.

4. M.-C. Yoon, S. Cho, M, Suzuki, A. Osuka, D. Kim, *J. Am. Chem. Soc.* **2009**, *131*, 7360.

5. M. Umetani, T. Tanaka, T. Kim, D. Kim, A. Osuka, *Angew. Chem. Int. Ed.* **2016**, *55*, 8095.

6. A. Yamaji, H. Tsurugi, Y. Miyake, K. Mashima, H. Shinokubo, *Chem. Eur. J.* **2016**, *22*, 3956.

7. T. Yonezawa, S. A. Shafie, S. Hiroto, H. Shinokubo, *Angew. Chem. Int. Ed.* **2017**, *56*, 11822.

8. T. M. Krygowski, M. K. Cyranski, *Chem. Rev.* **2001**, *101*, 1385.

9. Z. Chen, C. S. Wannere, C. Corminboeuf, R. Puchta, P. v. R. Schleyer, *Chem. Rev.* **2005**, *105*, 3842.

10. D. Geuenich, K. Hess, F. Köhler, R. Herges, *Chem. Rev.* **2005**, *105*, 3758.

Chapter 6　　**Summary of This Thesis**

Although antiaromatic compounds have attracted much attention in fields of organic chemistry, theoretical chemistry, and materials chemistry due to their distinct properties, further development in the area of antiaromatic compounds have been hampered by their unstable natures and consequent synthetic difficulties. Nevertheless, rigid and highly delocalized π-systems of porphyrinoids have offered a relatively wide-range of research on synthesis and properties of antiaromatic porphyrinoids. Norcorrole is the especially noteworthy antiaromatic porphyrinoid among them. In spite of the distinct antiaromaticity based on its 16π-electron system, norcorrole shows exceptional stability and is easily preparable in a gram-scale synthesis. Consequently, the author regarded norcorrole as a promising motif to transform the chemistry of antiaromatic compounds.

In this thesis, the author has described synthesis of novel antiaromatic norcorrole derivatives through the peripheral modifications employing several different approaches. The peripherally modified norcorroles underwent various changes in their properties depending on the fashions of functionalization.

Chapter 2 has described the method to introduce various aryl groups to *meso*-positions of norcorroles. Although symmetrical substitution by electron-donating or -withdrawing aryl groups resulted in loss of the stability of norcorroles, dissymmetrical substitution allowed designing stable *meso*-modified norcorroles. The dissymmetric norcorroles displayed intense absorption bands in the low-energy region, which were assigned to CT transitions by several experimental and theoretical evidences. Since these norcorroles took various packing structures depending on the *meso*-substituents, their carrier conductivity was evaluated using TRMC technics.

Chapter 3 has dealt with the facile direct amination reaction of norcorrole. One or two amino groups readily attacked pyrrole-β positions of norcorrole to afford aminated norcorroles regioselectively in high yields. The regioselectivity of the aminations was nicely accounted for by molecular orbitals of norcorroles. The aminonorcorroles exhibited highly electron-rich character because of strong electronic perturbation by the introduced amino groups.

In Chapter 4 and Chapter 5, benzonorcorroles have been synthesized to investigated effects of the fused benzene ring on the antiaromaticity of norcorrole. The benzo-fusion resulted in significant decrease of the HOMO–LUMO gaps and enhancement of the antiaromaticity, which are in sharp contrast to conventional benzo-fused antiaromatic compounds. Furthermore, small HOMO–LUMO gap also induced diradical character of benzonorcorroles. As a distinct antiaromaticity is basically not compatible with a diradical character in a 4n π-electron system, the present benzonorcorroles can be regarded as new class of antiaromatic compounds.

These studies in this thesis not only demonstrates effective peripheral modification of the antiaromatic porphyrinoid toward drastic modulations of its properties, but also would help understanding of antiaromaticity from the perspectives of stability (Chapter 2), reactivity (Chapter 3), and ring current effects associated with HOMO–LUMO energy gaps (Chapter 4 and Chapter 5). The author believes that norcorrole still holds enormous potentials to design antiaromatic compounds with further fascinating structures and properties and hopes that this thesis will be contributory to such works in the future.

Experimental Section

Contents

E-1. Instruction and materials

^{1}H NMR (500 MHz), ^{13}C NMR (126 MHz) and ^{19}F NMR (470 MHz) spectra were recorded on a Bruker AVANCE III HD spectrometer. Chemical shifts were reported as the delta scale in ppm relative to $CDCl_3$ (δ = 7.26 ppm) or toluene-d_8 (2.08 ppm) for ^{1}H NMR and $CDCl_3$ (δ = 77.16 ppm) for ^{13}C NMR and hexafluorobenzene (δ = –164.90 ppm, external standard) for ^{19}F NMR. UV/vis/NIR absorption spectra were recorded on a JASCO V670 spectrometer. Mass spectra were recorded on a Bruker microTOF using ESI-TOF method for acetonitrile solutions. X-ray data were taken on a Bruker D8 QUEST X-ray diffractometer equipped with PHOTON 100 CMOS active pixel sensor detector and IμS microfocus source using Mo-Kα radiation (λ = 0.71073 Å) or a Rigaku CCD diffractometer (Saturn 724 with MicroMax-007) with Varimax Mo optics using graphite monochromated Mo-Kα radiation (λ = 0.71075 Å). Cyclic voltammograms were recorded on ALS electrochemical analyzer 612C. Measurements were performed in freshly distilled dichloromethane with 0.1 M tetrabutylammonium hexafluorophosphate as electrolyte. A three-electrode system was used and consisted of a grassy carbon working electrode, a platinum wire and $Ag/AgClO_4$ as the reference electrode. All potentials are referenced to the potential of ferrocene/ferrocenium cation couple. Unless otherwise noted, materials obtained from commercial suppliers were used without further purification.

E-2. Flash-photolysis time-resolved microwave conductivity measurements[1] (Chapter 2)

Transient photoconductivity was measured by flash-photolysis time-resolved microwave conductivity (FP-TRMC) method. A resonant cavity was used to obtain a high degree of sensitivity in the measurement of conductivity. The resonant frequency and the microwave power were set at ~9.1 GHz and 3 mW, respectively, so that the electric field of the microwave was sufficiently small not to disturb the motion of charge carriers. The value of conductivity is converted to the product of the quantum yield ϕ and the sum of charge carrier mobilities $\Sigma\mu$, by $\phi\Sigma\mu = \Delta\sigma (eI_0F_{light})^{-1}$, where e, I_0, F_{light}, and $\Delta\sigma$ are the unit charge of a single electron, incident photon density of excitation laser (photons/m^2), a correction (or filling) factor (/m), and a transient photoconductivity, respectively. The sample was set at the highest electric field in a resonant cavity. FP-TRMC experiments were performed at room temperature. The charge carriers were injected into the samples

via photo-ionization by direct excitation with a third harmonic generation (λ = 355 nm) light pulses from a Nd: YAG laser (spectra Physics, INDI-HG). The excitation density was tuned at 9.1×10^{15} cm^{-2} photons per pulse.
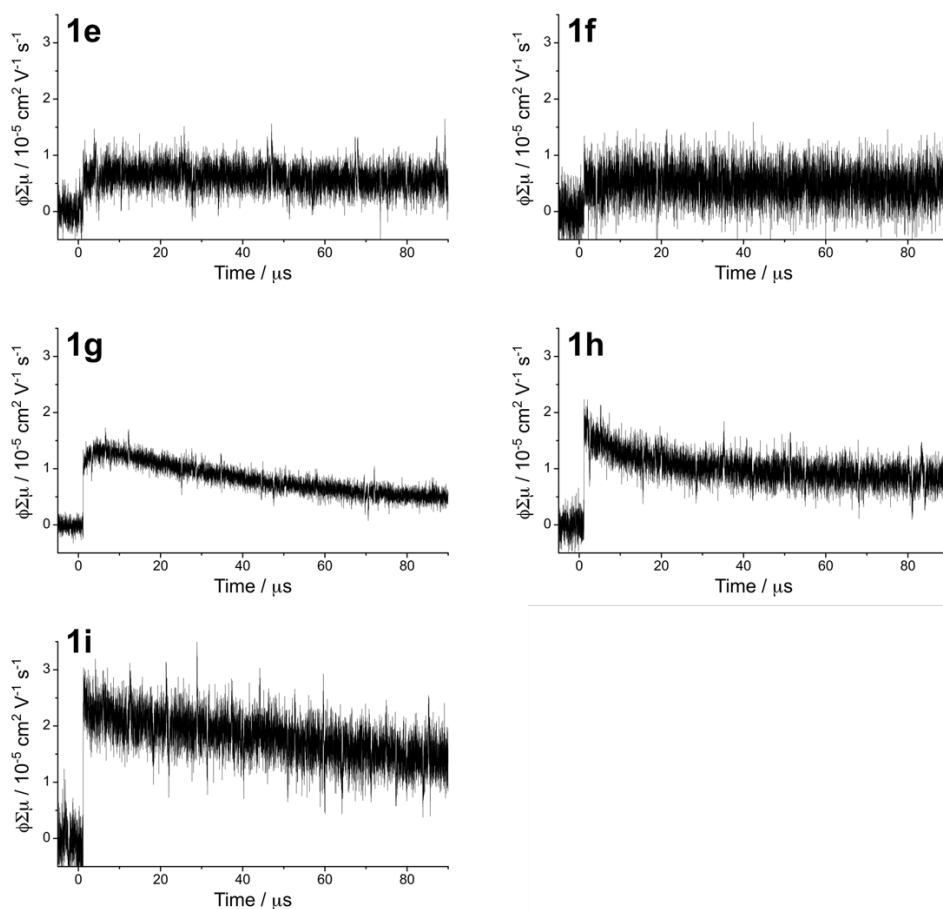

Figure E1. Time-resolved microwave conductivities **1e–1i**. Crystalline samples were used for measurement of **1e**, **1f**, **1h**, and **1i**, and a powder sample was used for measurement of **1g**.

E-3. Temperature dependent magnetic property (Chapter 4)

The solid-state temperature-dependent magnetic susceptibilities (x_pT) of **NiTBNc** were measured between 100 and 350 K under a magnetic field of 0.5 T on a Quantum Design MPMS-7 SQUID magnetometer. The solution-state temperature-dependent magnetic susceptibilities (x_pT) of **NiTBNc** were determined by the Evans method in toluene-d_8 solution using toluene as the chemical shift reference.[2] The temperature-dependent magnetic susceptibilities (x_pT_1) were also determined at various temperatures relative to that of high-spin Fe(TPP)Cl (x_pT_2 = 4.38 emu K mol^{-1}) according to $x_pT_1 = (\Delta n_1/\Delta n_2)^{1/2} x_pT_2$.[3] J_{S-T} values were derived from each measurements by the least-square curve fitting of the χ_pT values using the Bleaney–Bowers equation.[4]

E-4. Theoretical calculations

Chapter 2

All calculations were carried out using the *Gaussian 09* program.[5] Initial geometries of **1e** and **1i** were obtained from their X-ray structures. Part of the X-ray Structure of **1f** and **1i** was used as initial geometries of **1a** and **1d**, respectively. Full optimizations were performed with Becke's three-parameter hybrid exchange functional and the Lee–Yang–Parr correlation functional (B3LYP)[6,7] and a basis set consisting of SDD[8] for Ni and 6-31G(d) for the rest (denoted as 6-31(G)+SDD). The calculated absorption wavelengths and oscillator strengths were obtained with the TD-DFT method at the RB3LYP/6-31(G)+SDD level.

Chapter 3

All calculations were carried out using the *Gaussian 09* program. Part of the X-ray Structure of **2b** was used as initial geometries of **2a'** and **2b'**. Full optimizations were performed with Becke's three-parameter hybrid exchange functional and the Lee–Yang–Parr correlation functional (B3LYP) and a basis set consisting of SDD for Ni and 6-31G(d) for the rest). The calculated absorption wavelengths and oscillator strengths were obtained with the TD-DFT method at the RB3LYP/6-31G(d)+SDD level.

Chapter 4

All calculations were carried out using the *Gaussian 09* program. Initial geometries of **NiTBNc** and **NiDBNc** were obtained from their X-ray structures. Calculations were performed with Becke's three-parameter hybrid exchange functional and the Lee–Yang–Parr correlation functional (B3LYP) and the SDD basis set was used for Ni. Geometry optimizations were performed at the RB3LYP/6-31G(d)+SDD level of approximation. Frequency analysis for the optimized geometry was performed in order to confirm the local minimum. J_{S-T} values were estimated with the total energies and $<S^2>$ values of the open-shell singlet and triplet configurations.[9] The diradical character, y, was inferred from the occupation number of the lowest unoccupied natural orbital (LUNO) calculated at the LC-UBLYP/6-31G(d)+SDD level using the DFT-optimized geometries.[10] The calculated absorption wavelengths and oscillator strengths were obtained with the TD-DFT method at the RB3LYP/6-31G(d)+SDD level.

Chapter 5

All calculations were carried out using the *Gaussian 09* program. Initial geometries of **H₂TBNc** and **H₂Nc** were obtained from their X-ray structures. Calculations were performed with Becke's three-parameter hybrid exchange functional and the Lee–Yang–Parr correlation functional (B3LYP) and the SDD basis set was used for Ni. The calculated absorption wavelengths and oscillator strengths were obtained with the TD-DFT method at the RB3LYP/6-31G(d)+SDD level.

E-5. Synthetic procedures and compounds data

Chapter 2
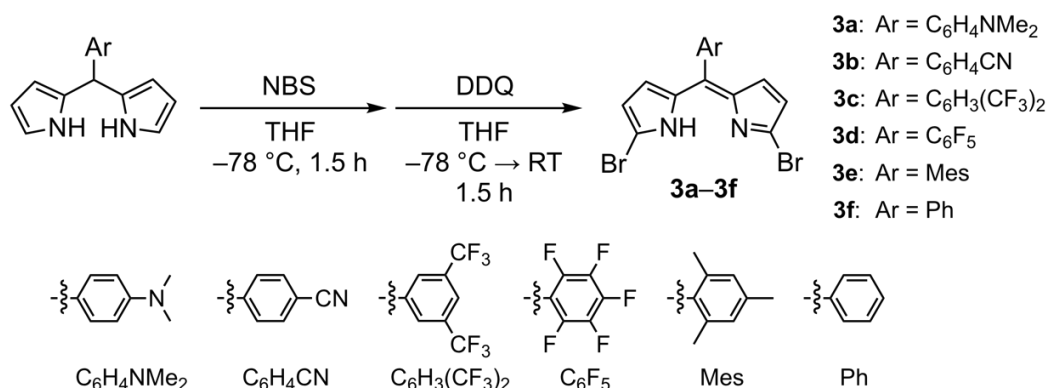
Scheme E1. Synthesis of α,α'-Dibromodipyrrins **3a–3f**. **3c–3f** were prepared according to literature procedures.[11-14]

meso-4-Dimethylaminophenyl-α,α'-dibromodipyrrin 3a

A two-necked flask containing *meso*-4-dimethylaminophenyldipyrromethane[15] (1.04 g, 3.92 mmol) was evacuated and then refilled with N_2. To the flask, dry THF (55 mL) was added and the solution was cooled to −78 °C. After *N*-bromosuccinimide (1.40 g, 7.87 mmol) was added to the solution in two portions at a 30 min interval, the mixture was stirred for 1 h. Then 2,3-dichloro-5,6-dicyano-1,4-benzoquinone (DDQ, 891 mg, 3.93 mmol) was added in three portions every 15 min. The resulting mixture was stirred at −78 °C for 10 min and then warmed to room temperature. After stirring for additional 1 h, the reaction mixture was filtered through a short pad of alumina (CH_2Cl_2 as an eluent) and then evaporated. Purification by silica-gel column chromatography (CH_2Cl_2 as an eluent) afforded the title compound **3a** in 50% (825 mg, 1.96 mmol) as a red solid.

^{1}H NMR (500 MHz, CDCl$_3$): δ 12.54 (brs, ^{1}H, NH), 7.37 (d, *J* = 8.9 Hz, 2H, aryl), 6.74 (d, *J* = 8.9 Hz, 2H, aryl), 6.63 (d, *J* = 4.2 Hz, 2H, *β*-H), 6.35 (d, *J* = 4.2 Hz, 2H, *β*-H), 3.05 (s, 6H, NMe$_2$) ppm. ^{13}C NMR (126 MHz, CDCl$_3$): δ 151.6, 141.3, 140.3, 133.1, 130.3, 128.1, 123.2, 119.8, 111.2, 40.4 ppm. HR-MS (ESI-MS): *m/z* = 421.9686, calcd for (C$_{17}$H$_{16}$Br$_2$N$_3$)$^+$ = 421.9686 [(M + H)$^+$].

meso-4-Cyanophenyl-α,α'-dibromodipyrrin 3b

A two-necked flask containing *meso*-4-cyanophenyldipyrromethane[16] (1.24 g, 5.01 mmol) was evacuated and then refilled with N_2. To the flask, dry THF (70 mL) was added and the solution was cooled to −78 °C. After *N*-bromosuccinimide (1.78 g, 10.0 mmol) was added to the solution in two portions at a 30 min interval, the mixture was stirred for 1 h. Then DDQ (1.14 g, 5.02 mmol) was added in two portion at a 30 min interval. The resulting mixture was stirred at −78 °C for 10 min then warmed to room temperature. After stirring for additional 1 h, the reaction mixture was filtered through a short pad of alumina (CH_2Cl_2 as an eluent) and then evaporated. Purification by silica-gel column chromatography (CH_2Cl_2/hexane = 1/1 as an eluent) afforded the title compound **3b** in 80% (1.61 g, 3.99 mmol) as an orange solid.

^{1}H NMR (500 MHz, CDCl$_3$): δ 12.37 (brs, 1H, NH), 7.76 (d, J = 8.5 Hz, 2H, aryl), 7.56 (d, J = 8.5 Hz, 2H, aryl), 6.36 (d, J = 4.3 Hz, 2H, β-H), 6.35 (d, J = 4.3 Hz, 2H, β-H) ppm. ^{13}C NMR (126 MHz, CDCl$_3$): δ 140.3, 139.9, 136.5, 131.9, 131.4, 130.8, 129.7, 121.3, 118.3, 113.4 ppm. HR-MS (ESI-MS): m/z = 403.9204, calcd for (C$_{16}$H$_{10}$Br$_2$N$_3$)$^+$ = 403.9216 [(M + H)$^+$].
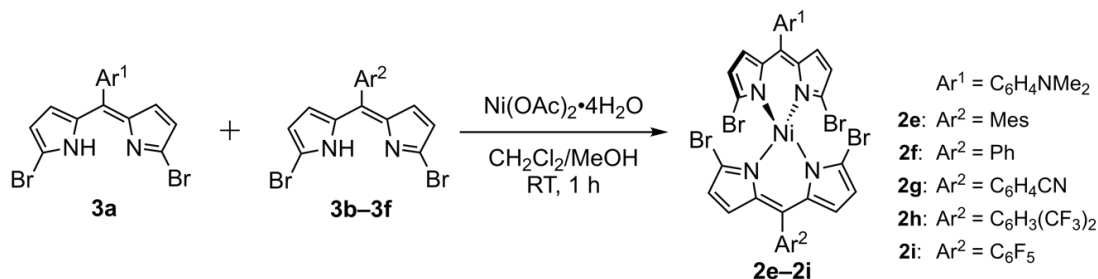
Scheme E2. Synthesis of α,α'-Dibromodipyrrins Ni^{II} complexes **2e–2i**.

Dissymmetric α,α'-dibromodipyrrin dimer Ni^{II} complex 2e

N(II) acetate tetrahydrate (175 mg, 0.703 mmol) dissolved in CH$_2$Cl$_2$/MeOH (10 mL/10 mL) was slowly added to a CH$_2$Cl$_2$/MeOH (40 mL/10 mL) solution of **3a** (295 mg, 0.700 mmol) and **3e**[13] (294 mg, 0.700 mmol) and the mixture was stirred for 1 h at room temperature. After the solvent was removed, silica-gel column chromatography (CH$_2$Cl$_2$/hexane = 2/3 as an eluent) was performed to collect the second eluting band. The residue after evaporation was washed with MeOH and the title compound **2e** was obtained in 35% (222 mg, 0.247 mmol) as a green solid.

HR-MS (ESI-MS): m/z = 897.8537, calcd for (C$_{35}$H$_{30}$Br$_4$N$_5$Ni)$^+$ = 867.8540 [(M + H)$^+$].

Dissymmetric α,α'-dibromodipyrrin dimer Ni^{II} complex 2f

Ni^{II} acetate tetrahydrate (125 mg, 0.502 mmol) dissolved in CH$_2$Cl$_2$/MeOH (7 mL/7 mL) was slowly added to a CH$_2$Cl$_2$/MeOH (30 mL/7 mL) solution of **3a** (211 mg, 0.501 mmol) and **3f**[14] (189 mg, 0.500 mmol) and the mixture was stirred for 1 h at room temperature. After the solvent was removed, silica-gel column chromatography (CH$_2$Cl$_2$/hexane = 1/1 as an eluent) was performed to collect the second eluting band. The residue after evaporation was washed with MeOH, and the title compound **2f** was obtained in 29% (124 mg, 0.145 mmol) as a green solid.

HR-MS (ESI-MS): m/z = 855.8057, calcd for (C$_{32}$H$_{24}$Br$_4$N$_5$Ni)$^+$ = 855.8070 [(M + H)$^+$].

Dissymmetric α,α'-dibromodipyrrin dimer Ni^{II} complex 2g

Ni^{II} acetate tetrahydrate (125 mg, 0.502 mmol) dissolved in CH$_2$Cl$_2$/MeOH (7 mL/7 mL) was slowly added to a CH$_2$Cl$_2$/MeOH (30 mL/7 mL) solution of **3a** (211 mg, 0.501 mmol) and **3b** (202 mg, 0.501 mmol), and the mixture was stirred for 1 h at room temperature. After the solvent was removed, silica-gel column chromatography (CH$_2$Cl$_2$/hexane = 2/1 as an eluent) was performed to collect the second eluting band. The residue after evaporation was washed with MeOH, and the title compound **2g** was obtained in 40% (177 mg, 0.201 mmol) as a green solid.

HR-MS (ESI-MS): m/z = 880.8031, calcd for (C$_{33}$H$_{23}$Br$_4$N$_6$Ni)$^+$ = 880.8023 [(M + H)$^+$].

### Dissymmetric α,α'-dibromodipyrrin dimer Ni[II] complex 2h

Ni[II] acetate tetrahydrate (187 mg, 0.751 mmol) dissolved in $CH_2Cl_2/MeOH$ (11 mL/11 mL) was slowly added to a $CH_2Cl_2/MeOH$ (54 mL/16 mL) solution of **3a** (316 mg, 0.750 mmol) and **3c**[11] (386 mg, 0.751 mmol), and the mixture was stirred for 1 h at room temperature. After the solvent was removed, silica-gel column chromatography (CH_2Cl_2/hexane = 1/1 as an eluent) was performed to collect the second eluting band. The residue after evaporation was washed with MeOH, and the title compound **2h** was obtained in 37% (274 mg, 0.276 mmol) as a green solid.

HR-MS (ESI-MS): *m/z* = 991.7821, calcd for $(C_{34}H_{22}Br_4F_6N_5Ni)^+$ = 991.7818 $[(M + H)^+]$.

Dissymmetric α,α'-dibromodipyrrin dimer Ni[II] complex 2i

Ni[II] acetate tetrahydrate (175 mg, 0.703 mmol) dissolved in $CH_2Cl_2/MeOH$ (10 mL/10 mL) was slowly added to a $CH_2Cl_2/MeOH$ (40 mL/10 mL) solution of **3a** (295 mg, 0.700 mmol) and **3d**[12] (328 mg, 0.701 mmol), and the mixture was stirred for 1 h at room temperature. After the solvent was removed, silica-gel column chromatography (CH_2Cl_2/hexane = 1/1 as an eluent) was performed to collect the second eluting band. The residue after evaporation was washed with MeOH, and the title compound **2i** was obtained in 38% (254 mg, 0.269 mmol) as a green solid.

HR-MS (ESI-MS): *m/z* = 945.7604, calcd for $(C_{32}H_{19}Br_4F_5N_5Ni)^+$ = 945.7599 $[(M + H)^+]$.
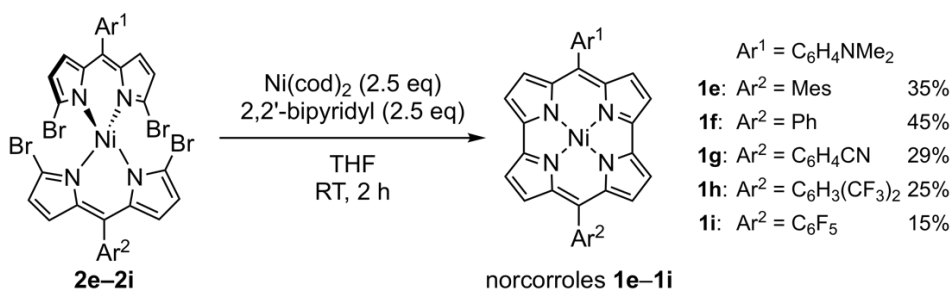
Scheme E3. Synthesis of dissymmetric norcorroles **1e–1i**.

Dissymmetric norcorrole 1e

Dipyrrin complex **2e** (89.8 mg, 0.100 mmol), bis(1,5-cyclooctadiene)nickel (68.8 mg, 0.250 mmol) and 2,2'-bipyridyl (39.0 mg, 0.250 mmol) were dissolved in dehydrated THF (8 mL) and the solution was stirred for 2 h at room temperature inside a glove box. After taking out the flask of the glove box, the reaction mixture was filtered through a short pad of alumina (CH_2Cl_2 as an eluent) immediately and then evaporated. The residue was purified by silica-gel column chromatography (CH_2Cl_2/hexane = 1/1 as an eluent) and the collected blue band was concentrated and washed with hexane. Recrystallization from CH_2Cl_2/acetonitrile afforded the title compound **1e** in 35% (20.5 mg, 35.4 μmol) as a dark purple solid.

^{1}H NMR (500 MHz, $CDCl_3$): δ 6.35 (s, 2H, Mes), 6.09 (d, *J* = 9.0 Hz, 2H, aryl), 5.95 (d, *J* = 9.0 Hz, 2H, aryl), 2.79 (s, 6H), 2.78 (s, 6H), 2.76 (d, *J* = 4.2 Hz, 2H, β-H), 2.26–2.25 (m, 4H, *β*-H), 2.17 (d, *J* = 4.2 Hz, 2H, *β*-H), 1.89 (s, 3H, *ortho*-Me) ppm. ^{13}C NMR (126 MHz, $CDCl_3$): δ 167.2, 164.7, 159.5, 156.4, 154.0, 146.0, 145.2, 136.9, 134.1, 130.5, 129.4, 128.1, 126.9, 122.9, 119.4, 114.3, 113.7, 109.1, 40.0, 20.8, 18.1 ppm.

UV/vis/NIR (CH$_2$Cl$_2$): λ_{max} (ε [M^{-1}cm^{-1}]) = 262 (34000), 426 (40000), 623 (34000) nm. HR-MS (ESI-MS): *m/z* = 577.1790, calcd for (C$_{35}$H$_{29}$N$_5$Ni)$^+$ = 577.1771 [(M)$^+$]. Single crystals were obtained by vapor diffusion of acetonitrile into a chlorobenzene solution of **1e**. C$_{35}$H$_{29}$N$_5$Ni, M_w = 578.34, monoclinic, P2$_1$/c, *a* = 11.547(4) Å, *b* = 7.327(2) Å, *c* = 32.081(9) Å, β = 96.234(5)°, *V* = 2698.4(14) Å^3, *Z* = 4, *R* = 0.0320 (*I* > 2.0 σ(*I*)), R_w = 0.0917 (all data), GOF = 1.077.

Dissymmetric norcorrole 1f

Dipyrrin complex **2f** (85.6 mg, 0.100 mmol), bis(1,5-cyclooctadiene)nickel (68.8 mg, 0.250 mmol) and 2,2'-bipyridyl (39.0 mg, 0.250 mmol) were dissolved in dehydrated THF (8 mL) and the solution was stirred for 2 h at room temperature inside a glove box. After taking out the flask of the glove box, the reaction mixture was filtered through a short pad of alumina (CH$_2$Cl$_2$ as an eluent) immediately and then evaporated. The residue was purified by silica-gel column chromatography (CH$_2$Cl$_2$/hexane = 1/1 as an eluent) and the collected blue band was concentrated and washed with hexane. Recrystallization from CH$_2$Cl$_2$/acetonitrile afforded the title compound **1f** in 45% (24.4 mg, 45.5 μmol) as a dark purple solid.

^{1}H NMR (500 MHz, CDCl$_3$): δ 6.96 (t, *J* = 7.4 Hz, 1H, Ph), 6.77 (m, 2H, Ph), 6.18 (dd, *J* = 1.3, 8.4 Hz, 2H, Ph), 6.13 (d, *J* = 9.1 Hz, 2H, aryl), 5.96 (d, *J* = 9.1 Hz, 2H, aryl), 2.87 (d, *J* = 4.2 Hz, 2H, β-H), 2.79 (s, 6H, NMe$_2$), 2.68 (d, *J* = 4.2 Hz, 2H, β-H), 2.37 (d, *J* = 4.2 Hz, 2H, β-H), 2.35 (d, *J* = 4.2 Hz, 2H, β-H) ppm. ^{13}C NMR (126 MHz, CDCl$_3$): δ 167.3, 164.5, 159.3, 156.9, 154.0, 145.8, 145.0, 131.9, 131.5, 130.9, 130.2, 127.9, 123.2, 121.8, 119.4, 114.3, 113.6, 109.1, 40.0 ppm. UV/vis/NIR (CH$_2$Cl$_2$): λ_{max} (ε [M^{-1}cm^{-1}]) = 261 (32000), 426 (39000), 628 (36000) nm. HR-MS (ESI-MS): *m/z* = 535.1295, calcd for (C$_{32}$H$_{23}$N$_5$Ni)$^+$ = 535.1301 [(M)$^+$]. Single crystals were obtained by pouring hexane into a chloroform solution of **1f**. C$_{32}$H$_{23}$N$_5$Ni, M_w = 536.26, monoclinic, P2$_1$/n, *a* = 14.9222(10) Å, *b* = 10.1071(7) Å, *c* = 16.9856(11) Å, β = 111.902(2)°, *V* = 2376.9(3) Å^3, *Z* = 4, *R* = 0.0301 (*I* > 2.0 σ(*I*)), R_w = 0.0819 (all data), GOF = 1.092.

Dissymmetric norcorrole 1g

Dipyrrin complex **2g** (88.1 mg, 0.100 mmol), bis(1,5-cyclooctadiene)nickel (68.8 mg, 0.250 mmol) and 2,2'-bipyridyl (39.0 mg, 0.250 mmol) were dissolved in dehydrated THF (8 mL) and the solution was stirred for 2 h at room temperature inside a glove box. After taking out the flask of the glove box, the reaction mixture was filtered through a short pad of alumina (CH$_2$Cl$_2$ as an eluent) immediately and then evaporated. The residue was purified by silica-gel column chromatography (CH$_2$Cl$_2$/hexane = 4/1 as an eluent) and the collected blue band was concentrated and washed with hexane and a small amount of CH$_2$Cl$_2$. The title compound **1g** was obtained in 29% (16.1 mg, 28.7 μmol) as a dark purple solid. ^{1}H NMR (500 MHz, CDCl$_3$): δ 7.05 (d, *J* = 8.6 Hz, 2H, aryl), 6.22 (d, *J* = 8.6 Hz, 2H, aryl), 6.04 (d, *J* = 9.1 Hz, 2H, aryl), 5.89 (d, *J* = 9.1 Hz, 2H, aryl), 2.76 (s, 6H, NMe$_2$), 2.65 (d, *J* = 4.0 Hz, 2H, β-H), 2.32 (d, *J* = 4.2 Hz, 2H, β-H), 2.14 (d, *J* = 4.0 Hz, 2H, β-H), 2.10 (d, *J* = 4.2 Hz, 2H, β-H) ppm. UV/vis/NIR (CH$_2$Cl$_2$): λ_{max} (ε [M^{-1}cm^{-1}]) = 259 (32000), 430 (35000), 645 (35000) nm. HR-MS (ESI-MS): *m/z* = 560.1250, calcd for (C$_{33}$H$_{22}$N$_6$Ni)$^+$ = 560.1254 [(M)$^+$]. Single crystals were obtained by vapor diffusion of methanol into a chloroform solution of **1g**. C$_{16.5}$H$_{11}$N$_3$Ni$_{0.5}$, M_w = 280.64,

monoclinic, $C2/c$, $a = 10.7913(16)$ Å, $b = 23.085(4)$ Å, $c = 9.7956(12)$ Å, $\beta = 98.370(14)°$, $V = 2414.3(6)$ Å^3, $Z = 8$, $R = 0.0902$ ($I > 2.0$ $\sigma(I)$), $R_w = 0.2609$ (all data), GOF = 1.070.

Dissymmetric norcorrole 1h

Dipyrrin complex **2h** (99.2 mg, 0.100 mmol), bis(1,5-cyclooctadiene)nickel (68.8 mg, 0.250 mmol) and 2,2'-bipyridyl (39.0 mg, 0.250 mmol) were dissolved in dehydrated THF (8 mL) and the solution was stirred for 2 h at room temperature inside a glove box. After taking out the flask of the glove box, the reaction mixture was filtered through a short pad of alumina (CH$_2$Cl$_2$ as an eluent) immediately and then evaporated. The residue was purified by silica-gel column chromatography (CH$_2$Cl$_2$/hexane = 1/2 as an eluent) and the collected green band was concentrated and washed with hexane. Recrystallization from CH$_2$Cl$_2$/acetonitrile afforded the title compound **1h** in 25% (16.5 mg, 24.5 μmol) as a dark purple solid. ^{1}H NMR (500 MHz, CDCl$_3$): δ 7.41 (s, 1H, aryl), 6.65 (s, 2H, aryl), 6.11 (d, $J = 9.1$ Hz, 2H, aryl), 5.91 (d, $J = 9.1$ Hz, 2H, aryl), 2.89 (d, $J = 4.2$ Hz, 2H, β-H), 2.56 (d, $J = 4.3$ Hz, 2H, β-H), 2.39–2.37 (m, 4H, β-H) ppm. ^{19}F NMR (470 MHz, CDCl$_3$): δ −66.6 ppm. UV/vis/NIR (CH$_2$Cl$_2$): λ_{max} (ε [M^{-1}cm^{-1}]) = 260 (29000), 430 (33000), 649 (32000) nm. HR-MS (ESI-MS): m/z = 671.1056, calcd for (C$_{34}$H$_{21}$F$_6$N$_5$Ni)$^+$ = 671.1049 [(M)$^+$]. Single crystals were obtained by vapor diffusion of hexane into a 1,2-dichloroethane solution of **1h**. C$_{51}$H$_{31.5}$F$_9$N$_{7.5}$Ni$_{1.5}$, $M_w = 1008.40$, monoclinic, $P2_1/c$, $a = 17.128(4)$ Å, $b = 11.539(2)$ Å, $c = 21.492(4)$ Å, $\beta = 94.759(4)°$, $V = 4233.1(14)$ Å^3, $Z = 4$, $R = 0.0695$ ($I > 2.0$ $\sigma(I)$), $R_w = 0.1885$ (all data), GOF = 1.083.

Dissymmetric norcorrole 1i

Dipyrrin complex **2i** (94.6 mg, 0.100 mmol), bis(1,5-cyclooctadiene)nickel (68.8 mg, 0.250 mmol) and 2,2'-bipyridyl (39.0 mg, 0.250 mmol) were dissolved in dehydrated THF (8 mL) and the solution was stirred for 2 h at room temperature inside a glove box. After taking out the flask of the glove box, the reaction mixture was filtered through a short pad of alumina (CH$_2$Cl$_2$ as an eluent) immediately and then evaporated. The residue was purified by silica-gel column chromatography (CH$_2$Cl$_2$/hexane = 2/1 as an eluent) and the collected green band was concentrated and washed with hexane. Recrystallization from CH$_2$Cl$_2$/hexane afforded the title compound **1i** in 15% (9.6 mg, 15.3 μmol) as a dark purple solid.

^{1}H NMR (500 MHz, CDCl$_3$): δ 5.91 (d, $J = 9.1$ Hz, 2H, aryl), 5.83 (d, $J = 9.1$ Hz, 2H, aryl), 2.75 (s, 6H, NMe$_2$), 2.28 (d, $J = 4.2$, 2H, β-H), 1.84 (d, $J = 4.3$ Hz, 2H, β-H), 1.75 (d, $J = 4.2$ Hz, 2H, β-H), 1.71 (d, $J = 4.3$ Hz, 2H, β-H) ppm. ^{19}F NMR (470 MHz, CDCl$_3$): δ −140.1, −156.7, −163.0 ppm. UV/vis/NIR (CH$_2$Cl$_2$): λ_{max} (ε [M^{-1}cm^{-1}]) = 261 (31000), 433 (39000), 645 (33000) nm. HR-MS (ESI-MS): m/z = 625.0842, calcd for (C$_{32}$H$_{18}$F$_5$N$_5$Ni)$^+$ = 625.0830 [(M)$^+$]. Single crystals were obtained by vapor diffusion of hexane into a dichloromethane solution of **1i**. C$_{32}$H$_{18}$Cl$_2$F$_5$N$_5$Ni, $M_w = 697.12$, monoclinic, $P2_1/c$, $a = 16.003(2)$ Å, $b = 10.6329(14)$ Å, $c = 17.070(2)$ Å, $\beta = 100.125(4)°$, $V = 2859.4(7)$ Å^3, $Z = 4$, $R = 0.0694$ ($I > 2.0$ $\sigma(I)$), $R_w = 0.1479$ (all data), GOF = 1.078.
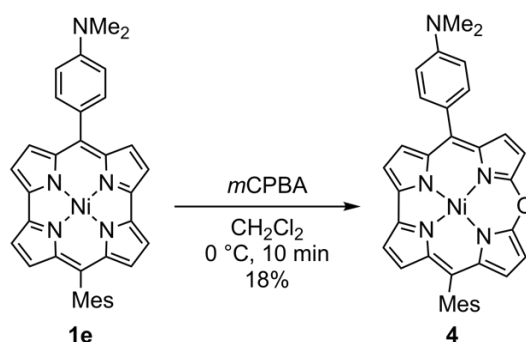
Scheme E4. Synthesis of 10-oxacorrole **4**.

10-Oxacorrole 4

m-Chloroperoxybenzoic acid (*m*CPBA, 3.6 mg, 21 μmol) was added to a solution of norcorrole **1e** (5.8 mg, 10 μmol) in CH$_2$Cl$_2$ (10 mL). After stirring the solution for 10 min at 0 °C, the reaction was quenched by the addition of NaHCO$_3$ aq. to extract mixture with CH$_2$Cl$_2$. The collected organic layer was dried over MgSO$_4$, and then evaporated. The crude product was purified by silica-gel column chromatography (CH$_2$Cl$_2$/hexane = 1/1 as an eluent) and the collected band was washed with small amount of hexane and methanol. The title compound **4** was obtained in 18% (1.1 mg, 1.9 μmol) as a brown solid.

^{1}H NMR (500 MHz, CDCl$_3$): δ 8.18 (d, J = 4.6 Hz, 1H, β-H), 7.87 (m, 2H, β-H), 7.83 (d, J = 8.7 Hz, 2H, aryl), 7.79 (d, J = 4.6 Hz, 1H, β-H) 7.78 (d, J = 4.6 Hz, 1H, β-H), 7.59 (d, J = 4.6 Hz, 1H, β-H), 7.52 (d, J = 4.3Hz, 1H, β-H), 7.51 (d, J = 4.3Hz, 1H, β-H), 7.10 (s, 2H. aryl), 6.99 (d, J = 8.7 Hz, 2H, aryl), 3.16 (s, 6H, NMe$_2$), 2.49 (s, 3H, *para*-Me), 1.98 (s, 6H, *ortho*-Me) ppm. ^{13}C NMR (126 MHz, CDCl$_3$): δ 153.7, 153.6, 150.8, 147.4, 147.1, 138.1, 137.9, 136.5, 134.5, 134.2, 134.1, 133.9, 133.9, 133.2, 132.7, 129.8, 129.6, 127.9, 127.8, 126.4, 125.8, 116.6, 116.4, 111.6, 109.0, 108.5, 40.7, 21.4, 20.8 ppm. UV/vis/NIR (CH$_2$Cl$_2$): λ_{max} (ε [M^{-1}cm^{-1}]) = 388 (56000), 554 (12000), 628 (7200), 679 (13000) nm.

Chapter 3
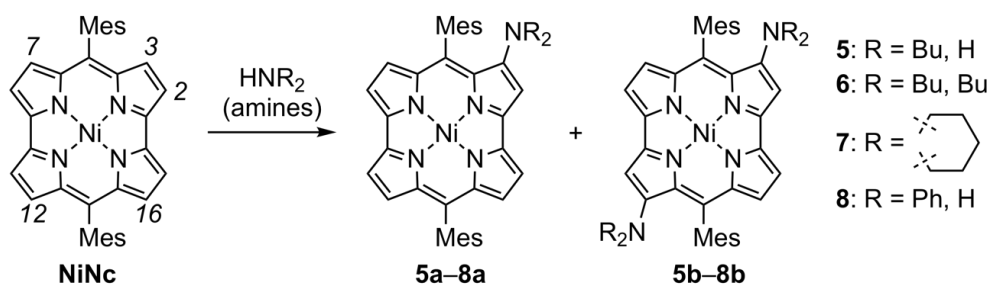
Scheme E5. Synthesis of aminonorcorroles **5–8**.

Aminonorcorroles 5a and 5b

Dimesitylnorcorrole **NiNc** (20.0 mg, 34.6 μmol) was dissolved in butylamine (2 mL) and stirred at room temperature for 1 h under air. The solution was neutralized by NH$_4$Cl aq., extracted with CH$_2$Cl$_2$, and the organic layer was dried over MgSO$_4$. The residue after evaporation was purified by silica-gel column chromatography

(CH$_2$Cl$_2$/hexane = 1/1 as an eluent) to provide **5a** in 45% (10.0 mg, 15.4 μmol) and **5b** in 52% (12.9 mg, 17.9 μmol) as dark brown solids.

5a: ^{1}H NMR (500 MHz, CDCl$_3$): δ 6.57 (s, 2H, Mes), 6.46 (s, 2H, Mes), 3.36 (d, *J* = 4.7 Hz, 1H, *β*-H), 3.25 (d, *J* = 4.7 Hz, 1H, *β*-H), 3.19 (d, *J* = 3.7 Hz, 1H, *β*-H), 3.09 (d, *J* = 3.9 Hz, 1H, *β*-H), 2.81 (d, *J* = 3.7 Hz, 1H, *β*-H), 2.73 (d, *J* = 3.9 Hz, 1H, *β*-H), 2.67 (s, 6H, *ortho*-Me), 2.67 (s, 6H, *ortho*-Me), 2.20 (s, 1H, *β*-H), 2.27 (td, *J* = 6.0, 5.3 Hz, 2H, alkyl), 2.05 (t, *J* = 5.3 Hz, 1H, NH), 2.01 (s, 3H, *para*-Me), 1.98 (s, 3H, *para*-Me), 0.71–0.57 (m, 7H, alkyl) ppm, ^{13}C NMR (126 MHz, CDCl$_3$): δ 173.5, 171.7, 161.6, 154.2, 151.0, 148.7, 145.7, 145.1, 144.6, 138.2, 137.9, 137.1, 136.9, 135.5, 134.8, 133.4, 128.9, 128.2, 128.1, 127.3, 121.0, 118.7, 116.3, 113.9, 112.1, 88.4, 44.0, 30.3, 20.9, 19.2, 18.6, 18.4, 13.4 ppm, UV/vis/NIR (CH$_2$Cl$_2$): λ$_{max}$ (ε [M^{-1}cm^{-1}]) = 264 (26000), 444 (19000), 546 (9000), 908 (880) nm. HR-MS (ESI-MS): *m/z* = 647.2567, calcd for (C$_{40}$H$_{39}$N$_5$Ni)$^+$ = 647.2554 [(M)$^+$]. **5b**: ^{1}H NMR (500 MHz, CDCl$_3$): δ 6.67 (s, 4H, Mes), 4.05 (d, *J* = 3.7 Hz, 2H, *β*-H), 3.50 (d, *J* = 3.7 Hz, 2H, *β*-H), 3.00 (s, 2H, *β*-H), 2.57 (s, 12H, *ortho*-Me), 2.38 (t, *J* = 5.3 Hz, 2H, NH), 2.27 (td, *J* = 6.0, 5.3 Hz, 4H, alkyl), 2.09 (s, 6H, *para*-Me), 0.84–0.69 (m, 8H, alkyl), 0.64 (t, *J* = 7.0, 6H, alkyl) ppm, ^{13}C NMR (126 MHz, CDCl$_3$): δ 172.1, 160.3, 146.3, 143.2, 137.8, 136.0, 135.9, 135.8, 129.0, 128.4, 114.9, 112.9, 87.6, 44.0, 30.3, 21.0, 19.4, 18.8, 13.5 ppm, UV/vis/NIR (CH$_2$Cl$_2$): λ$_{max}$ (ε [M^{-1}cm^{-1}]) = 264 (31000), 336 (21000), 477 (54000), 939 (2600) nm, HR-MS (ESI-MS): *m/z* = 718.3331, calcd for (C$_{44}$H$_{48}$N$_6$Ni)$^+$ = 718.3288 [(M)$^+$], Single crystals were obtained by vapor diffusion of hexane into a chloroform solution of **5b**. C$_{22}$H$_{24}$N$_3$Ni$_{0.5}$, *M*$_w$ = 359.80, triclinic, *P*–1, *a* = 8.3884(8) Å, *b* = 8.4668(5) Å, *c* = 14.2802(12) Å, *α* = 95.006(6)°, *β* = 94.479(7)°, *γ* = 113.925(7)°, *V* = 916.34(14) Å^3, *Z* = 2, *R* = 0.0460 (*I* > 2.0 σ(*I*)), *R*$_w$ = 0.1197 (all data), GOF = 1.058.

Aminonorcorrole 6a

Dimesitylnorcorrole **NiNc** (5.0 mg, 8.7 μmol) was dissolved in dibutylamine (0.5 mL) and stirred at 80 °C for 2 h under air. The solution was neutralized by NH$_4$Cl aq., extracted with CH$_2$Cl$_2$, and the organic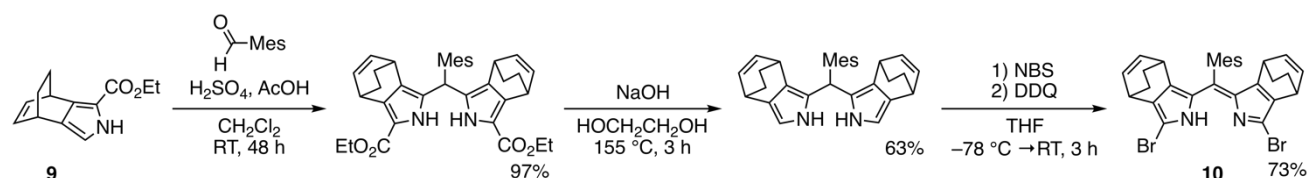 layer was dried over MgSO$_4$. The residue after evaporation was purified by silica-gel column chromatography (CH$_2$Cl$_2$/hexane = 1/2 as an eluent) to afford **6a** in 70% (4.3 mg, 6.1 μmol) as a dark brown solid.

^{1}H NMR (500 MHz, CDCl$_3$): δ 6.47 (s, 4H, Mes), 3.18 (d, *J* = 4.7 Hz, 1H, *β*-H), 3.25 (d, *J* = 4.7 Hz, 1H, *β*-H), 3.13 (d, *J* = 3.7 Hz, 1H, *β*-H), 3.12 (d, *J* = 3.7 Hz, 1H, *β*-H), 2.77 (d, *J* = 3.8 Hz, 1H, *β*-H), 2.70 (s, 6H, *ortho*-Me), 2.65 (s, 1H, *β*-H), 2.64 (d, *J* = 3.8 Hz, 1H, *β*-H), 2.61 (s, 6H, *ortho*-Me), 1.99 (s, 3H, *para*-Me), 1.98 (s, 3H, *para*-Me), 1.52 (t, *J* = 7.4 Hz, 4H, alkyl), 0.83–0.65 (m, 14H, alkyl) ppm, ^{13}C NMR (126 MHz, CDCl$_3$): δ 171.0, 170.4, 168.6, 152.1, 151.0, 148.8, 146.9, 145.2, 143.9, 140.9, 139.0, 136.9, 136.8, 134.8, 134.6, 133.9, 130.9, 128.7, 128.2, 128.1, 121.5, 119.3, 118.0, 113.8, 111.9, 101.4, 51.0, 29.1, 20.9, 20.6, 20.0, 19.1, 18.6, 13.8 ppm, UV/vis/NIR (CH$_2$Cl$_2$): λ$_{max}$ (ε [M^{-1}cm^{-1}]) = 267 (31000), 441 (29000), 566 (10000), 903 (1200) nm, HR-MS (ESI-MS): *m/z* = 703.3146, calcd for (C$_{44}$H$_{47}$N$_5$Ni)$^+$ = 703.3180 [(M)$^+$].

Aminonorcorrole 7b

Dimesitylnorcorrole **NiNc** (20.0 mg, 34.6 μmol) was dissolved in piperidine (2 mL) and stirred at room temperature for 1 h under air. The solution was neutralized by NH$_4$Cl aq., extracted with CH$_2$Cl$_2$, and the organic

layer was dried over MgSO$_4$. The residue after evaporation was purified by silica-gel column chromatography (CH$_2$Cl$_2$/hexane = 1/1 as an eluent) to afford **7b** in 80% (18.4 mg, 27.9 μmol) as a dark brown solid.

^{1}H NMR (500 MHz, CDCl$_3$): δ 6.55 (s, 4H, Mes), 3.74 (d, *J* = 3.7 Hz, 2H, *β*-H), 3.15 (s, 2H, *β*-H), 3.04 (d, *J* = 3.7 Hz, 2H, *β*-H), 2.54 (s, 12H, *ortho*-Me), 2.03 (s, 6H, *para*-Me), 1.76 (t, *J* = 5.4 Hz, 8H, methylene), 0.90 (m, 4H, methylene), 0.48 (m, 8H, methylene) ppm, ^{13}C NMR (126 MHz, CDCl$_3$): δ 169.3, 168.4, 145.6, 145.5, 140.1, 137.7, 136.6, 134.9, 130.7, 128.7, 118.1, 113.1, 100.6, 51.8, 24.1, 23.3, 20.9, 19.1 ppm, UV/vis/NIR (CH$_2$Cl$_2$): λ_{max} (ε [M^{-1}cm^{-1}]) = 265 (33000), 336 (20000), 488 (43000), 857 (2300) nm, HR-MS (ESI-MS): *m/z* = 742.3256, calcd for (C$_{46}$H$_{48}$N$_6$Ni)$^+$ = 742.3288 [(M)$^+$].

Aminonorcorroles 8a and 8b

Dimesitylnorcorrole **NiNc** (20.0 mg, 34.6 μmol) was dissolved in aniline (2 mL) containing a drop of tributylamine, and stirred at room temperature for 10 h under air. Aniline was removed by short silica gel column chromatography (CH$_2$Cl$_2$/hexane = 2/1 as an eluent), and then the residue was purified by silica-gel column chromatography (CH$_2$Cl$_2$/hexane = 1/1 as an eluent) to furnish **8a** in 72% (16.7 mg, 25.0 μmol) and **8b** in 17% (4.5 mg, 5.9 μmol) as dark brown solids. **8a**: ^{1}H NMR (500 MHz, CDCl$_3$): δ 6.86 (m, 2H, Ph), 6.69 (t, *J* = 7.5 Hz, 1H, Ph), 6.59 (s, 2H, Mes), 6.42 (s, 2H, Mes) 5.67 (dd, *J* = 8.8, 1.0 Hz, 2H, Ph), 3.53 (s, 1H, NH), 2.99 (d, *J* = 4.7 Hz, 1H, *β*-H), 2.85 (d, *J* = 4.7 Hz, 1H, *β*-H), 2.80 (s, 6H, *ortho*-Me), 2.79 (d, *J* = 3.9 Hz, 1H, *β*-H), 2.74 (s, 6H, *ortho*-Me), 2.71 (d, *J* = 3.8 Hz, 1H, *β*-H), 2.49 (d, *J* = 3.8 Hz, 1H, *β*-H), 2.48 (s, 1H, *β*-H), 2.40 (d, *J* = 3.9 Hz, 1H, *β*-H), 2.02 (s, 3H, *para*-Me), 1.95 (s, 3H, *para*-Me) ppm, ^{13}C NMR (126 MHz, CDCl$_3$): δ 174.2, 172.7, 156.1, 153.6, 153.2, 151.6, 146.4, 145.7, 145.5, 142.4, 138.6, 138.4, 136.9, 135.5, 134.4, 133.7, 129.1, 128.1, 127.5, 126.2, 123.1, 122.1, 118.9, 118.3, 118.2, 114.0, 112.6, 91.9, 20.9, 20.8, 18.3, 18.3 ppm, UV/vis/NIR (CH$_2$Cl$_2$): λ_{max} (ε [M^{-1}cm^{-1}]) = 264 (27000), 456 (20000), 569 (11000), 947 (1000) nm, HR-MS (ESI-MS): *m/z* = 667.2232, calcd for (C$_{42}$H$_{35}$N$_5$Ni)$^+$ = 667.2241 [(M)$^+$]. **8b**: ^{1}H NMR (500 MHz, CDCl$_3$): δ 6.93 (m, 4H, Ph), 6.73 (t, *J* = 7.5 Hz, 4H, Ph), 6.70 (s, 4H, Mes), 5.88 (dd, *J* = 8.8, 1.0 Hz, 4H, Ph), 4.02 (s, 2H, NH), 3.62 (d, *J* = 3.7 Hz, 2H, *β*-H), 3.29 (s, 2H, *β*-H), 3.14 (d, *J* = 3.7 Hz, 2H, *β*-H), 2.71 (s, 12H, *ortho*-Me), 2.11 (s, 6H, *para*-Me) ppm, ^{13}C NMR (126 MHz, CDCl$_3$): δ 173.1, 152.8, 148.9, 144.2, 139.8, 139.2, 138.4, 137.4, 136.1, 129.2, 129.1, 127.2, 122.7, 118.6, 116.8, 113.4, 91.8, 21.0, 18.6 ppm, UV/vis/NIR (CH$_2$Cl$_2$): λ_{max} (ε [M^{-1}cm^{-1}]) = 266 (33000), 501 (50000), 960 (3300) nm, HR-MS (ESI-MS): *m/z* = 758.2676, calcd for (C$_{48}$H$_{40}$N$_6$Ni)$^+$ = 758.2662 [(M)$^+$].

Chapter 4

Scheme E6. Synthesis of BCOD-fused dipyrrin **10** from BCOD-fused pyrrole **9**.

Bis-BCOD dipyrromethane diester

BCOD-fused pyrrole **9**[17] (1.09 g, 5.02 mmol) and 2,4,6-trimethylbenzaldehyde (557 mg, 3.76 mmol) were stirred in a mixture of acetic acid (12 mL) and CH_2Cl_2 (6 mL) with 5 drops of H_2SO_4 at room temperature for 48 h in the dark. The reaction mixture was neutralized by $NaHCO_3$ aq to extract the product with CH_2Cl_2. The organic layer was dried over $MgSO_4$ and filtrated. The residue after evaporation was purified by open silica-gel column chromatography (CH_2Cl_2, then AcOEt as eluents) to produce the title compound in 97% (1.38 g, 2.44 mmol) as a while or pale orange solid.

^{1}H NMR (500 MHz, $CDCl_3$): δ 8.03-7.97 (m, 2H, NH), 6.86 (s, 2H, Mes-aryl), 6.52-6.28 (m, 4H, olefin), 5.92-5.83 (m, 1H, *meso*), 4.35-4.32 (m, 2H, bridgehead), 4.30-4.22 (m, 4H, Et), 3.27-3.11 (m, 2H, bridgehead), 2.29 (s, 3H, *para*-Me), 2.00 (m, 6H, *ortho*-Me), 1.57-1.13 (m, 8H, methylene), 1.34 (t, J = 7.1 Hz, 6H, Et) ppm. ^{13}C NMR (126 MHz, $CDCl_3$): δ 161.7, 138.2, 138.1, 137.2, 137.2, 137.1, 137.0, 136.4, 136.3, 136.2, 136.0, 136.0, 135.8, 135.6, 135.5, 135.3, 135.2, 132.6, 132.5, 130.7, 130.6, 128.8, 128.6, 128.6, 125.9, 125.3, 125.2, 112.9, 112.7, 112.7, 112.3, 112.2, 59.9, 59.9, 37.1, 36.9, 34.0, 33.9, 33.8, 32.7, 32.7, 32.4, 26.5, 26.4, 26.4, 26.3, 21.0, 20.8, 20.8, 14.7 ppm. HR-MS (ESI-MS): m/z = 563.2914, calcd for $(C_{36}H_{39}N_2O_4)^+$ = 563.2904 $[(M - H)^+]$.

Bis-BCOD dipyrromethane

Bis-BCOD dipyrromethane diester (2.82g, 5.00 mmol) and sodium hydroxide (2.46 g, 61.5 mmol) in ethylene glycol (225 mL) were heated to 155 °C and stirred for 3 h in the dark. Dichloromethane was added to the flask after a cooling down in an ice bath, and the solution was washed with brine twice. The organic layer was dried over $MgSO_4$ and filtrated. The residue after evaporation was purified by open silica-gel column chromatography (CH_2Cl_2 as an eluent) to produce the title compound in 63% (1.33 g, 3.16 mmol) as a brown solid.

^{1}H NMR (500 MHz, $CDCl_3$): δ 7.25-7.19 (m, 2H, NH), 6.85-6.82 (m, 2H, Mes-aryl), 6.51-6.29 (m, 6H, olefin + pyrrole), 5.96-5.85 (m, 1H, *meso*), 3.80-3.76 (m, 2H, bridgehead), 3.26-3.05 (m, 2H, bridgehead), 2.29-2.27 (s, 3H, *para*-Me), 2.29-2.00 (m, 6H, *ortho*-Me), 1.55-1.22 (m, 8H, methylene) ppm. ^{13}C NMR (126 MHz, $CDCl_3$): δ 137.2, 137.1, 136.6, 136.5, 136.4, 136.4, 136.4, 136.4, 136.1, 136.1, 136.1, 136.0, 135.3, 135.3, 130.4, 130.3, 130.3, 130.2, 130.0, 126.0, 125.9, 125.6, 125.5, 121.9, 121.7, 121.1, 106.0, 106.0, 105.5, 105.4, 37.1, 37.0, 36.7, 33.6, 33.5, 33.5, 33.4, 32.5, 32.4, 32.2, 32.1 27.8, 27.7, 27.6, 27.1, 27.0, 27.0, 20.9, 20.9, 20.7, 20.6 ppm. HR-MS (ESI-MS): m/z = 419.2488, calcd for $(C_{30}H_{31}N_2)^+$ = 419.2482 $[(M - H)^+]$.
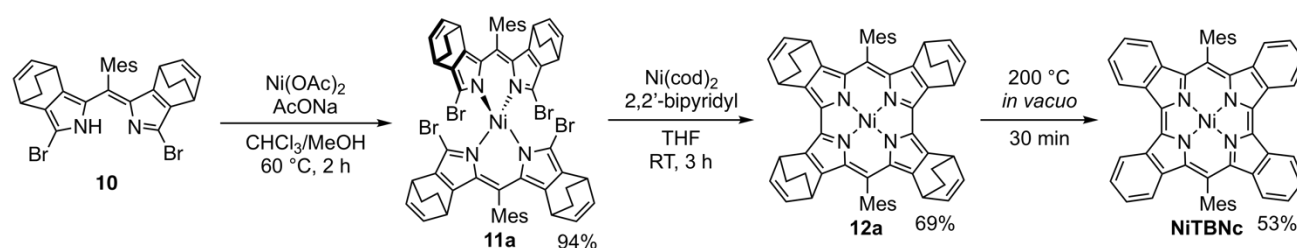
Bis-BCOD α,α'-dibromodipyrrin 10

A two-necked flask containing bis-BCOD dipyrromethane (1.33 g, 3.16 mmol) was evacuated and then refilled with N_2. To the flask, dry THF (50 mL) was added and the solution was cooled to –78 °C. After *N*-bromosuccinimide (NBS, 1.12 g, 6.30 mmol) was added to the solution in two portions at a 30 min interval, the mixture was stirred for 1 h. Then DDQ (714 mg, 3.15 mmol) was added in three portions every 15 min. The resulting mixture was stirred at –78 °C for 10 min and then warmed to room temperature. After stirring for additional 1 h, the reaction mixture was filtered through a short pad of alumina (CH_2Cl_2 as an eluent) and then

evaporated. Purification by open silica-gel column chromatography (CH$_2$Cl$_2$/hexane = 1/2 as an eluent) afforded **10** in 73% (1.32 g, 2.30 mmol) as an orange solid.

^{1}H NMR (500 MHz, CDCl$_3$): δ 11.91 (brs, 1H, NH), 6.99 (s, 2H, Mes-aryl), 6.40-6.33 (m, 2H, olefin), 6.08-6.03 (m, 2H, olefin) 3.84-3.74 (m, 2H, bridgehead), 4.48-4.34 (m, 2H, bridgehead), 2.43-2.40 (m, 3H, *para*-Me), 2.13-2.02 (m, 6H, *ortho*-Me), 1.42-1.01 (m, 8H, methylene) ppm. ^{13}C NMR (126 MHz, CDCl$_3$): δ 148.3, 148.3, 138.2, 138.2, 138.1, 137.2, 137.0, 136.8, 136.5, 136.5, 135.8, 135.7, 134.8, 134.7, 132.9, 132.8, 132.5, 132.5, 128.1, 128.1, 121.7, 121.7, 35.2, 33.6, 26.1, 25.9, 21.5, 19.9, 19.8, 19.7 ppm. HR-MS (ESI-MS): m/z = 577.0680, calcd for (C$_{30}$H$_{28}$Br$_2$N$_2$)$^+$ = 577.0674 [(M + H)$^+$].

Scheme E7. Synthesis of **NiTBNc**.

Bis-BCOD α,α'-dibromodipyrrin dimer Ni^{II} complex 11a

Ni^{II} acetate tetrahydrate (89.0 mg, 0.360 mmol), sodium acetate (98.8 mg, 1.20 mmol), and **10** (346 mg, 0.600 mmol) was dissolved in CHCl$_3$/MeOH (12 mL/6 mL) and heated to 60 °C. After stirring for 2 h, the solution was evaporated and open silica-gel column chromatography (CH$_2$Cl$_2$/hexane = 1/2 as an eluent) was performed to isolate **11a** in 94% (340 mg, 0.281 mg) as a deep red solid.

HR-MS (ESI-MS): m/z = 1208.0147, calcd for (C$_{60}$H$_{54}$Br$_4$N$_4$Ni)$^+$ = 1208.0394 [M$^+$].

Tetra-BCOD Ni^{II} norcorrole 12a

Dipyrrin complex **11a** (121 mg, 0.100 mmol), bis(1,5-cyclooctadiene)nickel (68.8 mg, 0.250 mmol) and 2,2'-bipyridyl (39.0 mg, 0.250 mmol) were dissolved in dehydrated THF (8 mL) and the solution was stirred for 3 h at room temperature inside a glove box. After taking out the flask of the glove box, the reaction mixture was filtered through a short pad of alumina (CH$_2$Cl$_2$ as an eluent) immediately and then evaporated. The residue was purified by silica-gel column chromatography (CH$_2$Cl$_2$/hexane = 1/2 as an eluent) and the collected brown band was concentrated and washed with hexane. The title compound **12a** was obtained in 69% (61.3 mg, 68.9 µmol) as a brown solid.

^{1}H NMR (500 MHz, CDCl$_3$): δ 6.36-6.06 (m, 4H, Mes-aryl), 5.18-4.69 (m, 8H, olefin), 3.50-2.55 (m, 12H, *ortho*-Me) 1.76 (s, 6H, *para*-Me), 0.58-0.35 (m, 4H, bridgehead), 0.28--0.22 (m, 16H, methylene), –0.72--0.75 (m, 4H, bridgehead) ppm. ^{13}C NMR (126 MHz, CDCl$_3$): δ 163.0 (br), 149.9 (br), 136.3, 135.0-132.6 (m), 131.8, 131.1, 127.9-127.7 (m), 125.2, 31.0, 24.0 (br), 23.6 (br), 20.8, 17.5, 17.3, 17.2, 17.1, 17.0, 16.9, 16.8, 16.7, 16.5 ppm. HR-MS (ESI-MS): m/z = 888.3712, calcd for (C$_{60}$H$_{54}$N$_4$Ni)$^+$ = 888.3696 [M$^+$].

Ni[II] tetrabenzonorcorrole (NiTBNc)

A solid sample of **12a** (100 mg, 0.112 mmol) was charged in a Kugelrohr, and heated at 200 °C for 30 min *in vacuo*. After cooling to room temperature, the resulting residue was recrystallized from toluene/MeOH, then toluene/MeCN inside a glove box. **NiTBNc** was obtained in 53% (50.5 mg, 64.9 μmol) as a dark brown crystal.

^{1}H NMR (500 MHz, toluene-d_8): δ 5.89 (s, 4H, Mes-aryl), 3.62 (s, 4H, benzo), 3.53 (s, 12H, *ortho*-Me), 2.91 (brs, 4H, benzo) 1.34 (s, 6H, *para*-Me), 0.61 (brs, 4H, benzo), 0.48 (d, J = 5.9 Hz, 4H, benzo) ppm. The ^{13}C NMR spectrum of **NiTBNc** was unobservable because of the broaden signals. UV/vis/NIR (CH$_2$Cl$_2$): λ_{max} (ε [M^{-1}cm^{-1}]) = 285 (48000), 449 (88000), 891 (4300), 1003 (6200) nm. HR-MS (ESI-MS): m/z = 776.2469, calcd for (C$_{52}$H$_{38}$N$_4$Ni)$^+$ = 776.2444 [M$^+$]. Single crystals were obtained by slow evaporation of toluene solution of **NiTBNc**. C$_{29.45}$H$_{22.89}$N$_2$Ni$_{0.50}$, M_w = 434.08, monoclinic, $P2_1/n$, a = 10.727 (4) Å, b = 16.223(6) Å, c = 12.946(5) Å, β = 100.899(6)°, V = 2212.2(15) Å^3, Z = 4, R = 0.0469 (I > 2.0 $\sigma(I)$), R_w = 0.1395 (all data), GOF = 1.012.
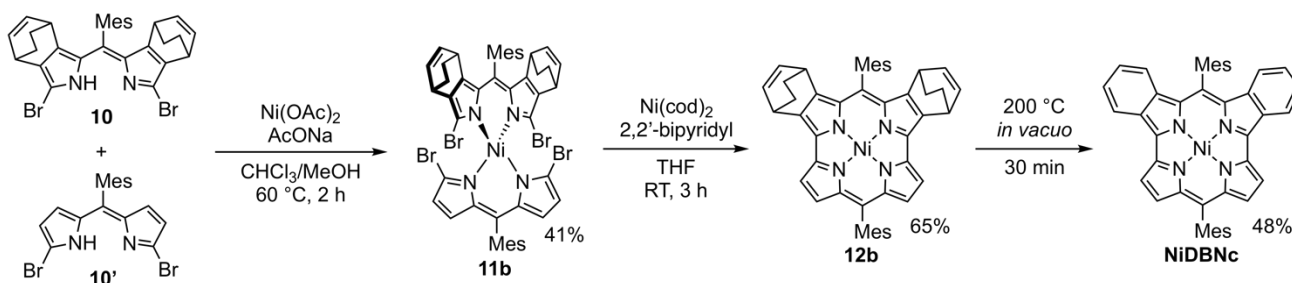
Scheme E8. Synthesis of **NiDBNc**.

Half & half dipyrrin dimer Ni[II] complex 11b

A flask was charged with Ni[II] acetate tetrahydrate (89.6 mg, 0.358 mmol), sodium acetate (98.4 mg, 1.20 mmol), **10** (173 mg, 0.300 mmol), and CHCl$_3$/MeOH (10 mL/10 mL). After starting to heat the flask in an oil bath which was heated to 60 °C in advance, the solution of α,α'-dibromodipyrrin **10'** (126 mg, 0.300 mmol) in CHCl$_3$ (10 mL) was added dropwise to the flask over 5 min. The mixture was stirred for 2 h at 60 °C. The residue resulted from the evaporation was purified by open silica-gel chromatography (CH$_2$Cl$_2$/hexane = 1/2 as an eluent) followed by GPC-HPLC (CHCl$_3$ as an eluent) operated overnight, to separate **11b** from homo-dimers. The middle band was taken from the GPC, and the additional purification by open silica-gel chromatography (CH$_2$Cl$_2$/hexane = 1/2 as an eluent) produced pure **11b** in 41% (130 mg, 0.123 mmol) as a deep red solid.

HR-MS (ESI-MS): m/z = 1051.9450, calcd for (C$_{48}$H$_{42}$Br$_4$N$_4$Ni)$^+$ = 1051.9451 [M$^+$].

Bis-BCOD Ni[II] norcorrole 12b

Dipyrrin complex **11b** (105 mg, 0.100 mmol), bis(1,5-cyclooctadiene)nickel (68.8 mg, 0.250 mmol) and 2,2'-bipyridyl (39.0 mg, 0.250 mmol) were dissolved in dehydrated THF (8 mL) and the solution was stirred for 3 h at room temperature inside a glove box. After taking out the flask of the glove box, the reaction mixture was filtered through a short pad of alumina (CH$_2$Cl$_2$ as an eluent) immediately and then evaporated. The residue was purified by silica-gel column chromatography (CH$_2$Cl$_2$/hexane = 1/2 as an eluent) and the collected brown

band was concentrated. Recrystallization from CH$_2$Cl$_2$/acetonitrile afforded **12b** in 65% (49.3 mg, 65.4 μmol) as a brown solid.

^{1}H NMR (500 MHz, CDCl$_3$): δ 6.30-6.13 (m, 4H, Mes-aryl), 5.20-4.87 (m, 4H, olefin), 3.26-2.68 (m, 12H, *ortho*-Me) 1.84-1.75 (m, 6H, *para*-Me), 1.15-1.03 (m, 4H, *β*-H), 0.63-0.60 (m, 2H, bridgehead), 0.51--0.05 (m, 8H, methylene), –0.45--0.47 (m, 2H, bridgehead) ppm. ^{13}C NMR (126 MHz, CDCl$_3$): δ 168.7, 168.5, 161.9, 161.9, 158.5, 158.5, 155.4, 155.3, 151.9, 151.7, 148.8, 148.7, 143.8, 143.7, 136.6, 136.6, 136.4, 136.1, 134.0, 133.6, 133.5, 133.4, 133.2, 132.9, 132.0, 132.0, 131.2, 131.2, 128.3, 128.2, 128.1, 128.1, 127.9, 127.9, 127.8, 125.6, 125.5, 113.7, 31.4, 30.7, 24.1, 24.0, 23.8, 23.6, 20.8, 20.6, 17.7, 17.6, 17.4, 17.4, 17.1, 17.1 ppm. HR-MS (ESI-MS): *m/z* = 732.2770, calcd for (C$_{48}$H$_{42}$N$_4$Ni)$^+$ = 732.2757 [M$^+$].

Ni^{II} dibenzonorcorrole (NiDBNc)

A solid sample of **12b** (50 mg, 68.1 μmol) was charged in a Kugelrohr, and heated at 200 °C for 30 min *in vacuo*. After cooling to room temperature, the resulting residue was recrystallized twice from toluene/MeCN inside a glove box. **NiDBNc** was obtained in 48% (22.1 mg, 32.6 μmol) as a dark red crystal.

^{1}H NMR (500 MHz, toluene-d_8): δ 5.95 (s, 2H, Mes-aryl), 5.77 (s, 2H, Mes-aryl), 3.65 (s, 2H, benzo), 3.59 (s, 6H, *ortho*-Me), 3.54 (s, 6H, *ortho*-Me) 3.11 (brs, 2H, benzo) 1.36 (s, 3H, *para*-Me), 1.29 (s, 3H, *para*-Me), 0.62 (s, 2H, benzo), 0.53 (brs, 2H, benzo), –2.79 (s, 2H, *β*-H), –3.87 (brs, 2H, *β*-H) ppm. The ^{13}C NMR spectrum of **NiDBNc** was unobservable because of the broaden signals. UV/vis/NIR (CH$_2$Cl$_2$): λ_{max} (ε [M^{-1}cm^{-1}]) = 278 (40000), 477 (40000), 565 (20000) nm. HR-MS (ESI-MS): *m/z* = 676.2159, calcd for (C$_{44}$H$_{34}$N$_4$Ni)$^+$ = 676.2131 [M$^+$]. Single crystals were obtained by vapor diffusion of acetonitrile into a chlorobenzene/diethylether solution of **NiDBNc** under argon atmosphere. C$_{88}$H$_{68}$N$_8$Ni$_2$, M_w = 1354.92, orthorhombic, $P2_12_12_1$, a = 31.2359(8) Å, b = 25.5017(9) Å, c = 8.2940(2) Å, V = 6606.7(3) Å^3, Z = 4, R = 0.0608 (I > 2.0 $\sigma(I)$), R_w = 0.1489 (all data), GOF = 1.045.

Chapter 5
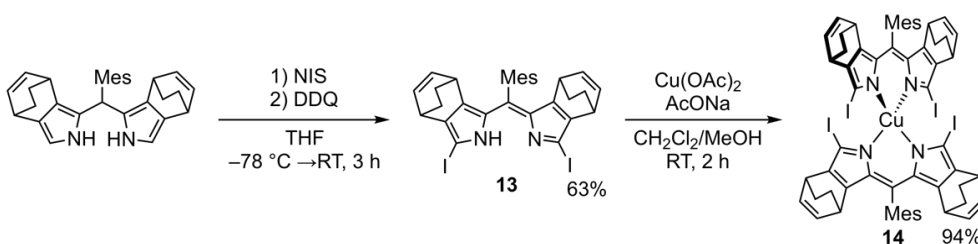
Scheme E9. Synthesis of Bis-BCOD α,α'-diiododipyrrin dimer Cu^{II} complex **14**.

Bis-BCOD α,α'-diiododipyrrin 13

A two-necked flask containing bis-BCOD dipyrromethane (1.09 g, 2.59 mmol) was evacuated and then refilled with N$_2$. To the flask, dry THF (35 mL) was added and the solution was cooled to –78 °C. After *N*-iodosuccinimide (NIS, 1.17 g, 5.20 mmol) was added to the solution in two portions at a 30 min interval, the mixture was stirred for 1 h. Then DDQ (588 mg, 2.59 mmol) was added in three portions every 15 min. The resulting mixture was stirred at –78 °C for 10 min and then warmed to room temperature. After stirring for

additional 30 min, the reaction mixture was filtered through a short pad of alumina (CH_2Cl_2 as an eluent) and then evaporated. Purification by open silica-gel column chromatography (CH_2Cl_2/hexane = 1/2 as an eluent) afforded **13** in 63% (1.09 g, 1.63 mmol) as an orange solid.

^{1}H NMR (300 MHz, $CDCl_3$): δ 12.04 (brs, 1H, NH), 6.99 (s, 2H, Mes-aryl), 6.40-6.33 (m, 2H, olefin), 6.07-6.01 (m, 2H, olefin) 3.65-3.61 (m, 2H, bridgehead), 2.49-2.44 (m, 2H, bridgehead), 2.43 (s, 3H, *para*-Me), 2.14-2.02 (m, 6H, *ortho*-Me), 1.45-0.98 (m, 8H, methylene) ppm.

Bis-BCOD α,α'-diiododipyrrin dimer Cu^{II} complex 14

Cu^{II} acetate monohydrate (120 mg, 0.601 mmol), sodium acetate (164 mg, 2.00 mmol), and **13** (670 mg, 1.00 mmol) was dissolved in $CHCl_3$/MeOH (24 mL/12 mL). After stirring for 2 h, the solution was evaporated, and the residue was recrystallized from CH_2Cl_2/MeOH. The resulting crystal was filtrated and washed with water, and MeOH to isolate **14** in 94% (660 mg, 0.471 mmol) as a deep red solid.
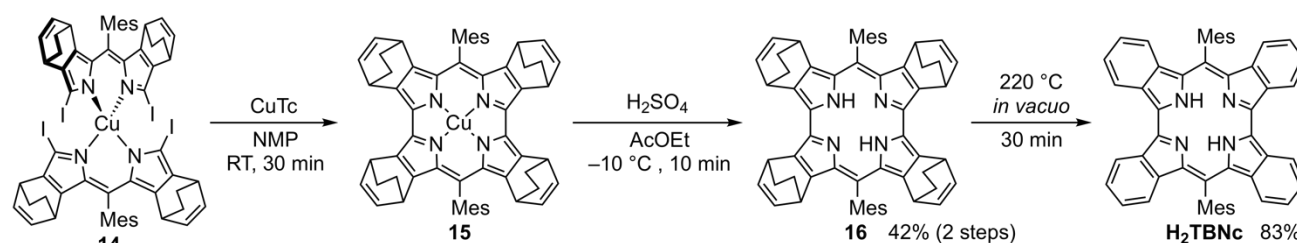
Scheme E10. Synthesis of free-base tetrabenzonorcorrole **H₂TBNc**.

Free-base tetra-BCOD norcorrole 16

To a flask charged with **14** (70.1 mg, 50.0 μmol) and Cu^I 2-thiophenecarboxylate (CuTc, 286 mg, 0.250 mmol)[18] was added NMP (30 mL) rapidly, and the solution was stirred for 15 min at room temperature inside a glove box. The flask was taken from the glove box to be treated with a sonicator, and the solution was stirred for additional 15 min at room temperature. The reaction mixture was extracted with AcOEt and washed with water, and brine. The organic layer was dried over Na_2SO_4, and the volume of the solution was reduced by a rotary evaporator. N_2 gas was bubbled through the resulting solution containing crude Cu^{II} norcorrole **15**. Then, H_2SO_4 (2 mL) was slowly added to the deoxygenated solution at 10 °C. After stirring for 10 min, the solution was cooled to –65 °C to be neutralized by aqueous ammonia. The mixture was allowed to warm and was washed with water. While the AcOEt layer was collected, the aqueous layer was extracted from CH_2Cl_2. The combined AcOEt layer and CH_2Cl_2 layer were dried over Na_2SO_4 and evaporated. The residue was purified by open silica-gel column chromatography (CH_2Cl_2, then CH_2Cl_2/MeOH = 9/1 as eluents) and a broad brown band was collected. Additional short silica-gel column chromatography (CH_2Cl_2 as an eluent) and recrystallization from CH_2Cl_2/MeOH were performed to remove residual Cu^{II} norcorrole **15**. The title compound **16** was isolated in 42% (17.4 mg, 20.9 μmol) as a brown solid. *Note: the purity of **16** need to be confirmed by UV/vis/NIR spectroscopy as well as ^{1}H NMR.

^{1}H NMR (500 MHz, $CDCl_3$): δ 34.24-34.08 (m, 2H, NH) 6.69-6.64 (m, 4H, Mes-aryl), 5.95-5.85 (m, 4H, olefin), 5.74-5.63 (m, 4H, olefin), 2.66-2.62 (m, 4H, bridgehead) 2.56-2.46 (m, 12H, *ortho*-Me), 2.17 (s, 6H,

para-Me), 1.54-1.51 (m, 4H, bridgehead), 1.31-0.76 (m, 16H, methylene) ppm. UV/vis/NIR (CH_2Cl_2): λ_{max} = 301, 398, 453, 940 nm.

Free-base tetrabenzonorcorrole H$_2$TBNc

A solid sample of **16** (16.7 mg, 20.0 μmol) was charged in a Kugelrohr, and heated at 220 °C for 30 min *in vacuo*. After cooling to room temperature, the resulting residue was recrystallized from toluene/MeCN inside a glove box. **H$_2$TBNc** was obtained in 83% (12.0 mg, 16.6 μmol) as a dark red crystal.

^{1}H NMR (500 MHz, toluene-d_8, −80 °C): δ 57.54 (s, 2H, NH), 6.18 (s, 4H, Mes-aryl), 5.36 (s, 4H, benzo), 5.21 (s, 4H, benzo), 4.50 (s, 4H, benzo), 3.83 (s, 4H, benzo), 2.99 (s, 12H, *ortho*-Me) 1.77 (s, 6H, *para*-Me) ppm. UV/vis/NIR (CH_2Cl_2): λ_{max} (ε [$M^{-1}cm^{-1}$]) = 262 (41000), 299 (28000), 413 (43000), 495 (38000), 1286 (240) nm. Single crystals were obtained by vapor diffusion of methanol into a toluene solution of **H$_2$TBNc** under argon atmosphere. $C_{29.5}H_{23.99}N_2$, M_w = 406.45, triclinic, P–1, a = 7.8763(6) Å, b = 10.2329(8) Å, c = 13.4047(10) Å, α = 84.031(2)°, β = 85.595(2)°, γ = 80.106(2)°, V = 1056.63(14) Å^3, Z = 2, R = 0.0677 (I > 2.0 $\sigma(I)$), R_w = 0.1650 (all data), GOF = 1.089.
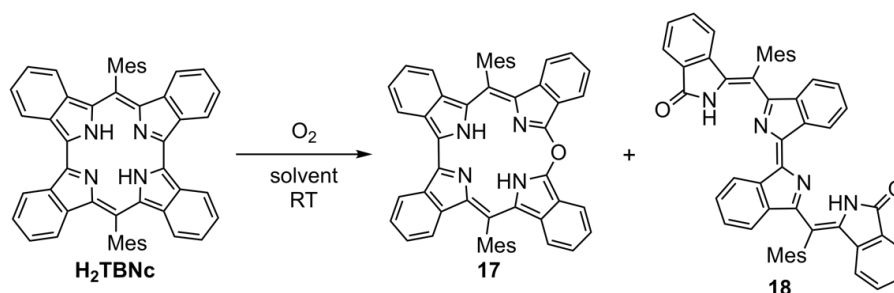
Scheme E11. Oxidation of **H$_2$TBNc**.

Oxidation of H$_2$TBNc by atmospheric dioxygen (17, 18)

A pure sample of **H$_2$TBNc** was dissolved in CH_2Cl_2/toluene and was left in air atmosphere. The change in the color of the solution was observed in a few minutes. After several hours, the solvent was evaporated and open silica-gel column chromatography (CH_2Cl_2/hexane, then CH_2Cl_2, then CH_2Cl_2/MeOH as eluents) was performed to collect bands of compounds **17** and **18**. Oxacorrle **17** was isolated as a green solid after recrystallization from CH_2Cl_2/MeOH, and bisdipyrrin **18** was isolated as a blue solid after washing with hexane.

17: ^{1}H NMR (500 MHz, CDCl$_3$): δ 9.40 (d, J = 8.2 Hz, 2H, benzo), 8.90 (d, J = 8.2 Hz, 2H, benzo), 7.81 (m, 2H, benzo), 7.72 (m, 2H), 7.61-7.52 (m, 8H, benzo), 7.36 (s, 4H, Mes-aryl), 2.69 (s, 6H, *para*-Me), 1.99 (s, 12H, *ortho*-Me) ppm. UV/vis/NIR (CH_2Cl_2): λ_{max}= 287, 392, 416, 433, 461, 580, 627, 670 nm. **18**: ^{1}H NMR (500 MHz, CDCl$_3$): δ 8.81 (d, J = 7.7 Hz, 2H, benzo), 7.91 (d, J = 7.4 Hz, benzo), 7.67-7.63 (m, 2H, benzo), 7.89-7.45 (m, 2H, benzo), 7.31-7.27 (m, 2H, benzo), 7.17-7.14 (m, 2H, benzo), 7.15 (s, 4H Mes-aryl), 6.27 (d, J = 7.9 Hz, 2H, benzo), 6.23 (d, J = 7.9 Hz, 2H, benzo), 2.53 (s, 6H, *para*-Me), 2.12 (s, 12H, *ortho*-Me) ppm. UV/vis/NIR (CH_2Cl_2): λ_{max}= 293, 363, 615, 659, nm. Single crystals were obtained by vapor diffusion of hexane into a CHCl$_3$ solution of **17**. $C_{52}H_{42}N_4O_2$, M_w = 754.89, monoclinic, $P2_1/n$, a = 9.5260(5) Å, b = 13.9187(6) Å,

c = 15.4793(7) Å, β = 103.7400(10)°, V = 1993.66(16) Å^3, Z = 2, R = 0.0366 (I > 2.0 $\sigma(I)$), R_w = 0.0964 (all data), GOF = 1.072.
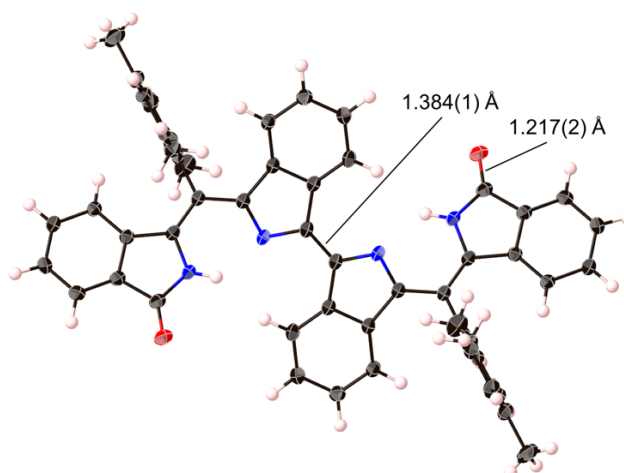
Figure E2. X-ray crystal structure of **18**. Atomic displacement parameters set at 50% probability.

E-6. References

1. S. Seki, A. Saeki, T. Sakurai, D. Sakamaki, *Phys. Chem. Chem. Phys.* **2014**, *16*, 11093.

2. D. F. Evans, D. A. Jakubovic, *J. Chem. Soc. Dalton Trans.* **1988**, 2927.

3. J. T. Groves, R. Quinn, T. J. McMurry, M. Nakamura, G. Lang, B. Boso, *J. Am. Chem. Soc.* **1985**, *107*, 354.

4. T. Ikeue, K. Furukawa, H. Hata, N. Aratani, H. Shinokubo, T. Kato, A. Osuka, *Angew. Chem. Int. Ed.* **2005**, *44*, 6899.

5. M. J. Frisch, G. W. Trucks, H. B. Schlegel, G. E. Scuseria, M. A. Robb, J. R. Cheeseman, G. Scalmani, V. Barone, B. Mennucci, G. A. Petersson, H. Nakatsuji, M. Caricato, X. Li, H. P. Hratchian, A. F. Izmaylov, J. Bloino, G. Zheng, J. L. Sonnenberg, M. Hada, M. Ehara, K. Toyota, R. Fukuda, J. Hasegawa, M. Ishida, T. Nakajima, Y. Honda, O. Kitao, H. Nakai, T. Vreven, J. A. Montgomery, Jr., J. E. Peralta, F. Ogliaro, M. Bearpark, J. J. Heyd, E. Brothers, K. N. Kudin, V. N. Staroverov, R. Kobayashi, J. Normand, K. Raghavachari, A. Rendell, J. C. Burant, S. S. Iyengar, J. Tomasi, M. Cossi, N. Rega, J. M. Millam, M. Klene, J. E. Knox, J. B. Cross, V. Bakken, C. Adamo, J. Jaramillo, R. Gomperts, R. E. Stratmann, O. Yazyev, A. J. Austin, R. Cammi, C. Pomelli, J. W. Ochterski, R. L. Martin, K. Morokuma, V. G. Zakrzewski, G. A. Voth, P. Salvador, J. J. Dannenberg, S. Dapprich, A. D. Daniels, Ö. Farkas, J. B. Foresman, J. V. Ortiz, J. Cioslowski, D. J. Fox, Gaussian, Inc., Wallingford CT, **2009**.

6. A. D. Becke, *Phys. Rev. A* **1988**, *38*, 3098.

7. C. Lee, W. Yang, R. G. Parr, *Phys. Rev. B* **1988**, *37*, 785.

8. M. Dolg, U. Wedig, H. Stoll, H. Preuss, *J. Chem. Phys.* **1987**, *86*, 866.

9. K. Yamaguchi, H. Fukui, T. Fueno, *Chem. Lett.* **1986**, 625.

10. K. Yamaguchi, In *Self-Consistent Field: Theory and Applications*, (Eds.; R. Carbó, M. Klobukowski) Elsevier, **1990**, pp 727–820.

11. H. Omori, S. Hiroto, H. Shinokubo, *Chem Commun.* **2016**, *52*, 3540.

12. S. Shimizu, Y. Ito, K. Oniwa, S. Hirokawa, Y. Miura, O. Matsushita, N. Kobayashi, *Chem Commun.* **2012**, *48*, 3851.

13. Y. Matano, T. Shibano, H. Nakano, H. Imahori, *Chem. Eur. J.* **2012**, *18*, 6208.

14. R. Nozawa, H. Tanaka, W.-Y. Cha, Y. Hong, I. Hisaki, S. Shimizu, J.-Y. Shin, T. Kowalczyk, S. Irle, D. Kim, H. Shinokubo, *Nat. Commun.* **2016**, *7*, 13620.

15. E. N. Durantini, *Molecules* **2001**, *6*, 533.

16. H. Chen, X.-B. Shao, X.-K. Jiang, Z.-T. Li, *Tetrahedron* **2003**, *59*, 3505.

17. S. Ito, T. Murashima, N. Ono, H. Uno, *Chem. Commun.* **1988**, 1661.

18. S. Zhang, D. Zhang, L. S. Liebeskind, *J. Org. Chem.* **1997**, *62*, 2312.

List of Publications

1. "Phosphorus(V) tetraazaporphyrins: porphyrinoids showing an exceptionally strong CT band between the Soret and Q bands"
   Taniyuki Furuyama, <u>Takuya Yoshida</u>, Daisuke Hashizume, Nagao Kobayashi, *Chem. Sci.* **2014**, *5*, 2466.

2. "Synthesis of Highly Twisted and Fully π-Conjugated Porphyrinic Oligomers"
   Satoru Ito, Satoru Hiroto, Sangsu Lee, Minjung Son, Ichiro Hisaki, <u>Takuya Yoshida</u>, Dongho Kim, Nagao Kobayashi, Hiroshi Shinokubo, *J. Am. Chem. Soc.* **2015**, *137*, 142.

3. "Synthesis and optical properties of tetraazaporphyrin phosphorus(V) complexes with electron-rich heteroatoms"
   <u>Takuya Yoshida</u>, Taniyuki Furuyama, Nagao Kobayashi, *Tetrahedron Lett.* **2015**, *56*, 1671.

4. "Fluorescence Enhancement of Tetraazaporphyrins by the Use of Bulky Substituent Effects"
   <u>Takuya Yoshida</u>, Taniyuki Furuyama, Mitsuo Asai, Nagao Kobayashi, *Chem. Lett.* **2015**, *44*, 1056.

5. "An Extremely Air-Stable 19π Porphyrinoid"
   <u>Takuya Yoshida</u>, Wen Zhou, Taniyuki Furuyama, Daniel B. Leznoff, Nagao Kobayashi, *J. Am. Chem. Soc.* **2015**, *137*, 9258.

6. "Synthesis of *meta*-methoxyphenyl substituted tetraazaporphyrin and corrolazine phosphorus(V) complexes"
   Taniyuki Furuyama, Yusuke Sugiya, <u>Takuya Yoshida</u>, Nagao Kobayashi, *J. Porphyrins Phthalocyanines* **2016**, *20*, 1075.

7. "Reversible Carbon–Carbon Bond Breaking and Spin Equilibria in Bis(pyrimidinenorcorrole)"
   Bin Liu, <u>Takuya Yoshida</u>, Xiaofang Li, Marcin Stępień, Hiroshi Shinokubo, Piotr J. Chmielewski, *Angew. Chem. Int. Ed.* **2016**, *55*, 13142.

8. "Enhancing the low-energy absorption band and charge mobility of antiaromatic Ni^{II} norcorroles by their substituent effects"
   <u>Takuya Yoshida</u>, Daisuke Sakamaki, Shu Seki, Hiroshi Shinokubo, *Chem. Commun.* **2017**, *53*, 1112.

9. "Direct amination of the antiaromatic Ni^{II} norcorrole"
   <u>Takuya Yoshida</u>, Hiroshi Shinokubo, *Mater. Chem. Front.* **2017**, *1*, 1853.

10. "Benzonorcorrole Ni^{II} Complexes: Enhancement of Paratropic Ring Current and Singlet Diradical Character by Benzo-Fusion"
    <u>Takuya Yoshida</u>, Kohtaro Takahashi, Yuki Ide, Jun-ya Fujiyoshi, Sangsu Lee, Yuya Hiraoka, Dongho Kim, Masayoshi Nakano, Takahisa Ikeue, Hiroko Yamada, Hiroshi Shinokubo, *Angew. Chem. Int. Ed.* **2018**, DOI: 10.1002/anie.201712961.

Acknowledgements

The author expresses sincere thanks to his all friend inside and outside the world of academia for their friendship and warm encouragement.

Last but not least, the author desire to deep gratitude beyond description to his parents, Dr. Yuichi Yoshida and Ms. Ikuko Yoshida. This thesis would not have appeared in the present form without their hearty encouragement and devoted support.

<div align="right">

Takuya Yoshida

吉田　拓矢

February 2018

</div>